DISCLAIMER NOTICE

THIS DOCUMENT IS BEST QUALITY PRACTICABLE. THE COPY FURNISHED TO DTIC CONTAINED A SIGNIFICANT NUMBER OF PAGES WHICH DO NOT REPRODUCE LEGIBLY.

CHESAPEAKE BAY INSTITUTE
The Johns Hopkins University

TECHNICAL REPORT XIX

SURFACE WAVES AT SHORT FETCHES AND LOW WIND SPEEDS—A FIELD STUDY

by Blair Kinsman

Volume I

Reference 60-1 May 1960

To: Mailing List

Since Volumes 2 and 3 containing the appendices to Technical Report No. XIX are very bulky, they are not being included in the general mailing. If, after considering the Tables of Contents in Volume 1 it is felt that the tabular and graphical material presented in Volumes 2 and 3 would be useful, copies may be secured by addressing a request to the Chesapeake Bay Institute, The Johns Hopkins University, Baltimore 18, Maryland.

D. W. Pritchard

CHESAPEAKE BAY INSTITUTE
THE JOHNS HOPKINS UNIVERSITY

TECHNICAL REPORT XIX

SURFACE WAVES AT SHORT FETCHES AND LOW WIND SPEEDS
A FIELD STUDY

Volume 1

by
Blair Kinsman

"If then, Socrates, amid the many opinions about the gods and the generation of the universe, we are not able to give notions which are altogether and in every respect exact and consistent with one another, do not be surprised. Enough, if we adduce probabilities as likely as any others; for we must remember that I who am the speaker, and you who are the judges, are only mortal men, and that we ought to accept the tale which is probable and enquire no further."

Plato, Timaeus

This report contains results of work carried out for the Office of Naval Research of the Department of the Navy under research project NR 083-016, Contract Nonr 248(20).

Reference 60-1
May 1960

D. W. Pritchard
Director

ABSTRACT

This is a study of 24 point records of surface waves made at short fetches and low windspeeds. It is found that the characteristic departure of the observed distribution of water heights from the Gaussian consists of an elevation of the positive tail, a depression of the negative tail, and a shifting of the mode toward negative values. The deformation is more pronounced for shorter fetches and lighter winds. Evidences of nonlinear interaction are found in the wave spectra, which tend to support the suggestion that a nonlinear theory of surface waves should be carried at least to third order for realistic results. It is found that for sharply peaked spectra the equilibrium range may not begin until frequencies are reached greater than three times the frequency at which the maximum power is located.

PREFACE

The material contained in this study took a considerable effort to gather, process, and present. Almost every member of the Chesapeake Bay Institute was at one time or another pressed into service. The author is grateful for all the assistance he received. He can not recognize individually all who have worked with him, but he would like to mention specifically Captain D. W. Booth of the R.V. MAURY, Mr. Edmund Schiemer who kept the instruments functioning, Mr. E. D. Stroup who made many of the pictures, Mr. R. W. Linfield who did the graphic arts work, Mrs. E. S. Shinn who digitized the records and drew many of the figures, Mrs. D. Raup and Mrs. T. A. Wastler who gave editorial assistance, and Mrs. W. C. Hof who did the typing. The author is grateful to Mr. R. Reightler and his staff in the Duplication Department of the Johns Hopkins University for the care and effort expended in printing this report. Thanks are also due to Mr. E. Mehr of New York University who supervised the author's novitiate in high-speed digital computing and who saw the numbers through the machine.

Finally the author is deeply grateful to three men: to Dr. D. W. Pritchard who encouraged and supported this work from its inception, to Dr. W. J. Pierson, Jr. who gave liberally of his time and experience, and to Dr. O. M. Phillips whose counsel in moments of despair provided a rational alternative to suicide.

Baltimore, Maryland — Blair Kinsman

May 1960

Volume 1

TABLE OF CONTENTS PAGE

Volume 2

TABLE OF CONTENTS PAGE

Volume 3

TABLE OF CONTENTS PAGE

Volume 1

LIST OF FIGURES

Volume 1

LIST OF TABLES

0.0 INTRODUCTION

The advance of science, as its history shows, proceeds on two legs, for it depends equally upon theory and observation. Without a guiding theoretical concept observation, controlled or passive, is at a loss to know what to observe or in what way. The Baconian notion of tables of presences and absences unguided by theory, while logically sound and intriguing to the imagination, never produced any startling results. On the other hand, theory must proceed by abstraction and simplification and, without observation to guide it, the selection of a fruitful set of assumptions from among the myriad alternatives becomes at best an improbable happy accident. It is seldom at any point of the advance that both legs are equally developed. The gait is usually a lop-sided hobble and there are times when science gives the distinct impression of riding a pogo stick.

The history of our understanding of ocean surface waves is the epitome of the history of science. Our understanding of water waves depends upon both theory and observation and the two have seldom, if ever, been in good balance. It seems strange that most people understand wave motion in any form by analogy with what they think they have seen of surface waves on the water; we really know very little about the process on which the analogy is based.

The problem can be simply stated. What we require is a solution of the equation of wave motion and the equations of motion for an incompressible, inviscid, constant-density fluid bounded by a free surface. If we formulate this in an Eulerian reference system, we have (Coulson, 1949)

(1) $\frac{\partial^2 \eta}{\partial x_i^2} = \frac{1}{c^2} \frac{\partial^2 \eta}{\partial t^2}$, the equation of wave motion,

where $\eta = \eta(x_1, x_2, t)$ is the displacement of the free surface and

(2) $\frac{D\mathbb{V}}{Dt} = \mathbb{g} - \frac{1}{\rho} \nabla p$, the equations of motion,

where $\mathbb{V}$ = the velocity vector,

$\mathbb{g}$ = the acceleration of gravity,

p = the pressure force,

ρ = the density of the water,

$\nabla \equiv \frac{\partial}{\partial x_1} + \frac{\partial}{\partial x_2} + \frac{\partial}{\partial x_3}$, the gradient operator, and

$\frac{D}{Dt} \equiv \frac{\partial}{\partial t} + u_i \frac{\partial}{\partial x_i}$, the Stokes derivative. There are also suitable boundary conditions. Equations (2) have already been much simplified from the full equations of motion. Since the bulk modulus of elasticity of water is only 5.25×10^{-5} atm, its viscosity only 1.79×10^{-2} dyne-sec/cm^2, and its changes in density in the oceans are of the order of a few thousandths of a gram/cm^3, the assumptions of incompressibility, zero viscosity, and constant density seem reasonable. Even with these simplifications equations (2) are intractable.

If we make the further assumption that the wave motion is irrotational, then it will be possible to express the velocity by a potential function Φ and our equations of motion become

(3) $\frac{\partial^2 \Phi}{\partial x_i^2} = 0$, Laplace's equation, and

(4) $\frac{p}{\rho} = \frac{\partial \Phi}{\partial t} - \frac{1}{2}\left\{\frac{\partial \Phi}{\partial x_i}\right\}^2 - g x_3$, Bernoulli's equation. At the

bottom boundary (or any other rigid boundary) the normal derivative of the potential function must be zero:

(5) $x_3 = -h(x_1,x_2)$, $\frac{\partial \Phi}{\partial n} = 0$. At the free surface

where $x_3 = \eta(x_1,x_2,t)$,

(6) $\eta = \frac{1}{g}\frac{\partial \Phi}{\partial t} - \frac{1}{2g}\left\{\frac{\partial \Phi}{\partial x_i}\right\}^2$, and

(7) $\frac{\partial \eta}{\partial t} = -\frac{\partial \Phi}{\partial x_3}$.

The problem as stated in equations (1) and (3) through (7) is nonlinear because of the presence of the terms $\left\{\frac{\partial \Phi}{\partial x_i}\right\}^2$ in (4) and (6). This is unfortunate because the mathematical techniques available for handling nonlinear equations are in a much less satisfactory state of development than are those for linear equations. Furthermore, because of the nonlinearity the principle of superposition cannot be invoked, and the powerful tool of Fourier analysis cannot be used. The problem can be linearized by making the additional assumptions that

(8) $\left\{\frac{\partial \Phi}{\partial x_i}\right\}^2 << \frac{\partial \Phi}{\partial t}$, and that

(9) ηk is small. The k is the wave number $\frac{2\pi}{\lambda}$. These reduce the problem to the solution of

(10) $\frac{\partial^2 \Phi}{\partial x_i^2} = 0$,

(11) $\frac{p}{\rho} = \frac{\partial \Phi}{\partial t} - g x_3$, at

(12) $x_3 = -h(x_1,x_2)$, $\frac{\partial \Phi}{\partial n} = 0$, and at

(13) $$x_3 = 0, \quad \eta = \frac{1}{g}\frac{\partial \Phi}{\partial t}, \text{ and}$$

(14) $$\frac{\partial \eta}{\partial t} = -\frac{\partial \Phi}{\partial x_3}.$$

It is with solutions to equations (1) and (3) to (7), or more often with equations (1) and (10) to (14), that the classical wave theory of the 19th century concerns itself. It engaged some of that century's best minds: among others, Airy, Boussinesq, Cauchy, Dirichlet, Gerstner, Helmholz, Kelvin, Krylov, Lamb, Poisson, Rankine, Rayleigh, and Stokes. That the problem has not lost its interest today is indicated by the publication of books such as Stoker's (1957) which are 19th century in spirit and contain many ingenious and novel contributions.

The classical solutions quite typically demand strict periodicity either in the wave form η or, if the problem has been linearized and superposition invoked, in the components η_i whose sum constitutes η. Now if there is one thing that even a cursory glance at the waves of the sea shows, it is that they are not periodic in any simple way. No two wave records ever seem to duplicate each other exactly. Lord Rayleigh is said to have remarked, "The basic law of the seaway is the apparent lack of any law." This seems to be a clear recognition of the fact that ocean waves are a stochastic process. Since a good theory of stochastic processes lay in the future, and since the 19th century was dominated by Newtonian determinism, even the giants in the field could do little beyond recognizing the chaotic nature of the real phenomenon. They could only elucidate the properties of their slightly more tractable, deterministic, periodic models.

Meanwhile, observations of waves were being made. Since the models bore so little relation to the process in nature, they afforded only feeble guidance to the observers, who measured what they could

as well as they could--often very well indeed. Only seldom does much light emerge from unguided observations of chaos. The measurements were of scant utility to the model makers, so each group went its own way and communication between the two became increasingly sporadic and difficult.

The two tools that brought an abrupt end to this sorry state of affairs were forged in the 1930's and 1940's. The first was an adequate theory of stochastic processes. Among the leading contributers were Blanc-Lapierre, Bochner, Doob, Feller, Fortet, Gnedenko, Khintchine, Kolmogorov, Lévy, and Slutsky. The second was primarily the work of Wiener (1930, 1949), who extended Fourier analysis to generalized harmonic analysis. The tools did not long lie idle. World War II brought a pressing need for wave forecasts on invasion beaches. Rice (1944, 1945) applied stochastic processes and generalized harmonic analysis to communications problems, thus making these techniques more intelligible to those not adepts of pure mathematics. Tukey (1949) concerned himself with the practical aspects of measuring power spectra.

There are four major insights which were necessary before the modern approach to waves could take form:

1) The conviction that the problem of bringing law to the confusion of the sea was in its essence a statistical problem not to be solved by deterministic formulations. This required a firm departure from the classical approach and a commitment to the then new and unfamiliar discipline of stochastic processes.

2) The realization that even under the new formulation the motion must still obey the classical equations. This is not trivial. There is no a priori reason to suppose that a statistic must propagate in the classical manner. In fact there are those which do not.

3) The identification of the two-variable spectrum as the ordering and governing principle in the apparent confusion.

4) The conception that the space-time function describing a given sea state must have a certain multivariate probability structure which, if stationary, can depend only on time and space coordinate differences.

These four concepts Pierson (1952, 1955) brought into relation and exploited in detail, the first three in 1952 and the fourth in 1955. During the decade preceding 1952 these ideas had breached. Sverdrup and Munk (1947) were well aware of the statistical nature of the problem but under the pressure of the war had no time to resolve it satisfactorily. Four related theoretical notes by Longuet-Higgins (1946), Barber (1946a, 1946b), and Barber, Collins, and Tucker (1946) use one or more of the basic ideas but not to produce a systematic theory of waves. The same is later true of Longuet-Higgins (1950), Rudnick (1951), and Birkhoff and Kotik (1952). Eckart (1946, 1953) made more extensive use of stochastic processes than any of these authors although he usually worked with correlation functions rather than spectra.

Pierson (1952), drawing largely on the ideas of Rice and Tukey, gave form, coherence, and definition to these inchoate loomings. He was familiar with the work of Sverdrup, Munk, Rudnick, Birkhoff, Kotik, and Eckart. There is no indication that he was familiar with the work of the British Admiralty group. Since the acceptance of the stochastic process approach there has been a rapid proliferation of mathematical models which agree with many more features of the observed seaway than did the classical models. There has also been a growing interest in the nonlinearity of the problem, e.g., work by Tick (1958) and Phillips (1960).

It is not surprising that Pierson (1952) finds very few wave observations that are even remotely useful in testing his theory. Unless observation programs are structurally related to the theory with which they are to be compared, they are usually inadequate. With the guidance on what to observe provided by the stochastic formulation, appropriate wave-measurement data have been accumulating at an accelerating pace. True, most of the data come from pressure records which are Gaussian to a high degree and can therefore yield little information about nonlinearity, since the high-frequency components have been filtered out.

Today, however, perhaps for the first time, theory and observation are on an equal footing: they can now effectively supplement each other. This paper is devoted to an analysis of a group of 24 surface records with particular attention to the evidences of nonlinearity.

1.0 THE WORK AREA

1.1 Desirable Characteristics

In the selection of an area for field work there are four primary considerations. The first is that it be a region of light winds. Most of the time the entire Chesapeake Bay is such a region, if one omits the winter months and ignores the notorious Chesapeake Bay squall. In practice, these squalls are remarkably hard to ignore, and one must either be ready to cut and run on very short notice or have extremely good ground tackle.

A second consideration is freedom from interference. Since our interest is in rather small wind-driven waves, any force other than wind that alters the water level will tend to obscure the phenomenon we wish to observe. A tideless piece of water would be ideal but, barring that, one in which the tidal ranges are small is usable. The astronomical tide in the upper Bay is quite small. For example, the Tide Tables (1958) seldom show a range greater than 18 inches for Baltimore. Another consideration that makes a small tidal range desirable is that it is usually accompanied by small tidal currents. In Chesapeake Bay, wind setup frequently produces a much larger change in water level than does tide. Experienced Bay watermen handling boats in constricted places usually pay more attention to the wind setup than to the stage of the tide. The author has observed differences of 4 feet or more in water level, due primarily to wind. Fortunately, the periods of these oscillations are so long compared with the record lengths required for small wind waves that these fluctuations can be ignored. The chief

difficulty they introduce is that instrument mountings must be adjustable through a rather large range.

A much more serious source of interference comes from passing boats. The body of Chesapeake Bay is a busy international thoroughfare. An oil tanker with a bone in her teeth produces a bow wave capable of drowning out and damaging almost any instrument rig. Small pleasure craft, while not so hard on instruments, can effectively prevent taking useful records. In this respect the Bay, while not ideal, is usable. With the development of a good network of highways on its periphery, many of its arms are no longer frequented by heavy commercial traffic and most pleasure boat owners are active only on week ends.

A third major consideration is that the working area have well-defined fetches in the directions from which the wind may be expected to blow. While this is not so easy to satisfy as might be supposed from the dendritic nature of the Bay, still, places can be found which combine this requirement with the two previous ones as well as with the fourth.

The fourth major consideration is that the working area have a uniform bottom deep enough not to interfere in any way with the development of waves in the range of interest. From the theory of small amplitude waves we have for deep water (Lamb, 1932, p. 365)

$$\sigma^2 = gk$$

where $\sigma = 2\pi/T$ = the frequency, and

$k = 2\pi/L$ = the wave number. Consequently,

$L = (g/2\pi)T^2$. If we take $g = 32.2$ ft/sec with L in feet and T in seconds,

$L = 5.12T^2$. Among hydrodynamicists, e.g., Stoker (1957), it is customary to consider that a wave is in deep water whenever the relative depth

$h/L > 1/2$. Since the exact expression is $\sigma^2 = gk \tanh 2\pi h/L$, this produces an error of only 0.37% due to the approximation. Using this criterion we find that waves with periods

$T < \sqrt{0.391h}$ sec or frequencies

$f > \sqrt{\frac{2.56}{h}}$ cps will be in deep water and undistorted.

1.2 Round Bay

The area selected for field work was Round Bay at the head of the Severn River (figure 1.1). This area, lying within 76°32'W and 76°34'W longitude and 39°02'N and 39°04'N latitude, has a long axis of a little more than 2 nautical miles ranging roughly NW-SE. The width of the main part is a bit less than 1 nautical mile. It is joined on the southwest by Little Round Bay. The bottom, which is mostly sandy mud, falls away steeply to a quite uniform depth of 20 to 22 feet; the extreme depth is 25 feet. Between east-west lines through Cedar Point (figure 1.2) and 39°02'N, and within the 18-foot contour, chart C & GS 566 shows 82 soundings whose mean is 20.8 feet with a standard deviation of ±1.4 feet; these depths are for mean low water. The only detached shoal within the 18-foot contour is a small one near the southern end of Round Bay.

The banks surrounding Round Bay are quite high and steep and are heavily wooded. In figure 1.2 the 40-foot elevation contour has been showed in order that some idea of the ruggedness of the surrounding country may be formed. It also shows the extreme heights on the northern and western sides, the wind directions for which wave records were made.

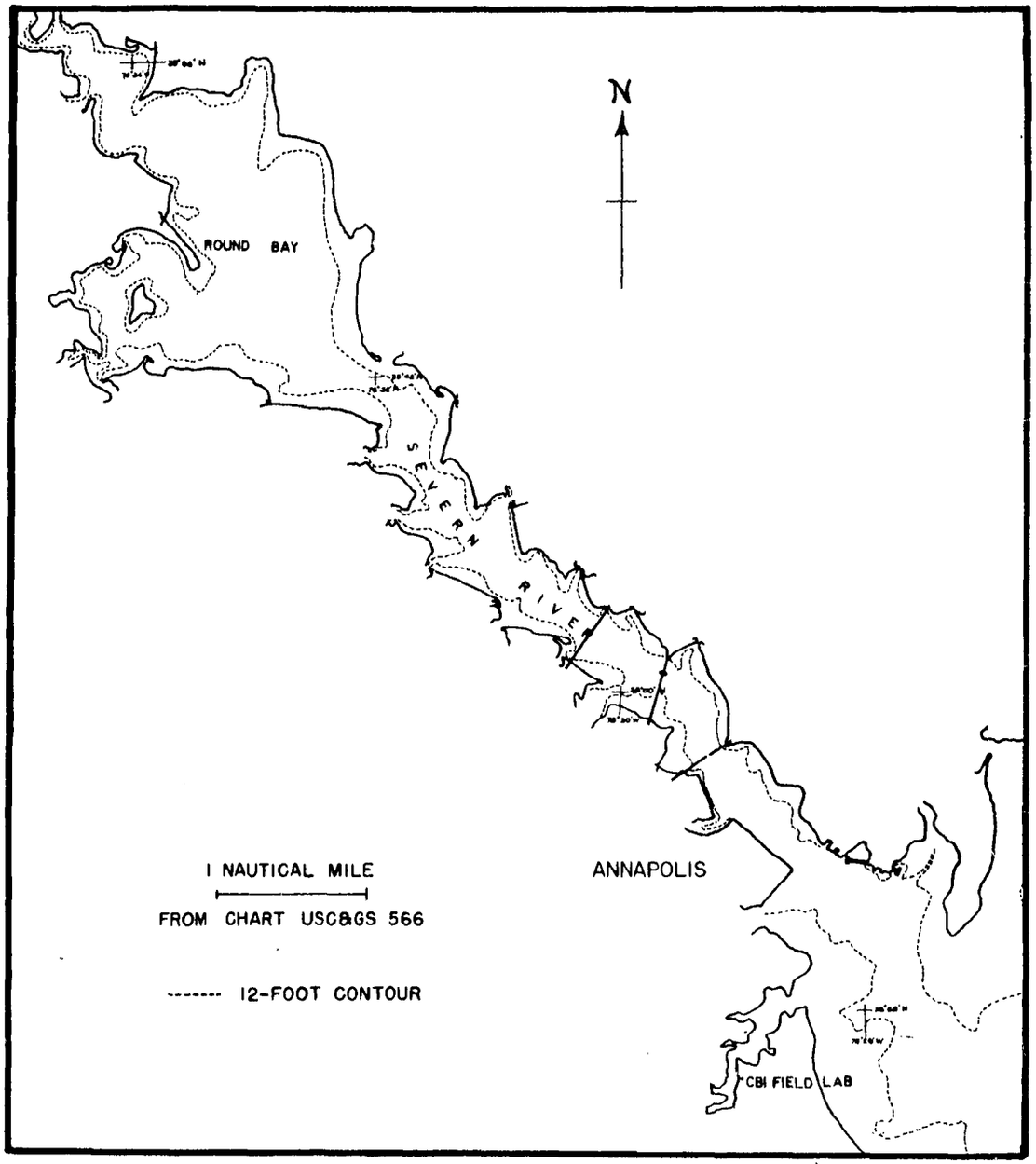

Figure 1.1 A Chart of the Severn River

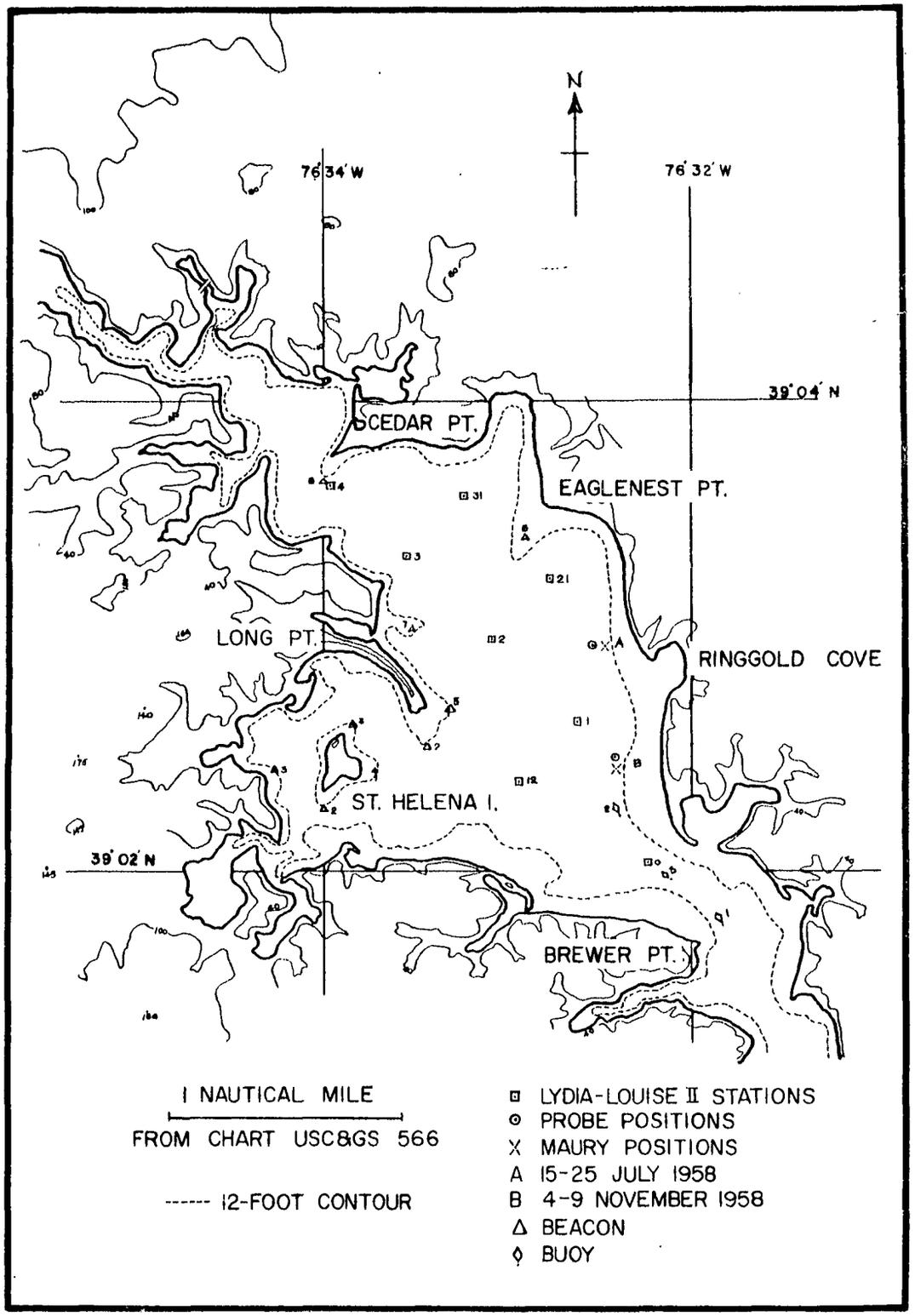

Figure 1.2 A Chart of Round Bay on the Severn River

There is no major source of fresh water for Round Bay. It is fed by a few very small streams which carry strictly local runoff. A generous estimate of the drainage area, including Round Bay itself, would be 25 square miles.

Round Bay meets all four primary considerations quite well. The U.S. Weather Bureau compilation "Local Climatological Data, Baltimore, Maryland," shows that for winds measured nearby the averages of the hourly speeds for July and for November from 1950 through 1957 were 8.6 and 10.3 mph, respectively. For both months the wind lay in the sector from south to north-northwest 66.1% of the time. It has been the author's experience, based on many years of racing sailboats, that the wind in the arms of Chesapeake Bay actually tends to follow the rivers. Thus, if we position the probe to take full advantage of the west-to-north sector at the sacrifice of the other directions, we can hope for a reasonably frequent occurrence of satisfactory observation conditions.

The wind often follows a rather common sequence. Usually there is a calm at sunrise, after which the wind springs up and strengthens until late afternoon. Toward sunset it dies away and either remains light and variable during the night or rises again 2 or 3 hours after sunset and continues to blow until dawn. This pattern offers the possibility, partly realized during the November cruise, of securing wave records tracing the history of waves produced by a single wind.

The tidal range in Round Bay is about a foot and the currents are correspondingly weak. No noticeable difficulty was encountered from wind setup in either July or November.

As may be seen from figure 1.1, Round Bay is well protected from shipping interference. There is no commercial traffic. The main

shipping lane lies about 2 nautical miles beyond the right-hand margin of the figure, and the Severn River is so crooked that waves from ships in the main part of Chesapeake Bay are almost certain to go ashore before reaching Round Bay.

Pleasure boats are a different problem and here the situation is not so happy. There are a great many based on Round Bay, and they are so active on week ends that it is virtually impossible to make any records except from 0000 to 0600. During the working week they are only a nuisance. At first, many of them laid alongside to ask the meaning of the signal we were flying (Answering Pennant, H, D: "I am engaged in submarine survey work. Stay clear."). An explanation and an invitation, during calms, to come aboard and inspect the gear soon brought a large measure of cooperation and the situation became tolerable.

The fetches are quite clearly defined for a natural environment. Figures 1.3 and 1.4 show them as they appeared for the July and November cruises. The sector of usable wind has been broken into smaller sectors, and a single fetch distance has been estimated for each in table 1.1 and figures 1.3 and 1.4.

Figures AI 1.01 to AI 1.15 and AI 2.01 to AI 2.06* show the depth profiles along the midlines of each subsector from probe position to windward shore. In most cases it is obvious that there will be no interference with the waves. In a few cases there are areas of shoal water toward the windward end of the subsector, particularly for subsectors passing over the bars extending from Eaglenest Point and Long Point (figure 1.2). The depths over the Long Point bar are very

*Figure and table numbers preceded by AI, AII, AIII, or AIV will be found in the appendix with the corresponding number.

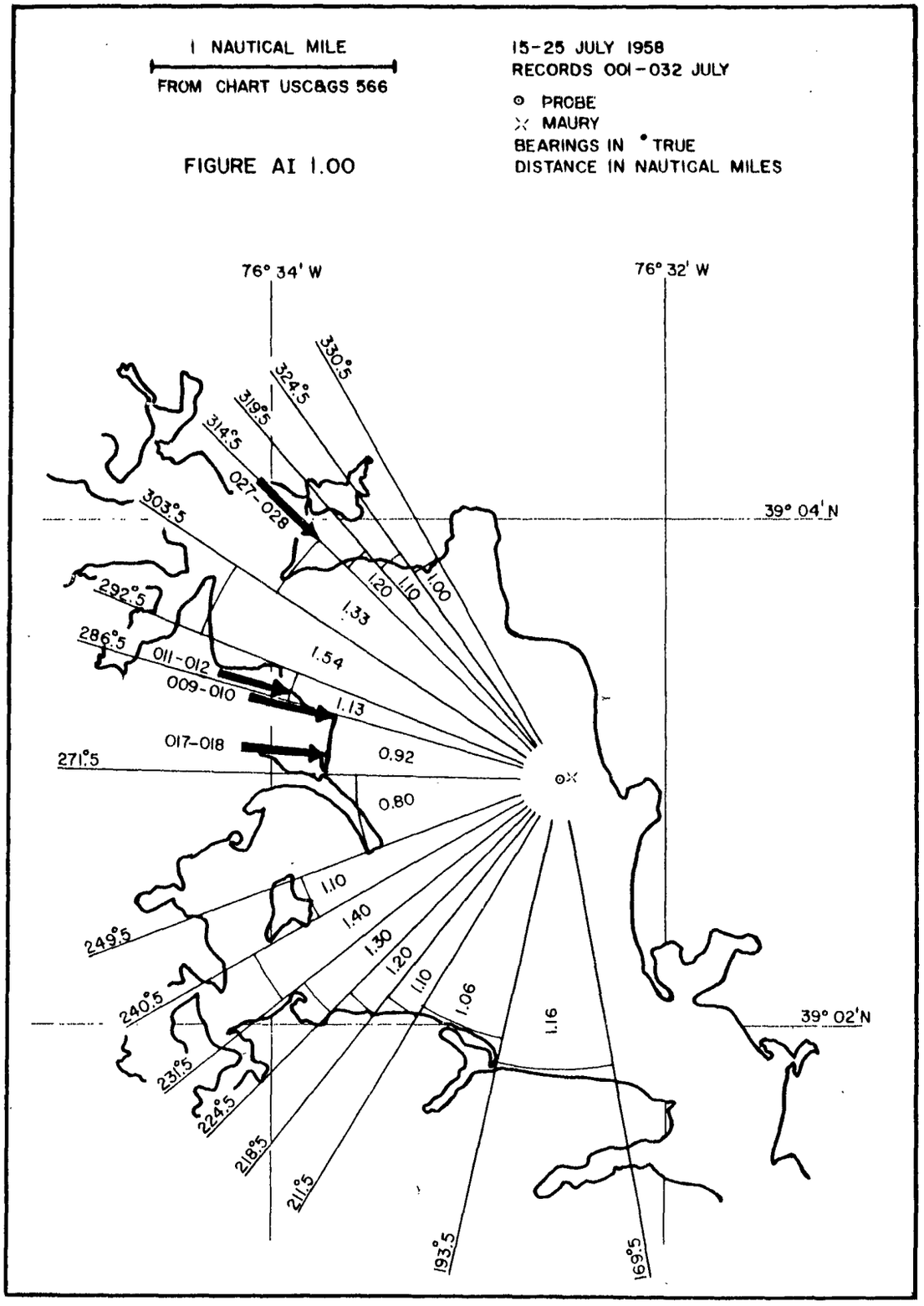

Figure 1.3 Wind Direction Sectors and Fetch Distances for the Probe Position During July

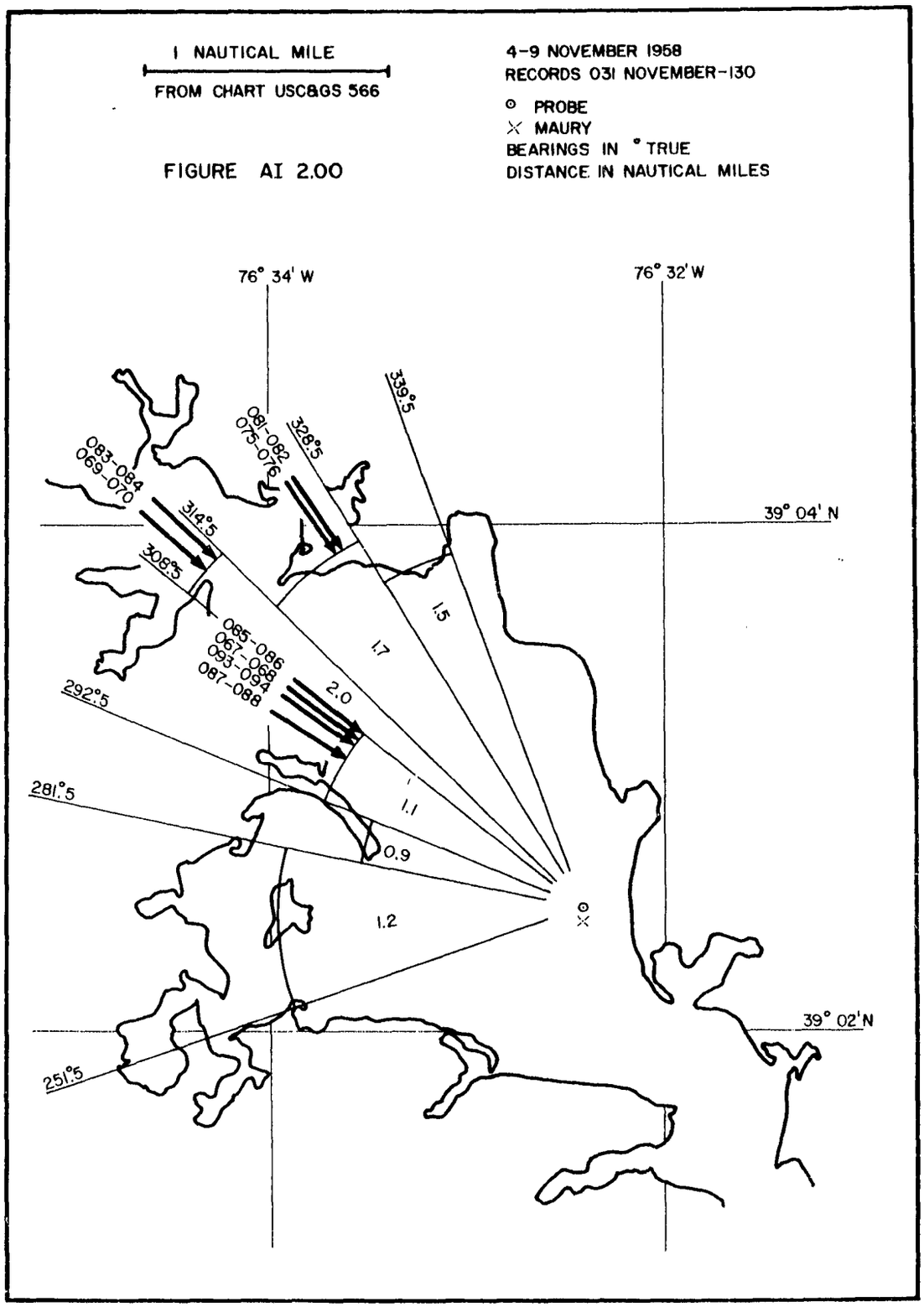

Figure 1.4 Wind Direction Sectors and Fetch Distances for the Probe Position During November

Table 1.1 Wind Sector Limits and Fetch Distances

July						November					
Sector			Fetch			Sector			Fetch		
From (°T)	To (°T)	Midline (°T)	(NM)	(ft)	(m)	From (°T)	To (°T)	Midline (°T)	(NM)	(ft)	(m)
170	193	181.5	1.16	7060	2152	252	281	266.5	1.2	7300	2225
194	211	202.5	1.06	6450	1966	282	292	287.0	0.9	5480	1670
212	218	215.0	1.10	6690	2039	293	309	301.0	1.1	6690	2039
219	224	221.5	1.20	7300	2225	310	314	312.0	2.0	12170	3709
225	231	228.0	1.30	7910	2411	315	328	321.5	1.7	10340	3152
232	240	236.0	1.40	8520	2597	329	339	334.0	1.5	9130	2783
241	249	245.0	1.10	6690	2039						
250	271	260.5	0.80	4870	1484						
272	286	279.0	0.92	5600	1707						
287	292	289.5	1.13	6880	2097						
293	303	298.0	1.54	9370	2856						
304	314	309.0	1.33	8090	2466						
315	319	317.0	1.20	7300	2225						
320	324	322.0	1.10	6690	2039						
325	330	327.5	1.00	6090	1856						

shallow, but they are relatively near the upwind end of the sector. Those over the Eaglenest Point bar are farther downwind but are 10 feet at their shallowest. It is thought that in neither case will waves generated by winds from those directions have grown to such a size by the time they reach the shoal areas that they will be much affected.

Applying the criterion for deep water $h/L > 1/2$, we find the values for period and frequency shown in table 1.2. Since light winds at fetches

Table 1.2 Limits on Frequencies, Lengths, and Periods of Waves Which May Be Considered To Be in Deep Water at the Probe Position

	July	November
Depth at wave probe (ft)	22	18
Length less than (ft)	44	36
Periods less than (sec)	2.93	2.65
Frequencies greater than (cps)	0.34	0.38

up to 2 nautical miles will probably not generate waves with periods and lengths which attain the maximum values, Round Bay meets the depth requirements satisfactorily.

Round Bay has other advantages as a work area. It is reasonably protected during squalls, and the holding ground is satisfactory. Its geographical location admits of ready access to both the Field Laboratory at Annapolis (figure 1.1) and the Chesapeake Bay Institute facilities in Baltimore. This convenience in getting replacement parts and using test facilities was particularly invaluable during July's preliminary work. Also, onshore recreation was available for the crew during unsatisfactory weather.

2.0 THE INSTRUMENTS

2.1 The Support Tower

The problem of mounting a probe for measuring small waves is a rather serious one. The spar and damping-disc system, cf. Upham (1955), often used in the open ocean is unsuitable. The errors introduced by the motions of the spar, negligible in measuring large waves, are not negligible for small ones. Since for small waves the work can be done in shallow water, a driven piling would answer if the permanent position selected were entirely suitable. Ideally, work should be possible at different places within an area and in different areas. An extended pile-driving program would soon become inordinately expensive, especially as in most cases the piles would have to be removed again at the conclusion of the work. Any solution to the problem must combine a large measure of the driven pile's rigidity with a reasonable degree of portability.

Our solution to the problem consists of a vertical column of 3-inch galvanized iron pipe bolted to a triangular base of 2-inch angle iron and 5 feet on each side (figures 2.1c, 2.2a, and AI 3.01*). The vertical column is made of 6-foot sections. The bottom section is threaded and screwed into a number 3 flange which is held by four 3/4-inch bolts welded to the base. To the upper end of the bottom section is welded a 12-inch length of 3-1/2-inch pipe which fits snugly over the 3-inch pipe for 2 inches. The next section slides into the remaining 10 inches and

*A complete set of diagrams of the support tower is included in appendix I.

Figure 2.1 Assembling the Instrument Support Tower

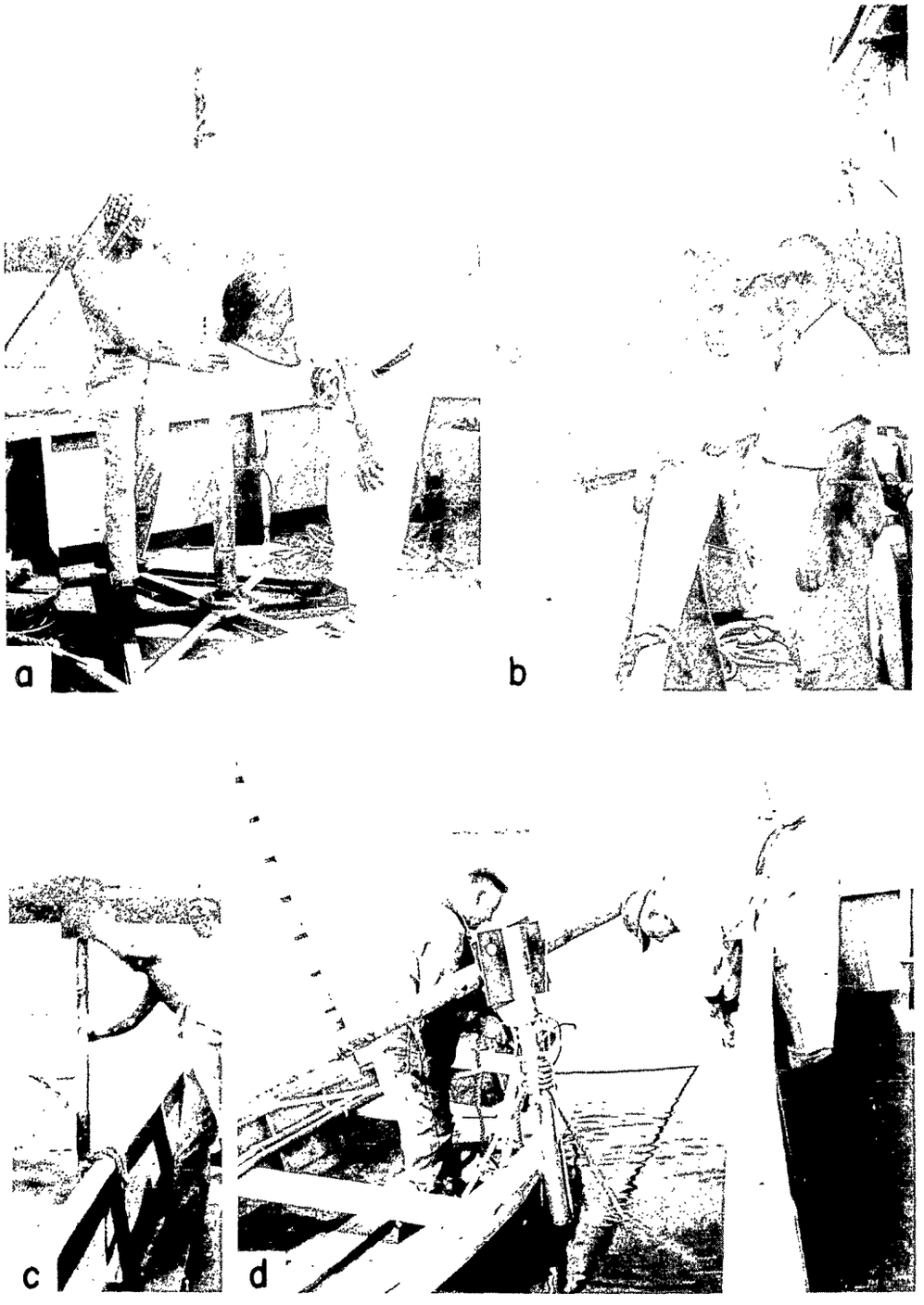

Figure 2.2 Other Phases of Installing the Instrument Support Tower

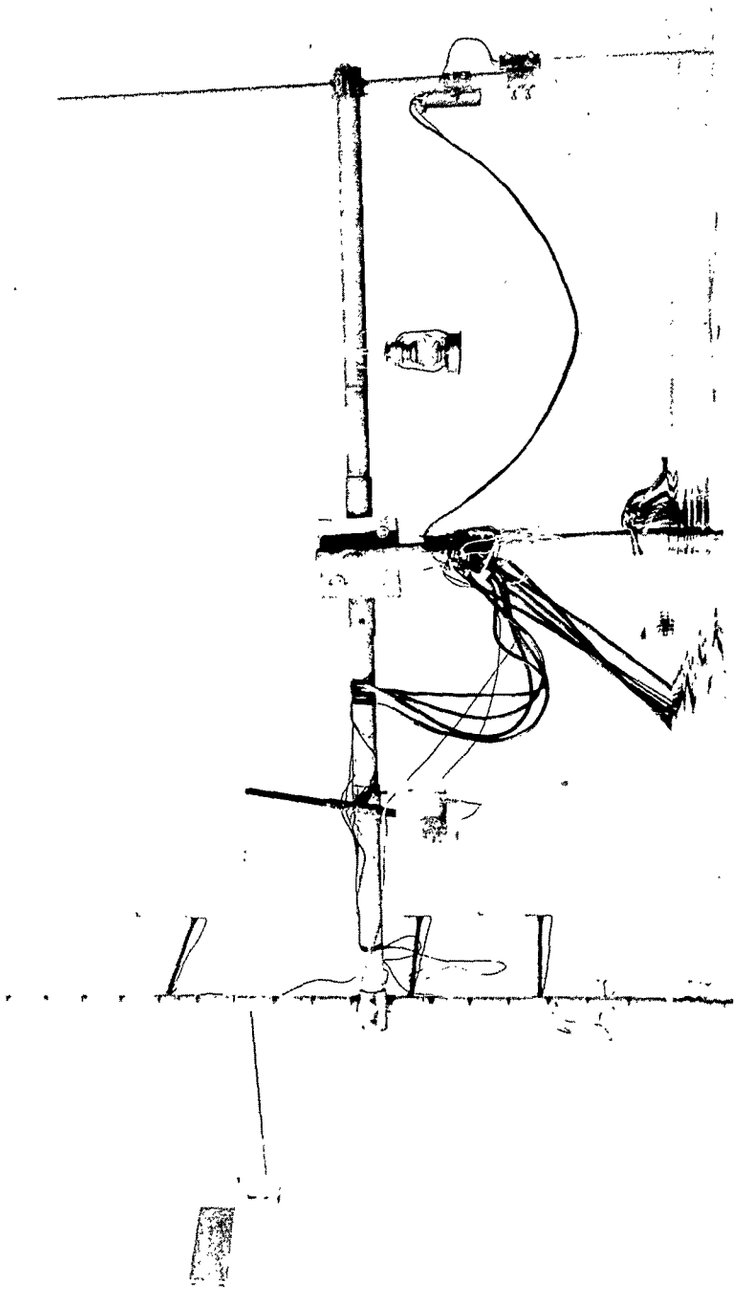

Figure 2.3 The Support Tower with the Probes in Position

The anemometer mast is a 9-foot length of 2-3/8-inch-o.d. aluminum pipe. Arms made of steel tubing are secured to it with hose clamps. The anemometers are held at a distance of 2 feet from the mast, the wind vane at 3 feet (figures 2.3 and AI 3.10). Vertical lines were painted on the anemometer mast and on the sleeve of the cross-arm clamp. These can mark a given radial setting when it is necessary to move the mast up or down.

The cross-arm clamp for the camera mount is similar to the other cross-arm clamps. The camera-mount arm of 1-15/16-inch-o.d. pipe slides through the 12-inch clamp sleeve and is held by a single set screw. At the end is a 3-1/4-inch by 6-inch sheet iron plate which is set at 45° to the arm. The camera is held to the plate by a strap and bolt arrangement (figures 2.1d, 2.3, AI 3.11, AI 3.12, and AI 3.13).

Handling the support tower has proved to be quite simple; it should be usable in depths of 50 feet or more as long as no very strong currents are present. The unassembled parts are carried on the afterdeck of the MAURY (figure 2.1a). When the MAURY has arrived at the probe position and has been anchored bow and stern to prevent her swinging, the bottom section is bolted to the triangular base (figure 2.2a); the first middle section can also be added at this time. A rolling hitch on the bottom section just below the welded sleeve provides a bight for the bill-hook from the MAURY's winch cable. The base and the first two sections are then swayed over the rail (figure 2.1c) and lowered until the top sleeve is at a convenient working height for the next section to be slipped in place and bolted (figure 2.2b). The support tower is lowered and more sections added until the upper end of the top section will extend 3 to 6 feet above the water. This last section carries a friction plate (figure 2.2c). As the tower increases in height during this operation there is only a small tendency to capsize; a man using one hand can keep

the tower upright, or a bight of light line loosely tied to the ship's rail will serve as well.

When the vertical column has been completed, the winch is let go with a run for the last foot to embed the base in the bottom; the tower must be oriented so that the wave probe will have an unobstructed "view" of the working sector. The two parts of the cross arm are now bolted together, the cross arm is bolted to the vertical column, and the bolts for the friction plates are inserted loosely. No care is taken at this time to get the cross arm horizontal; usually it must be cockbilled to clear the MAURY's rail. The cross-arm clamps are put on the cross arm and roughly positioned, and the masts are slid into their sleeves. Four anchors are carried out about 150 feet by skiff. The rodes are first brought back to the MAURY's afterdeck, where four or five men set the anchors firmly, and then tied to the tower. There is now no danger of the tower's toppling over. To locate the wave probe, sextant bearings are taken at the wave probe mast, which is inboard at this time, on identifiable marks showed on the chart (figure 2. 1b). The bill-hook of the windlass cable is then shaken free, and the MAURY slides from under the anchor rodes to take her station 300 feet to leeward of the sector of usable wind. Normally, the MAURY sets four anchors and determines her own position by sextant bearings.

The final adjustments are now made from a skiff (figures 2. 1d and 2. 2d). The anchor rodes are released one by one, tightened, and tied as low on the vertical column as possible. The cross arm is leveled with a spirit level and the friction plates are bolted together. The masts are then set vertically with the spirit level and the cross arms clamped. The plate of the camera mount is leveled horizontally. The entire tower installation can be completed in 1 to 1-1/2 hours. Figure 2.3 shows the tower with the probes in place.

When it becomes necessary to move the tower, it may be retrieved even more easily than it is set. Originally plans called for a SCUBA diver to attach the winch cable billhook to the lifting bight. Although the divers remedied some of the inevitable blunders occurring as assembly techniques were invented, they were not essential to the dismantling process. After the tower has been stripped of its probes, the MAURY eases alongside and the four anchor rodes are slackened. The tower anchors can hold the MAURY with proper attention to wind direction. The cross arm and masts are dismantled. A rolling hitch is thrown around the top vertical section; the billhook of the winch cable is inserted in this and a strain is taken. The anchor rodes are then transferred from the tower to the MAURY. The winch lifts the tower until the sleeve joining the top section to the adjacent middle section is just above the rail. The middle section is lashed to the rail, the lashing taking the full weight of the tower when the winch cable is removed. The top section is then unbolted and stowed, and the billhook is inserted in a new rolling hitch on the middle section below its lashing. The winch takes a strain on the hitch again and the lashing is cast off. The hoisting, lashing, and dismantling sequence is repeated until the original rolling hitch used in the lowering phase can be reached; then the remaining section and base are hoisted aboard. Finally, the anchors are retrieved from the skiff. The entire operation takes about three-quarters of an hour.

As a reasonably portable rig with a high degree of rigidity the support tower has proved quite satisfactory. Experience with it has not extended to deeper water, but no difficulties were encountered that would suggest that it could not be used in considerable depths. Some minor changes have been suggested during its use. There is no need to have two top sections; one 6-foot top section and a 3-foot middle section would be enough, since middle sections are easier to make. Also,

the cleat and ringbolt arrangement on the top section might well be omitted. The original intention was to use three anchors, pass the anchor rodes through the ringbolts, and secure them to the cleats. After a 3-hour interlude with the tower on its side in the mud, four anchors seemed advisable, and tying the anchor rodes directly to the vertical column proved simpler and better. The cleats and ringbolts were used as lashing points for probe cables, but they are unnecessary even for that. The fact that the anemometer mast is made of pipe and the wave-probe mast of tubing is an accident occurring because most of the tower was built from scrap. During the July cruise we discovered the steel probe mast was too heavy for easy adjustment so we replaced it in November with an aluminum tube. Although it was thin-walled, it was satisfactorily rigid and light, but care was necessary to avoid denting it with the set screws. Preferably, the clamps and fittings should take pipe throughout. Each component of the support tower is small enough for one man to handle it, although the work goes more rapidly with two men on the larger sections. However, taken as a whole, such a tower made mostly of galvanized iron pipe is heavy and cannot be handled without a good winch. Information has been received (personal communication from Mr. Joseph Pandolfo) that the Department of Meteorology and Oceanography at New York University has built a support tower similar to the one described here; theirs has a 6-foot-square base and is made of aluminum pipe. He reports that this tower was successfully set and retrieved with tackle rigged on the mizzen gaff using muscle power alone, since no winch was available. Also, the tower stood without guy anchors in a 2-knot current. Even with a winch available, aluminum pipe on a larger base, square rather than triangular, might be an improvement. One operating detail reported by Mr. Pandolfo, unnoticed during our operations with the winch, was the slow draining of water from the vertical pipe as it was being raised. With an adequate

winch this extra weight hardly matters, but when the tower must be raised by hand, drain holes could be drilled in each section.

2.2 The Wave Probe

The device used for measuring water level is essentially the capacitance probe developed by C. G. Whittenbury and B. L. Hicks and described in Hicks and Whittenbury (1956) and Whittenbury (1956). The probe itself is a 5-foot length of 1/2-inch-diameter cold-rolled steel rod spirally wrapped with a slightly overlapped single layer of tape; this plastic tape is 0.005 inch thick and 1 inch wide, and has a pressure-sensitive vinyl adhesive on one side. The tape was provided by the Enflo Corporation, Pennsauken, New Jersey, and has a dielectric constant between 2.2 and 2.3. The steel rod and the surrounding water form the plates of a variable capacitor. The circuit in which the probe is placed is designed to sense the varying capacitance as the water rises and falls on the probe and to translate it into a fluctuating voltage. The circuit is substantially linear in the range from 300 $\mu\mu$fd to 1000 $\mu\mu$fd, corresponding to an output voltage ranging from 50 to 150 volts (figure 2.4). So the part of the probe which must always remain immersed to give at least 300 $\mu\mu$fd will not be too long, the bottom 18 inches of the rod are wound with six layers of the tape. The topmost 6 inches of the rod are wrapped with electrical tape so that the probe clamp will grip it securely.

With a rod diameter of 1/2 inch it is probably safe to consider that the smallest waves visible to the probe will have a length of four times 1/2 inch or about 5 cm. Since our interest is in gravity waves and not in capillaries, the 1/2-inch diameter seems satisfactory. One advantage of using so heavy a rod is that it is rigid enough to be clamped at one end only, thus reducing interference from the probe mount.

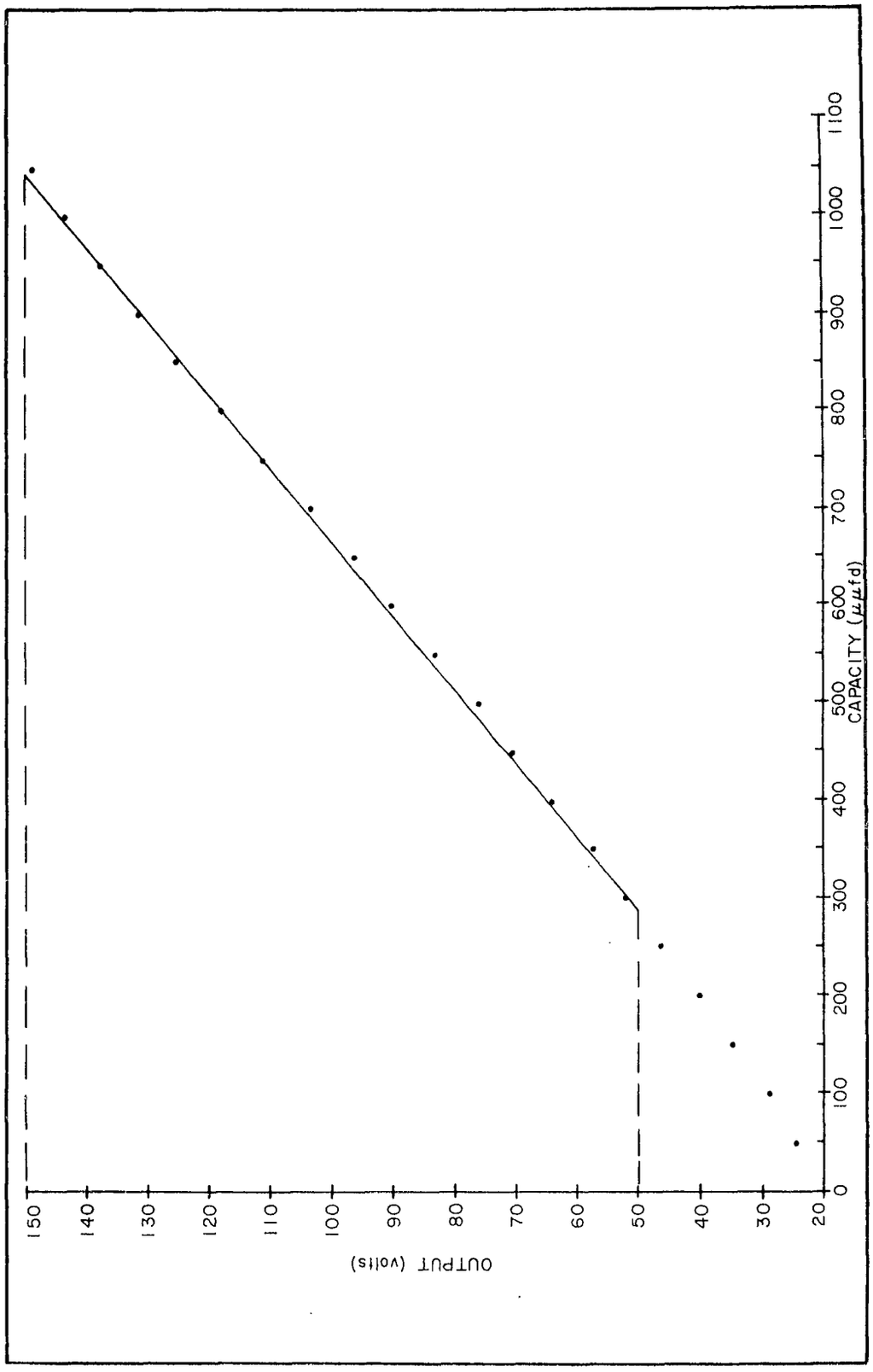

Figure 2.4 Circuit Linearity

Ideally, the dielectric coating of the wave probe should be applied evenly. This was originally thought to be a very critical matter, and much time was spent devising ingenious methods of obtaining uniformity. As it turned out, the evenness is not particularly critical. Reasonable care and quite crude methods will produce a satisfactory probe. One man holds the rod firmly and rotates it, while another applies the spiral winding of tape, adjusting it by eye; two men can apply one layer of tape to a 7-foot rod in less than half an hour.

The modifications of the electronics were made by Dr. Willis C. Gore, Associate Professor of Electrical Engineering, The Johns Hopkins University, who describes the instrument as follows:

"In operation, the function of these electronic devices (table 2.1, figures 2.5, 2.6, 2.7) is to give an output voltage which is proportional to the depth of immersion of the wave probe. In order to accomplish this, vacuum tube V_1 (table 2.1 and figure 2.5) is connected as a blocking oscillator which generates short pulses of voltage as shown in figures 2.8a and 2.9a. The time between these pulses, T_0, is determined by the product of the resistance and capacitance in its grid circuit, and $T_0 = KRC$. The capacitance C includes the capacitance of the wave probe which is a linear function of its immersion depth, L, ($C = aL + b$); therefore, $T_0 = K_1 + K_2$ or T_0 is proportional to L. The variable 5-M resistor is used to set the range of operation as it affects K_1 and K_2. The other half of V_1 is connected as a cathode follower to isolate the oscillator from the connecting cable to prevent unwanted loading effects.

"These pulses are amplified by the first half of V_2 and coupled by the diode buffer gate V_9 to the bi-stable flip-flop, V_3 (figure 2.6). The output of V_3 is a rectangular wave as shown in figures 2.8b and 2.9b which switches level with each incoming pulse. The output of V_3 is coupled through a cathode follower (the second half of V_2) to the Miller

Table 2.1 Parts List for the Blocking Oscillator, the Converter, and the Power Supply

R_1	5 M	R_{17}	330 K	R_{33}	25 K	C_1	Probe	V_1	12AT7	T_1	UTC H 49
R_2	5 M	R_{18}	22 K, 2 W	R_{34}	33 K, 2 W	C_2	0.01 μfd	V_2	12AT7	T_2	Stancor P6134
R_3	5.6 K	R_{19}	18 K, 2 W	R_{35}	10 K	C_3	0.03 μfd	V_3	12AT7		
R_4	1 K	R_{20}	27 K, 2 W	R_{36}	15 K, 1 W	C_4	0.1 μfd	V_4	6AL5	T_3	Merit P3152
R_5	1 K	R_{21}	12 K, 1 W	R_{37}	25Ω, 25 W; IRC	C_5	0.1 μfd	V_5	6AS6		
R_6	1 K	R_{22}	220 K	R_{38}	5.6 K, 10%	C_6	10 $\mu\mu$fd	V_6	12AU7		
R_7	100 K	R_{23}	330 K	R_{39}	5.6 K, 10%	C_7	100 $\mu\mu$fd	V_7	6AL5	S_1	DPDT
R_8	39 K	R_{24}	330 K	R_{40}	5.6 K, 10%	C_8	25 $\mu\mu$fd	V_8	6AK5	S_2	DPST
R_9	10 K	R_{25}	5.1 M	R_{41}	5.6 K, 10%	C_9	100 $\mu\mu$fd	V_9	6AL5		
R_{10}	330 K	R_{26}	150 K	R_{42}	470 K, 10%	C_{10}	750 $\mu\mu$fd	V_{10}	6X4	L_1	20 HY; 50 ma
R_{11}	220 K	R_{27}	330 K	R_{43}	91 K, 5%	C_{11}	0.1 μfd	V_{11}	5Y3GT		
R_{12}	10 K	R_{28}	5.6 K, 2 W	R_{44}	180 K, 10%	C_{12}	0.01 μfd	V_{12}	OD3	M_1	Weston voltmeter model 301; 0-150 v, 1000Ω/v
R_{13}	330 K	R_{29}	12 K	R_{45}	50 K, AB CLU 5031	C_{13}	8 mfd, 600 v	V_{13}	6AQ5		
R_{14}	39 K	R_{30}	39 K, 4 W			C_{14}	30 mfd, 450 v	V_{14}	12AX7		
R_{15}	60 K	R_{31}	4 M, 1%	R_{46}	68 K, 10%	C_{15}	30 mfd, 450 v	V_{15}	5651		
R_{16}	220 K	R_{32}	3.3 K	R_{47}	100 K, 10%					F_1	3 a, 250 v

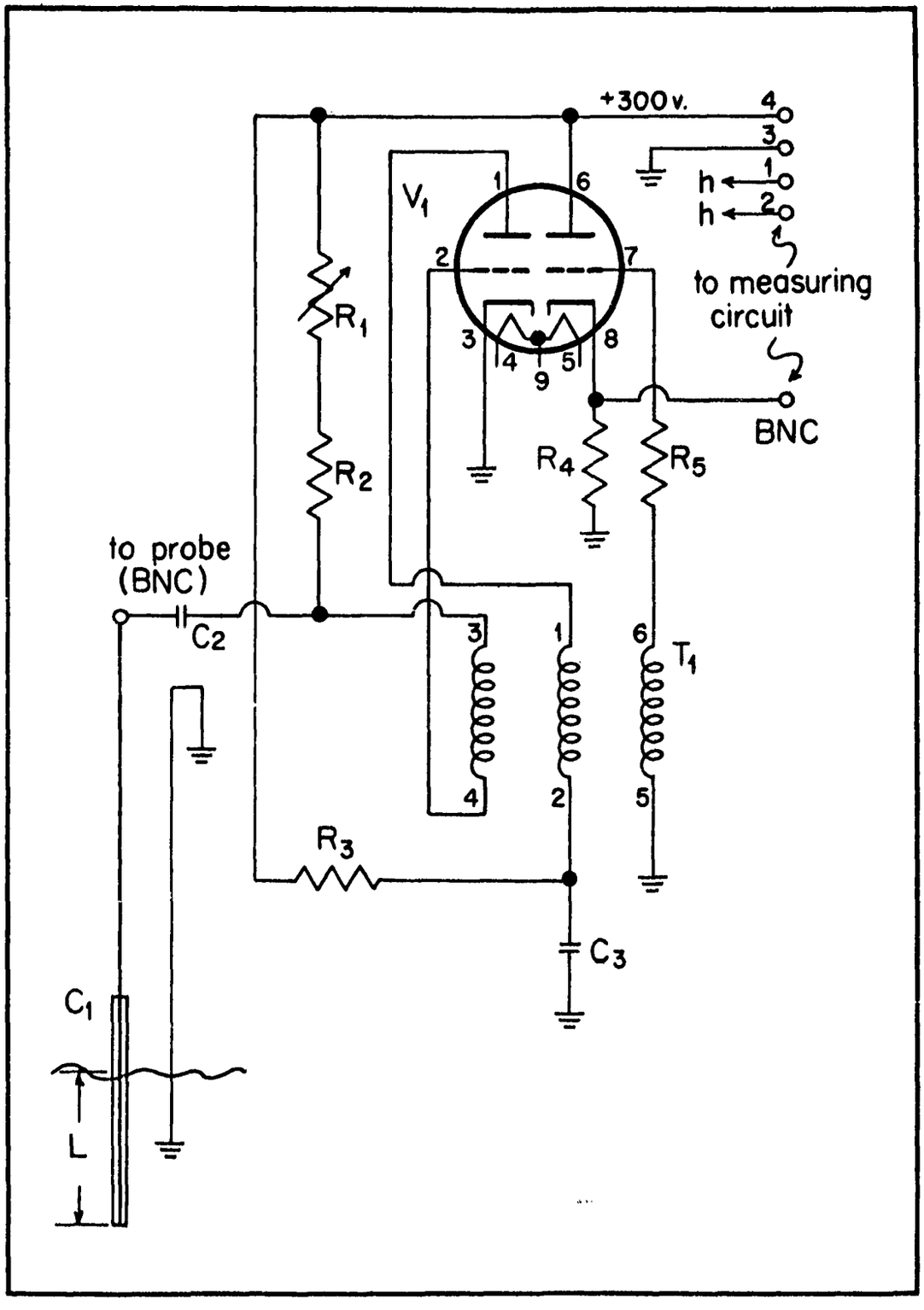

Figure 2.5 Circuit Diagram of the Blocking Oscillator at the Wave Probe

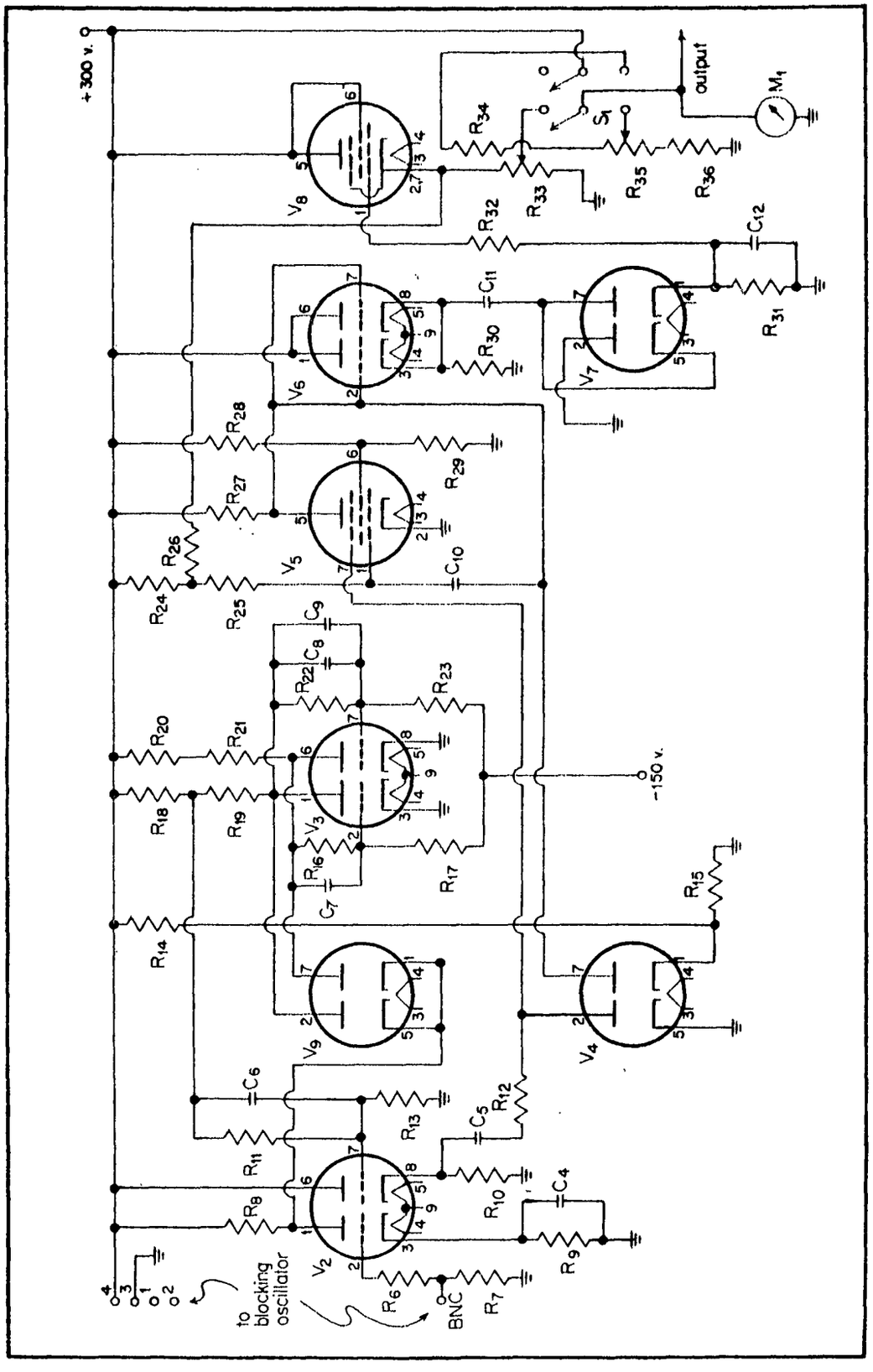

Figure 2.6 Circuit Diagram of the Converter

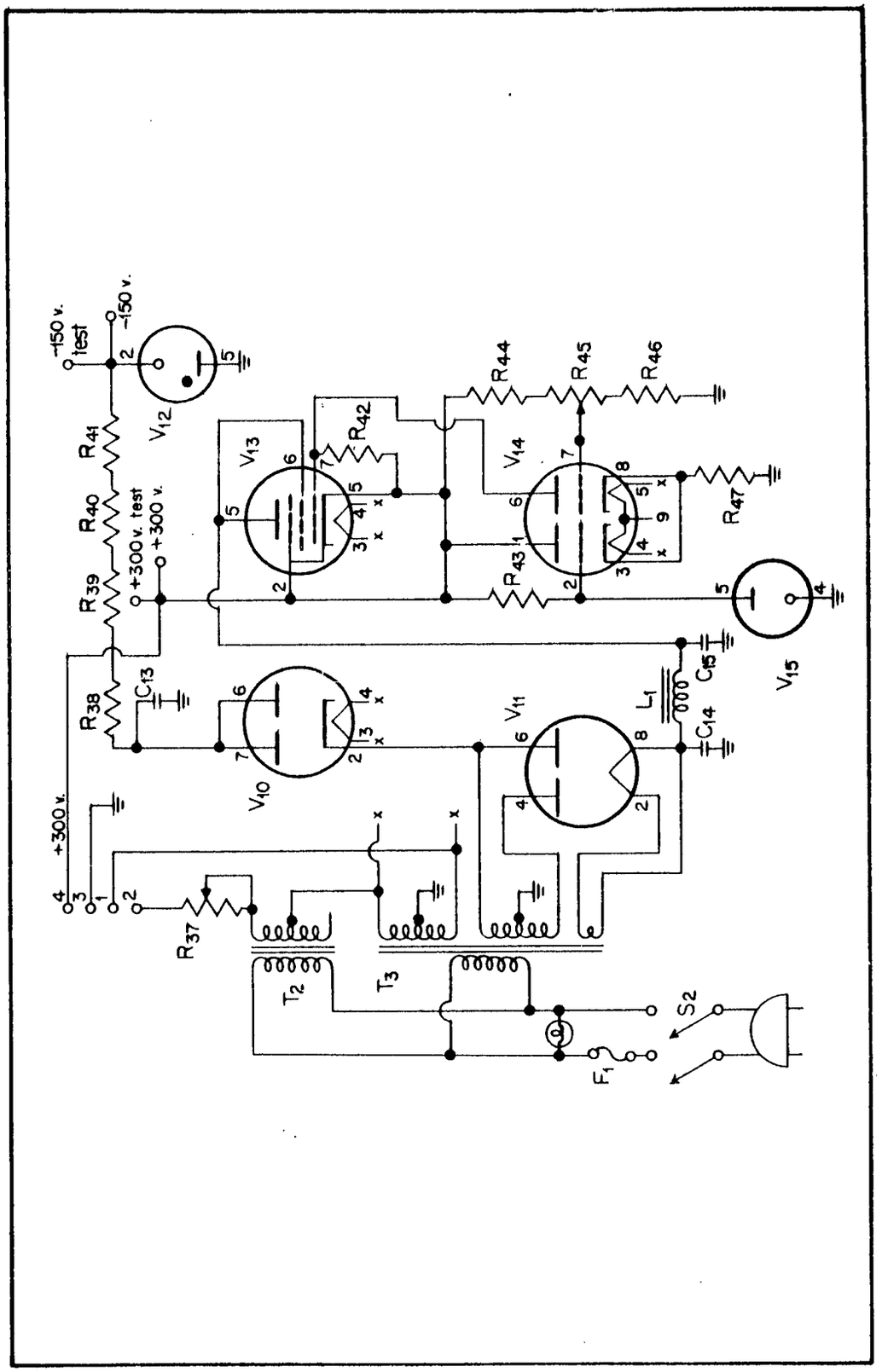

Figure 2.7 Circuit Diagram of the Power Supply for the Wave Probe

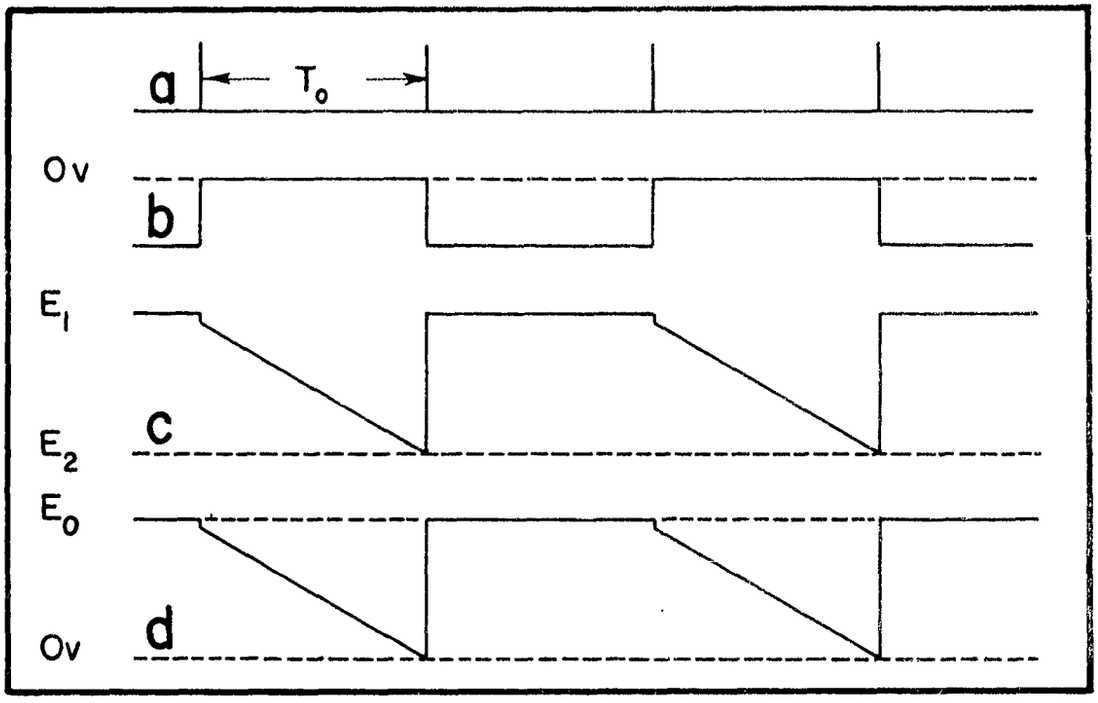

Figure 2.8 Schematic Representation of the Processing of a Pulse with an Interval T_0 by the Wave Probe

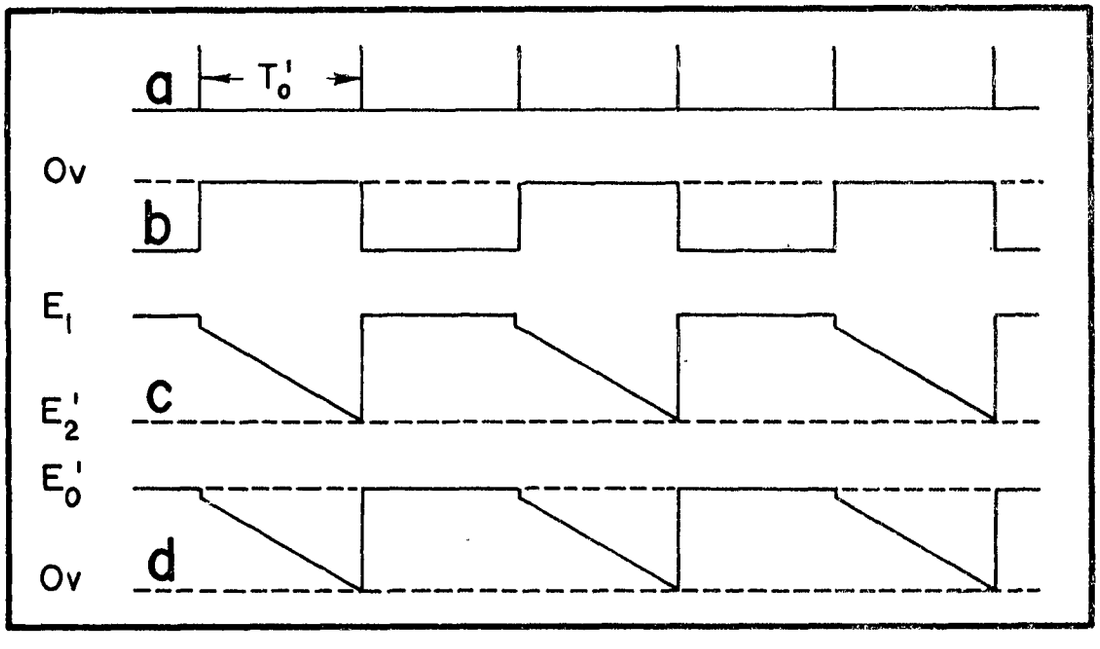

Figure 2.9 Schematic Representation of the Processing of a Pulse with an Interval T_0' by the Wave Probe

integrator circuit V_5. The first half of diode V_5 clamps the most positive going part of the output wave form at 0 volts.

"With the application of this positive going wave form the Miller integrator (V_5) is turned on; its plate voltage starts decreasing linearly with time as shown in figures 2.8c and 2.9c. The voltage at the start of this wave form, E_1, is maintained by the clamping action of the second half of V_4. When the positive going input to V_5 stops, the output voltage returns to its original voltage. The voltage E_2 is determined by the time the Miller integrator is left on, which is the time T_0. Figures 2.8 and 2.9 show similar wave forms for different values of T_0. In particular, one notes that $(E_1 - E_2)$ is proportional to $T_0 = K_1L + K_2$. Therefore, $E_1 - E_2 = M(K_1L + K_2)$.

"The output of V_5 is coupled through the double cathode follower, V_6, to the peak-to-peak reading voltmeter V_7. The first half of V_7 clamps the most negative going part of the output at 0 volts, as shown in figures 2.8d and 2.9d, while the second half of V_7 detects the most positive going part E_0. Since $E_0 = E_1 - E_2 = M(K_1L + K_2)$, we have the fact that E_0 is proportional to the immersion depth of the wave probe, L. This voltage E_0 is coupled through the cathode follower, V_8, to prevent loading by the voltmeter. The connection of a 150-K resistor from the output to the grid circuit of V_5 was done to make the over-all response more linear. This was necessary because of very small effects which have been neglected in this discussion.

"The power supply necessary is +300 volts at 25 milliamperes and -150 volts at 1 milliampere. These voltages are supplied from regulators to prevent calibration changes due to input voltage changes. The rectifier, V_9, (figure 2.7) supplies the +300 volts which are regulated by the amplifier-regulator V_{12} and V_{10}. The reference voltage

is supplied by V_{11}. The negative supply comes from the rectifier V_{13} and is regulated by the reference tube V_{14}."

For field work, the pulse system has a great advantage. Very long leads can be used so that one can keep out of the way of the probe. Attenuation in the leads is no problem since it is only the frequency of the pulse that needs to be measured, not the power of the signal.

Since the circuit is linear over the range from 50 to 150 volts, as a safety factor only the range from 60 to 140 volts was used. Shortly before each record was to be made, two men went out to the support tower in a skiff. On a hand signal from the MAURY the probe was raised or lowered until the voltage was fluctuating around 100 volts. The signal was recorded on a 6-channel Brush Instruments oscillograph model BL 266 using electric writing. The associated Brush DC amplifier model BL 536 offers sensitivities which make full scale correspond to 90 to 110 volts at 0.5 volt/line, 80 to 120 volts at 1 volt/line, or 60 to 140 volts at 2 volts/line. Most of the records included in this report were made at 1 volt/line, and none at 0.5 volt/line.

In addition to the six recording channels the oscillograph carries a timer and an event marker. The event marker was used to monitor the chart paper for drift. As delivered, the timer made pips in the left-hand chart margin at 1-second intervals. This was modified by replacing the cam that actuated the microswitch with a 10-toothed chain sprocket wheel whose teeth had been turned down to a suitable size. With this the time pips are entered every 0.1 second. Several runs timed by stop watch and inspected for evenness showed that the division secured was at least as good as it would be using the nominal chart speed and mechanically dividing the record. In some records a slight binding in the chart drive momentarily slowed the paper. The increased density of the timing

pips revealed this situation, and their presence made it possible to salvage the records.

Calibration of the wave probe proved to be rather difficult. A number of efforts made in the laboratory showed that the instrument had a very slow drift of a volt or two over periods of a couple of hours and that a continuous soaking of 7 weeks made no appreciable change in its characteristics, but they also showed that the relation between water height and voltage depended strongly on the geometry of the ground path. In the field the support tower provides the ground. It was not desirable to use a calibration made in the laboratory and extrapolated to the field configuration through a rather involved theoretical development containing several questionable links. For this reason a cylindrical tank 8 feet in diameter and 8 feet deep was constructed and filled with water whose conductivity was adjusted to approximately that of the field situation. The tank was big enough so that sections of the tower could be mounted in it for a ground and the probe could be suspended at the same distance from the ground as in field use. The tank was roofed to keep out dirt and screened from the wind (figure 2.10). It was in this tank that the static calibrations were made and the dynamic response explored.

For the static calibration the probe was suspended on 3/32-inch hydrographic wire with an insulator just above the probe (figure 2.11a). The wire passed over a 6-inch sheave and was led down over a second sheave alongside a meter stick. Stops were placed on the meter stick so that the instrument would not read less than 50 nor more than 150 volts (figure 2.11b). A small cylinder clamped to the wire between the stops served as an index to read against the meter stick. The voltmeter used was a Weston DC model 430, serial no. 27893 (E21-313) with 0-to-300- and 0-to-150-volt scales.

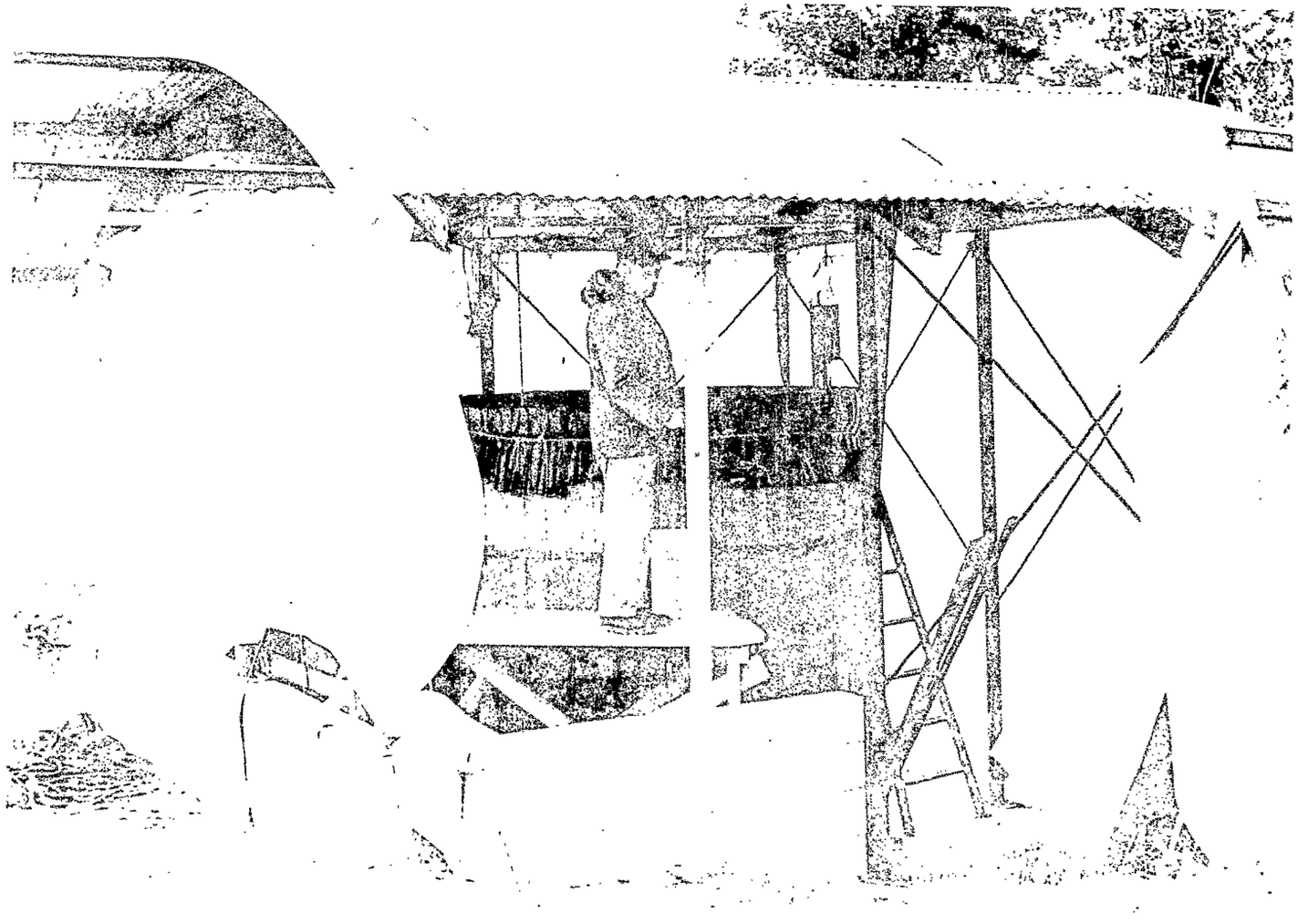

Figure 2.10 General View of the Calibration Apparatus

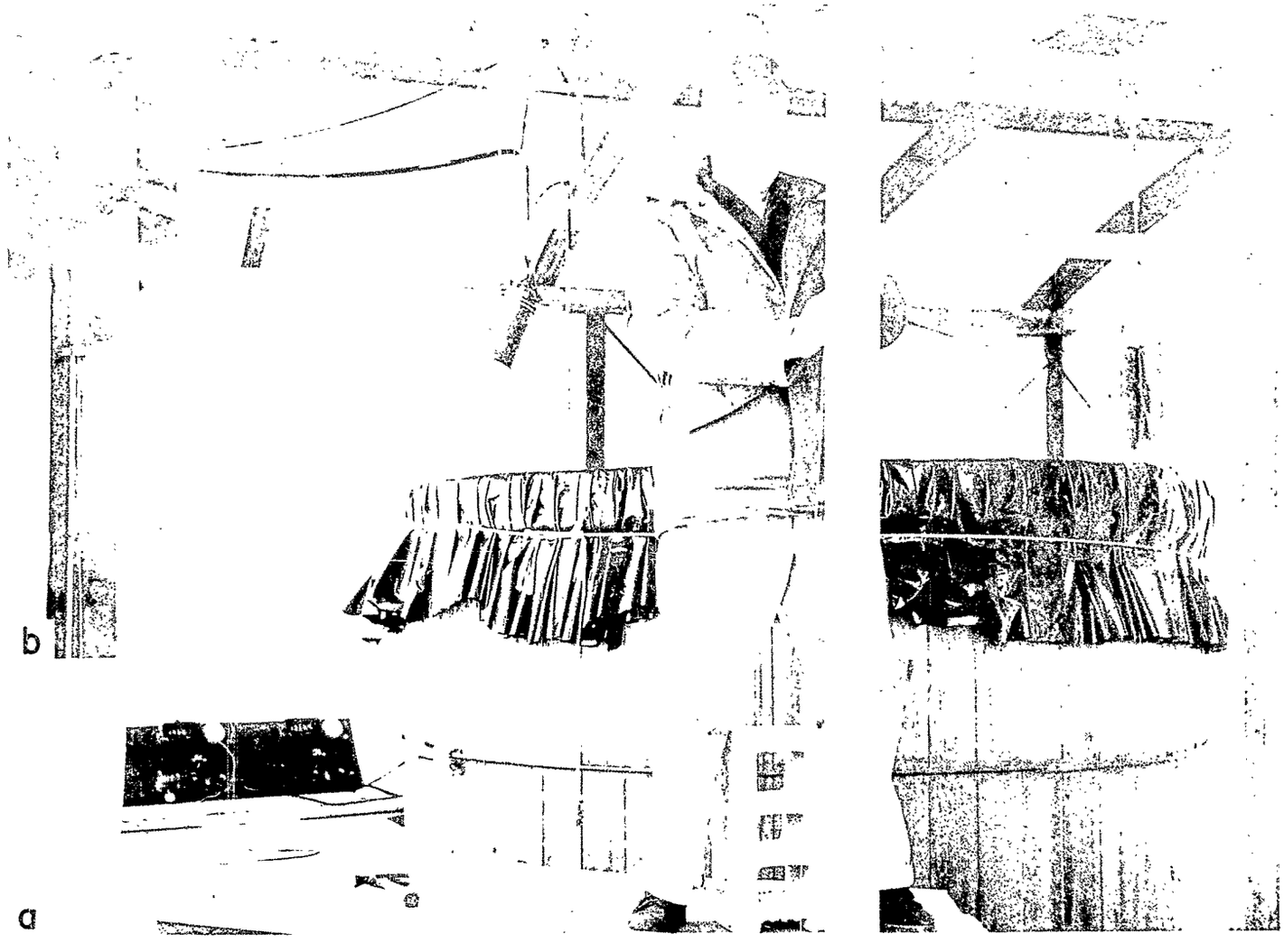

Figure 2.11 Close View of the Calibration Apparatus

The probe was withdrawn from the water from 90 cm to 50 cm on the meter stick by 5-cm intervals and then lowered again by 5-cm intervals. The position of the probe could be repeated to less than 0.25 mm. The cycle was repeated 25 times and took 2 hours and 10 minutes to complete. At each position the voltage was read to the nearest 0.1 volt. The values obtained are given in table AI 1.1.

Since previous work had indicated that the probe was sufficiently sensitive to detect whether the meniscus was bent up or down, the 50 values at each level were separated into two sets, one in which the water rose (the probe immersed) to reach the level, and one in which the water fell (the probe withdrew). Because the length of time required to make the measurements was roughly that of the long-period instrument drift, the secular trend was compensated by averaging the first two readings at each level and the last two readings at each level. The time drift was considered to be linear, and the intermediate values were adjusted as though they were evenly spaced. The mean values and the standard deviations for each level are showed in table 2.2. The differences between the means rising and falling have an average value of 0.69 volt with a standard deviation of 0.08 volt. (The calibration value of 2.20 volts/cm, which we shall discuss later, makes this difference due to meniscus between rising and falling water about 0.3 cm, which seems reasonable from casual observation.)

The means of the rising and falling sets have been plotted in figure 2.12. Each point has 25 measures. The average standard deviation is 0.362 volt and the standard deviation of the standard deviations is 0.055 volt. It can be seen that these points are not strictly linear; there is a slight bow downward in each line which is most strongly marked at the ends.

Table 2.2 Mean Values of the Voltage Corresponding to the Several Levels of Probe Immersion Used in the Static Calibration

Nominal Level (cm)	Rising		Falling		Difference (volts)
	Mean (volts)	σ (volts)	Mean (volts)	σ (volts)	
50	-	-	55.73	0.318	-
55	67.58	0.287	68.40	0.330	0.82
60	79.48	0.250	80.15	0.214	0.67
65	90.87	0.333	91.50	0.244	0.63
70	101.99	0.363	102.70	0.358	0.71
75	112.89	0.282	113.56	0.331	0.67
80	123.52	0.354	124.29	0.380	0.77
85	133.68	0.375	134.24	0.420	0.56
90	142.59	0.378	-	-	-

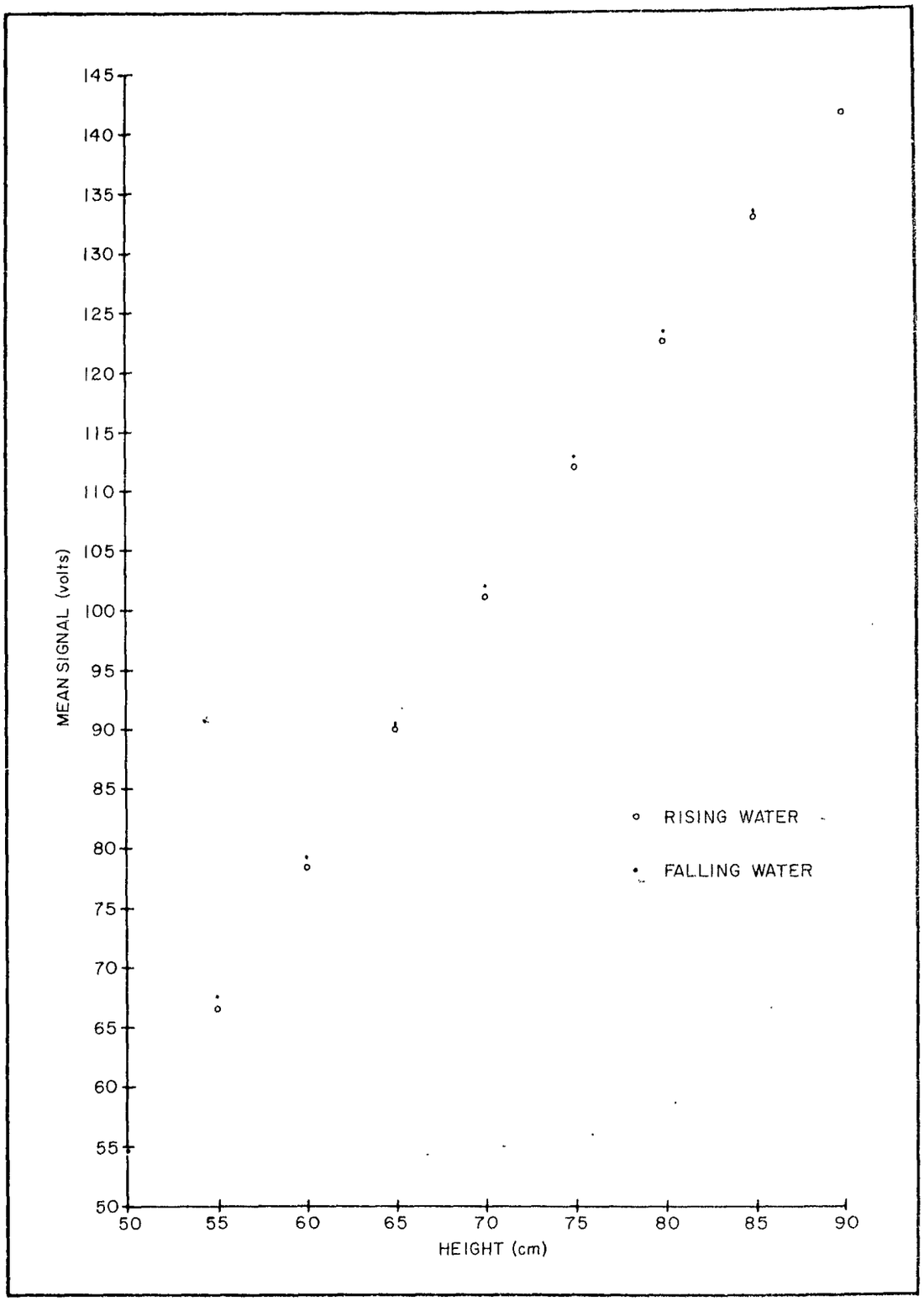

Figure 2.12 Mean Values of the Static Calibration

It is a question, in fitting a calibration curve to these points, whether it is worth while taking into account the slight curvature and the difference between rising and falling water, or whether in view of other errors inherent in the work it may not be just as serviceable to lump rising and falling water together and use a straight line. In addition, the way in which the instrument is used in the field has a bearing on the problem.

In the field before each record is made, the probe is adjusted so that the signal is centered at approximately 100 volts. Each channel on the Brush oscillograph paper is 40 lines wide, and sensitivities of 0.5, 1, and 2 volts/line are available corresponding to ranges of 90 to 110, 80 to 120, and 60 to 140 volts. Thus during operation at 0.5 volt/line only values corresponding to that section of the calibration curve ranging from a nominal 65 cm to 75 cm can appear on the chart. For 1 volt/line the range is 60 to 80 cm, and for 2 volts/line, 55 to 85 cm. Therefore, the end points corresponding to 50 cm and 90 cm should always be omitted from the static calibration, and in any case extreme values are of rare occurrence. It seemed wise to make separate calibration curves for each of the three sensitivities.

Furthermore, two sets of calibration curves were made, a linear set lumping both rising and falling water together, and a quadratic set each of which was actually a pair of curves, one to use when the water was rising and one when the water was falling. The fits were made by the method of least squares and are showed in table 2.3.

In order to test whether the linear calibrations were adequate, two simulated wave records were made at each of the three sensitivities by oscillating the probe manually in what was hoped was a random manner. The method is discussed later. These records were about 2.5 minutes

Table 2.3 Least-Squares Fits to the Means of the Static Calibration Data

	Sensitivity (volts/line)		Regression Equation (x in volts; y in cm)	Standard Error of Estimate (volts)
Linear	0.5		$x = -52.015 + 2.204y$	0.469
	1		$x = -52.212 + 2.204y$	0.509
	2		$x = -52.287 + 2.201y$	0.716
Quadratic	0.5	Falling	$x = -86.702 + 3.205y - 0.0071y^2$	0.315
		Rising	$x = -74.253 + 2.834y - 0.0045y^2$	0.328
	1	Falling	$x = -74.018 + 2.841y - 0.0045y^2$	0.313
		Rising	$x = -76.742 + 2.905y - 0.0050y^2$	0.320
	2	Falling	$x = -81.014 + 3.051y - 0.0061y^2$	0.343
		Rising	$x = -82.321 + 3.065y - 0.0062y^2$	0.326

long. Each record was read at 0. 1-second intervals, twice with the linear calibration and twice with the paired quadratic calibration. The 24 sets of 1500 values that resulted, 8 for each sensitivity, were subjected to all the statistical analyses applied to the field records. Comparisons could then be made between differences in values resulting from repeated readings with the same calibration curve and differences in values which arose from repeated readings with different calibration curves. The results showed that the differences arising from repeated readings with the different calibrations were of substantially the same size as those arising from repeated readings with the same calibration. From this comparison it was concluded that no real improvement was to be expected from using the refined double quadratic calibration and that the linear calibration was sufficient.

To explore the dynamic response of the instrument, one should ideally subject it to a wave motion of a known form. This proved to be impossible, principally because waves of exactly known form are almost impossible to generate on such a scale that the field configuration of the instrument can be maintained. As a compromise it was decided to oscillate the probe in the water. This fails to duplicate the effect of waves in the field in three ways: the probe accelerates past the water rather than water accelerating past the probe under the action of gravity; the water does not have the horizontal and vertical velocities associated with the orbital velocities found in a wave; finally, the probe in the field is always subjected to wind when waves are present, while the tank must be sheltered. This wind tends to break up the sheath of water draining down the probe and, consequently, to decrease the runoff time. The net effect of these differences makes the response of the probe more sluggish in the test tank than it would be in the field; the results obtained in the tank may be considered as an upper limit on the probe response.

To get a separate account of the motion to which the probe was subjected, a potentiometer was attached to the shaft of the 6-inch sheave from which the probe was suspended; the potentiometer was then used as a voltage divider. Its signal was recorded on one channel of the Brush oscillograph while the report of the motion coming from the probe was simultaneously recorded on another. At each of the three sensitivities a 2.5-minute simulated wave record was made which was read at 0.1-second intervals. These records differed from the field records in having a much bigger proportion of large oscillations. Thus the test records are more demanding than those obtained under field conditions.

Correlation and crosscorrelation functions (figures 2.13 to 2.15 and tables AI 2.1.1 to 2.3.1, AI 3.1.1 to 3.3.1, and AI 4.1.1 to 4.3.1), spectra, cospectra, and quadrature spectra (figures 2.16 to 2.18 and tables AI 2.1.2 to 2.3.2, AI 3.1.2 to 3.3.2, and AI 4.1.2 to 4.3.2) were computed for each sensitivity. If the two spectra and the cospectrum were identical while the quadrature spectrum was zero, the instrument would be one in which the probe signal reported exactly the changes in the environment without any lag; such an instrument may be called "perfect." It is clear that the wave probe is not "perfect," although it is worth noting that the spectra and the cospectrum all lie within each other's confidence limits and are in this sense statistically indistinguishable, and that the quadrature spectrum is relatively small. An "ideal" instrument would show the two spectra identical while the phase shift determined from the cospectrum and quadrature spectrum would be constant.

If $f_{xx}(\mu)$ denotes the spectrum of the standard, i.e., our potentiometer, and $f_{yy}(\mu)$ the spectrum of the probe; and $c(\mu)$ and $q(\mu)$ the cospectrum and quadrature spectrum of x with y, we can express a number of functions that are useful in appraising the behavior of the instrument.

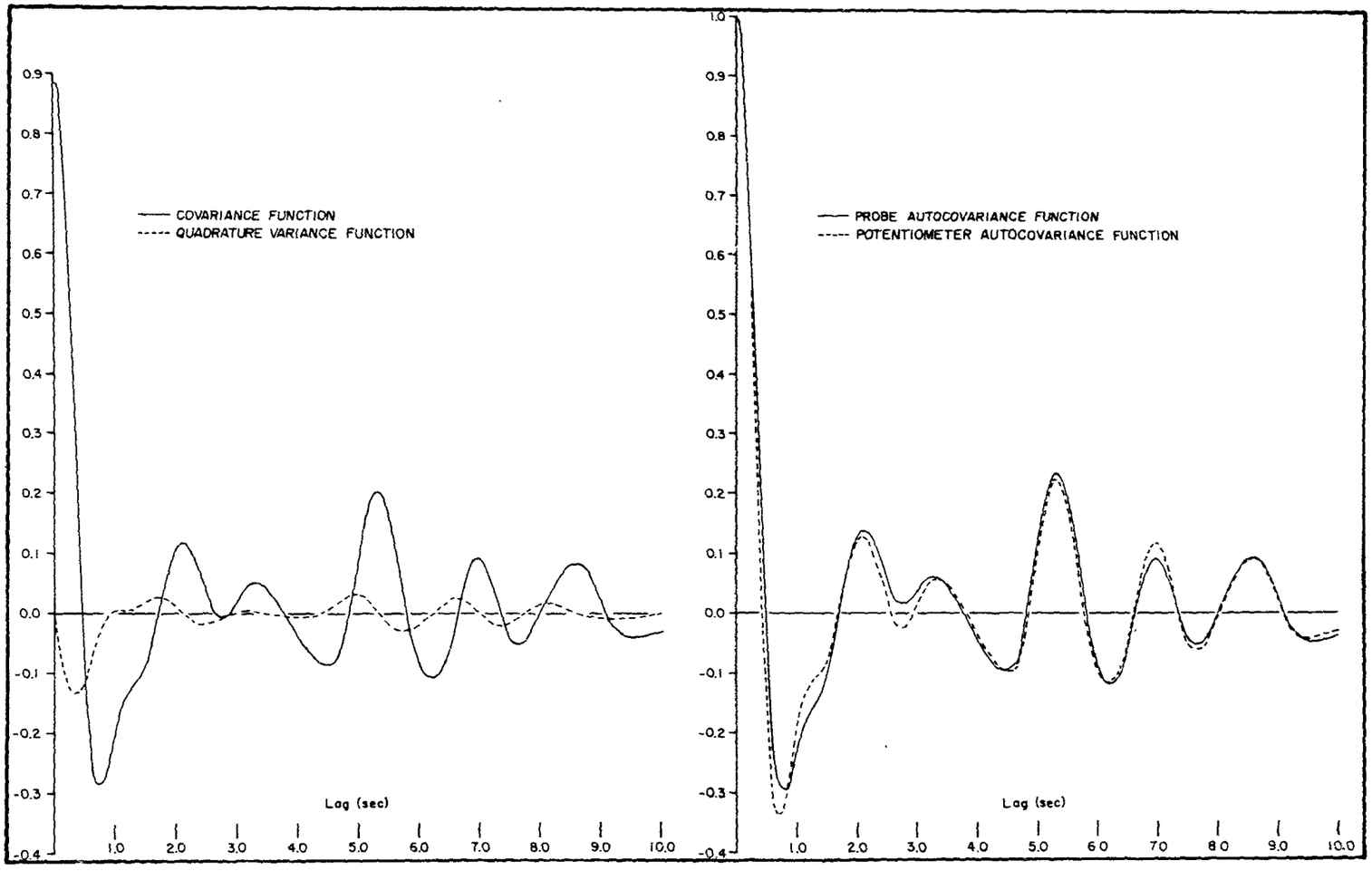

Figure 2.13 Dynamic Response Variance Functions at 0.5 volt/line

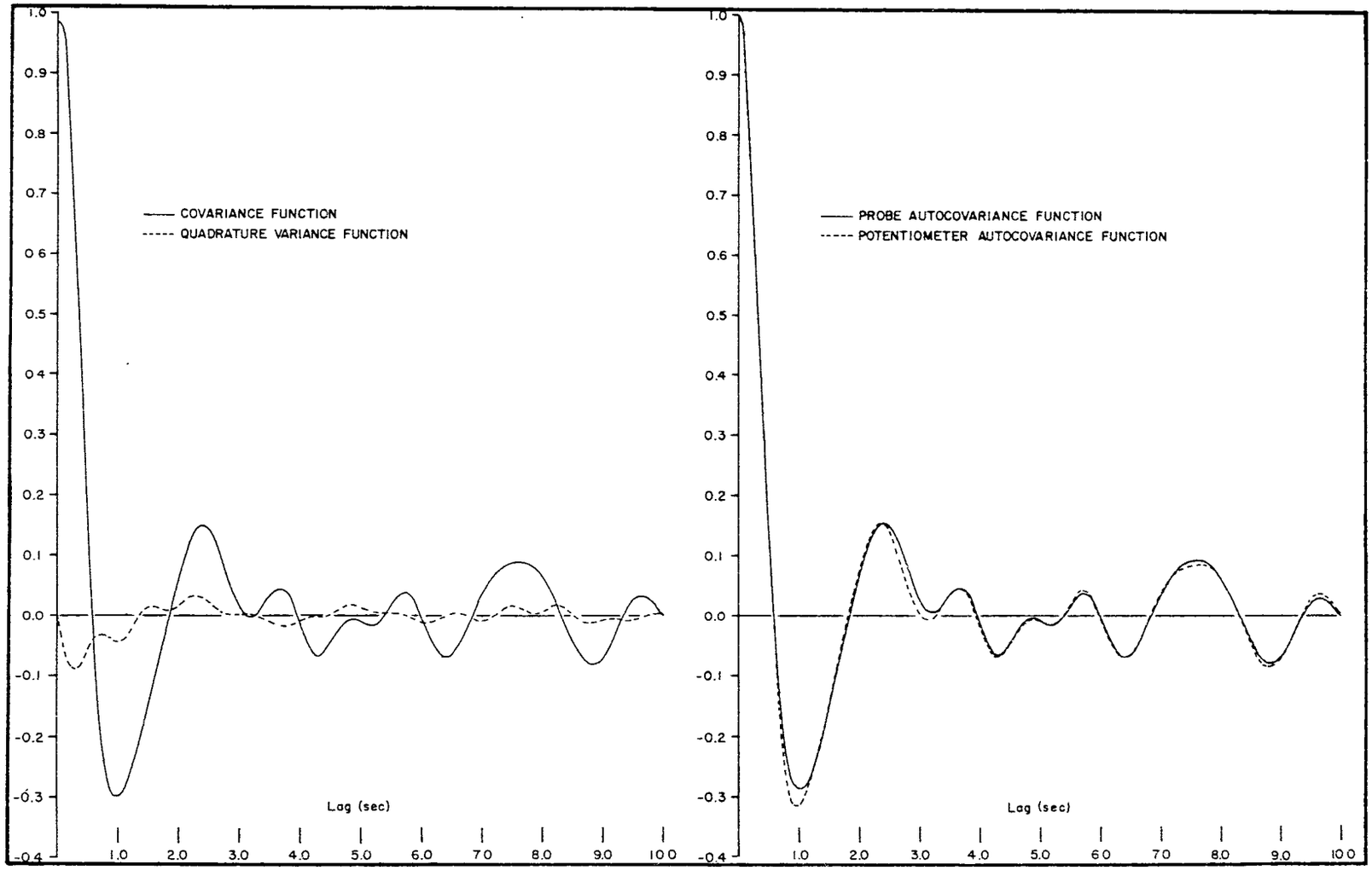

Figure 2.14 Dynamic Response Variance Functions at 1 volt/line

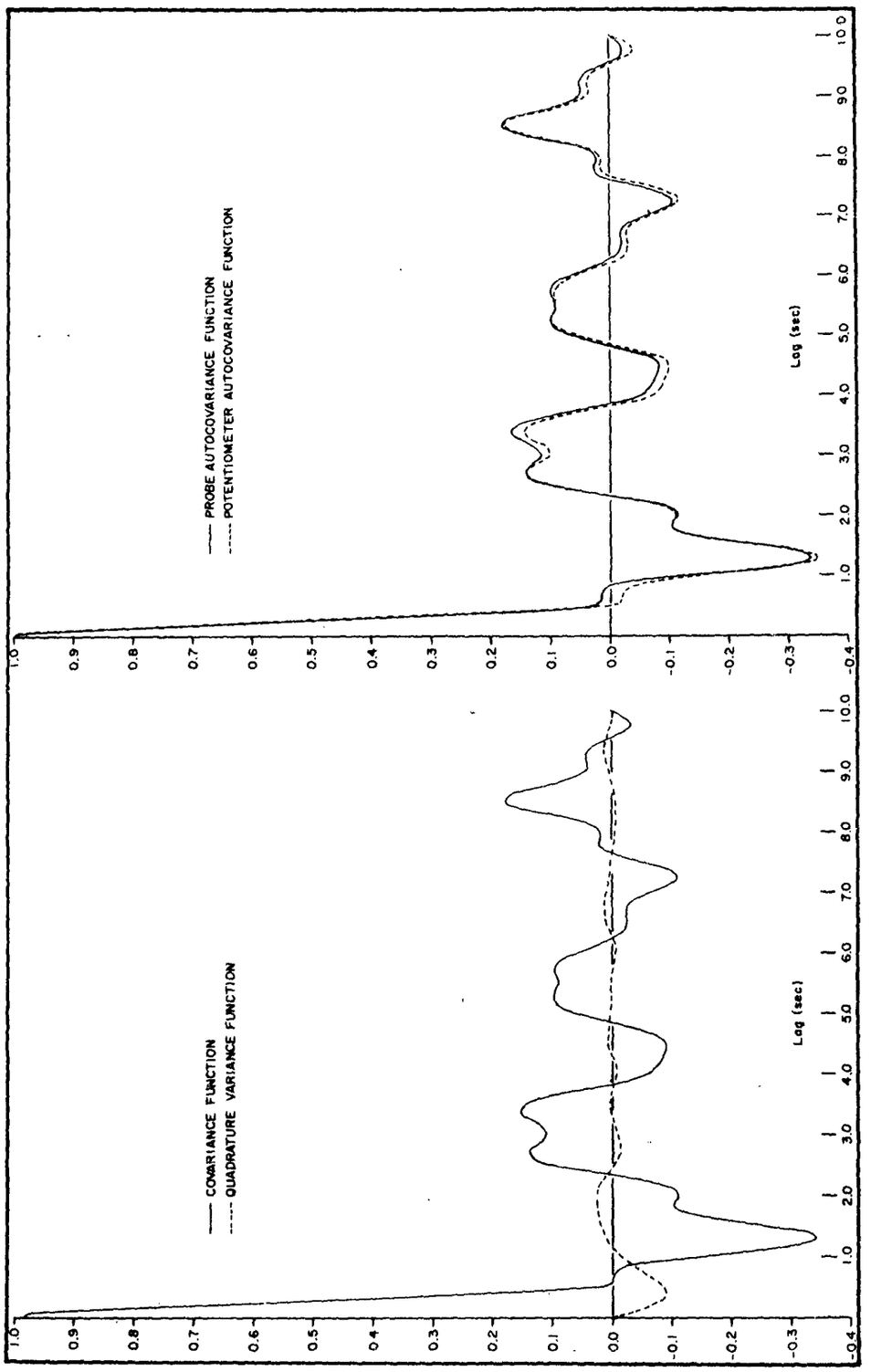

Figure 2.15 Dynamic Response Variance Functions at 2 volts/line

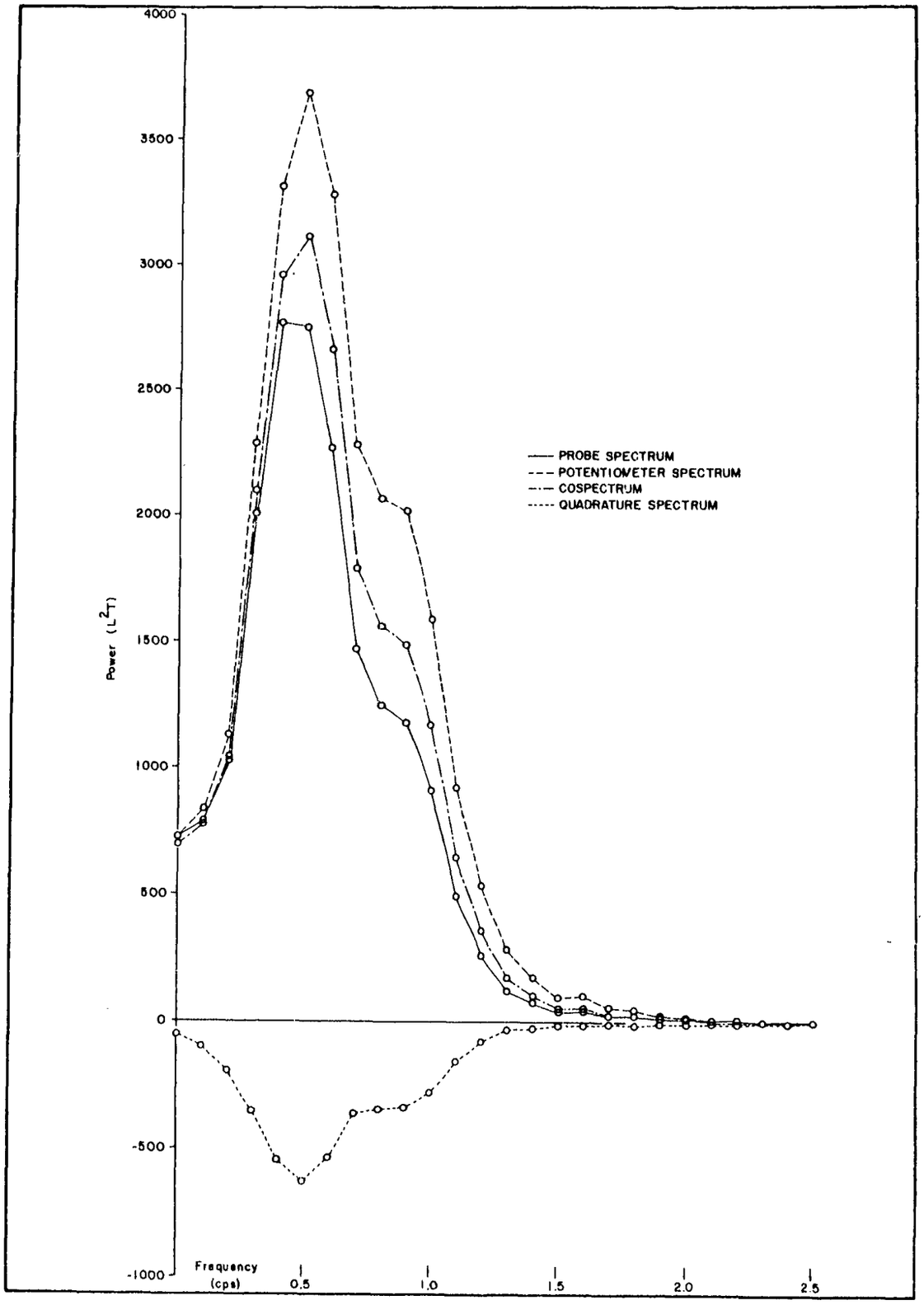

Figure 2.16 Dynamic Response Spectra at 0.5 volt/line

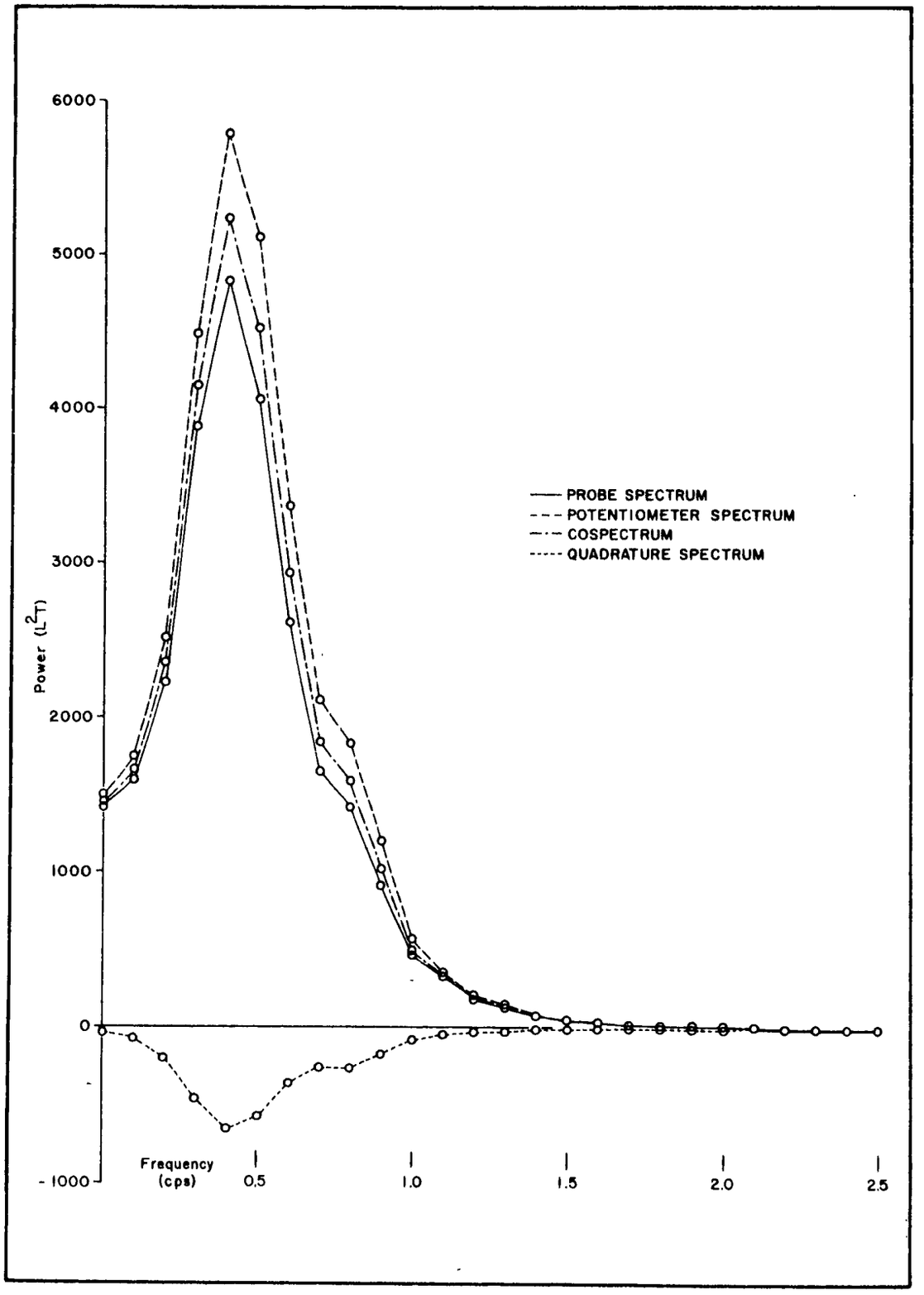

Figure 2.17 Dynamic Response Spectra at 1 volt/line

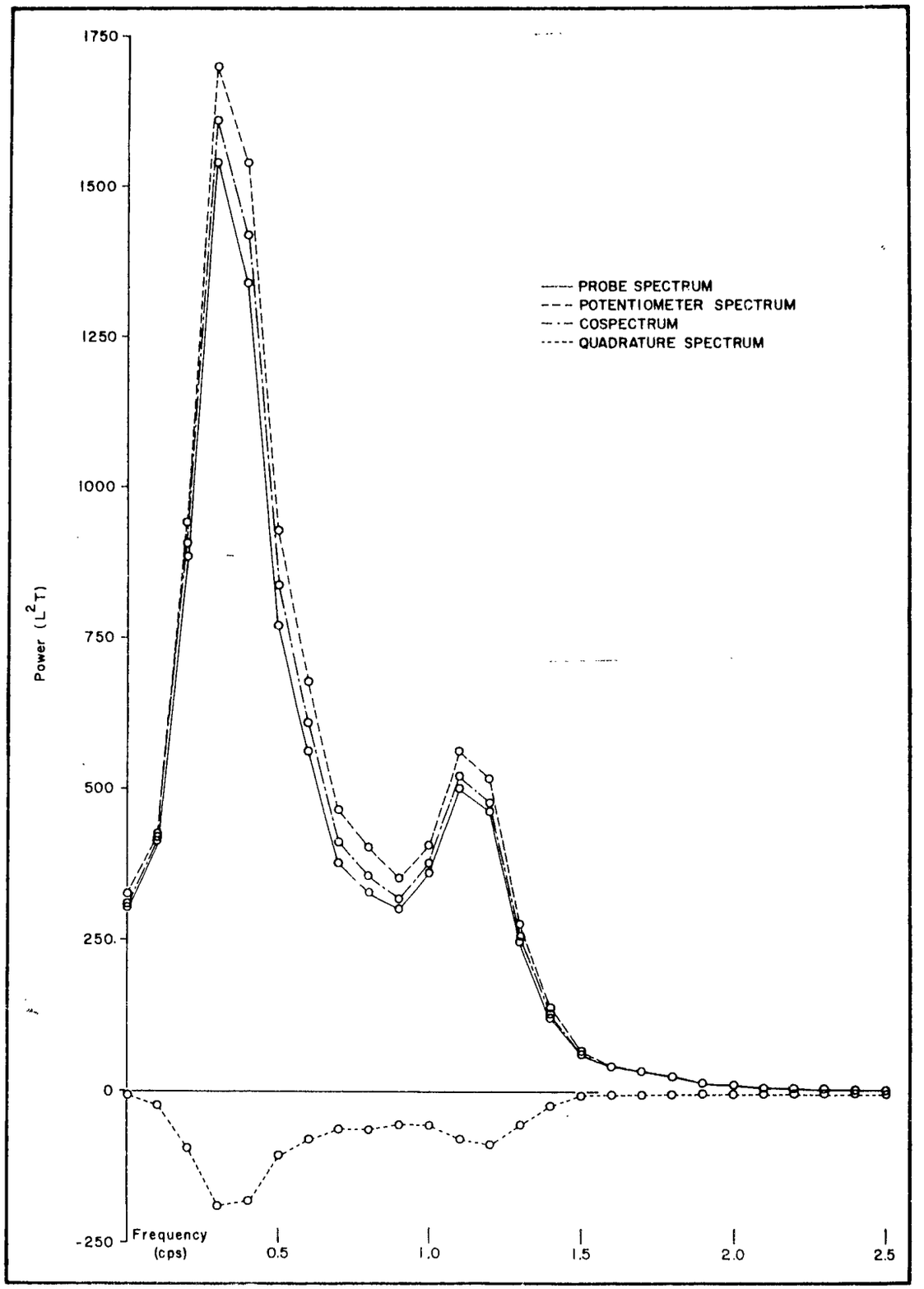

Figure 2.18 Dynamic Response Spectra at 2 volts/line

They are:

1) The coherence $\frac{c^2 + q^2}{f_{xx} f_{yy}}$, which may be thought of as a kind of correlation coefficient between the two signals for each frequency. The closer this is to one, the better the instrument.

2) The phase shift Arg(c + iq). An instrument that shifted all frequencies the same amount would produce a signal directly related to the process in the environment.

3) The transfer function f_{xx}/f_{yy}, which represents the factor by which the spectrum of the instrument record must be multiplied to give the spectrum of the standard record. The values of these functions are given in tables AI 2.4, AI 3.4, and AI 4.4 and showed in figures 2.19 to 2.21.

Preliminary studies of the July records showed that there was no appreciable energy in the waves at frequencies higher than 2.5 cps. Thus we need be concerned only about the response of the instrument to frequencies less than 2.5 cps. An inspection of the coherences shows that the instrument responds very well to frequencies from 0.0 to 1.5 cps, less well to frequencies from 1.6 to 2.0 cps, and rather poorly in the range from 2.1 to 2.5 cps. Actually the deterioration in quality may not be nearly so rapid as the numbers indicate. The energy in the test records at frequencies from 1.5 to 2.0 cps is about two orders of magnitude smaller than the energy at frequencies from 0.0 to 1.0 cps, while that at 2.0 to 2.5 is three orders of magnitude less. Thus the apparent incoherence may well be due chiefly to the increasing relative importance of the background noise.

The phase shift is equally encouraging at frequencies below which the noise becomes important, being quite stable at about -0.2 radians. The transfer functions show some loss of energy at the lower frequencies

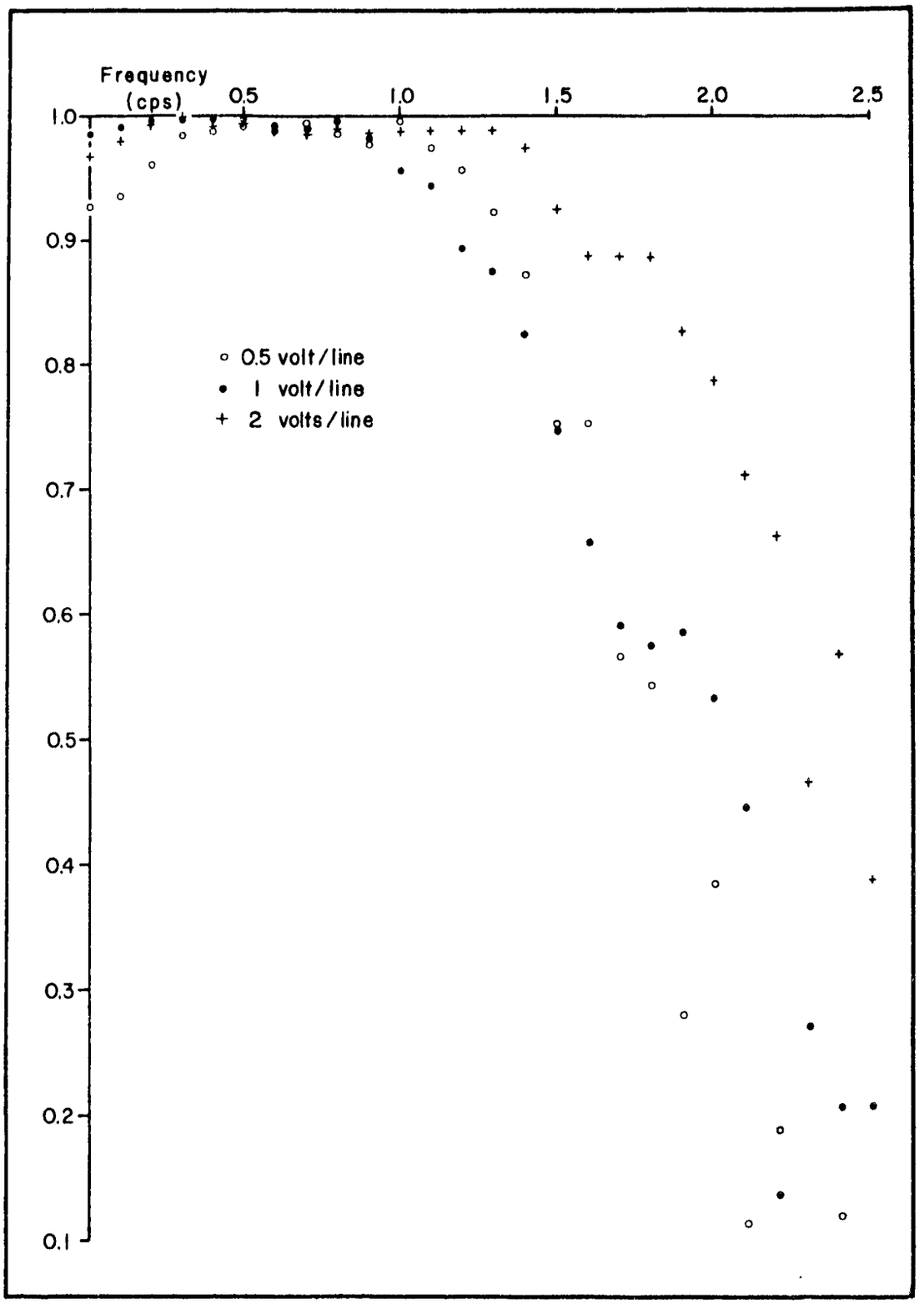

Figure 2.19 Dynamic Response Coherence

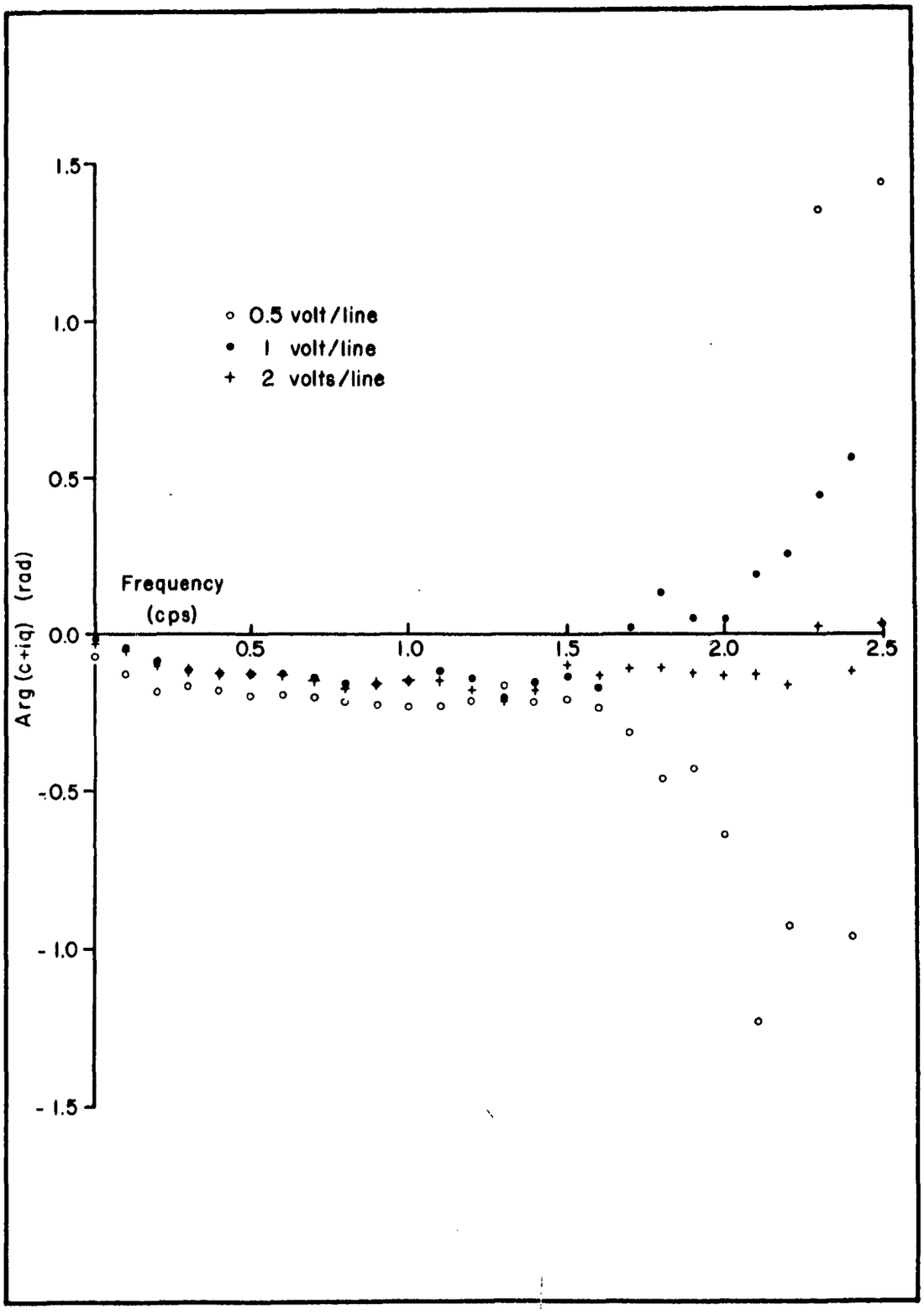

Figure 2.20 Dynamic Response Phase Shift

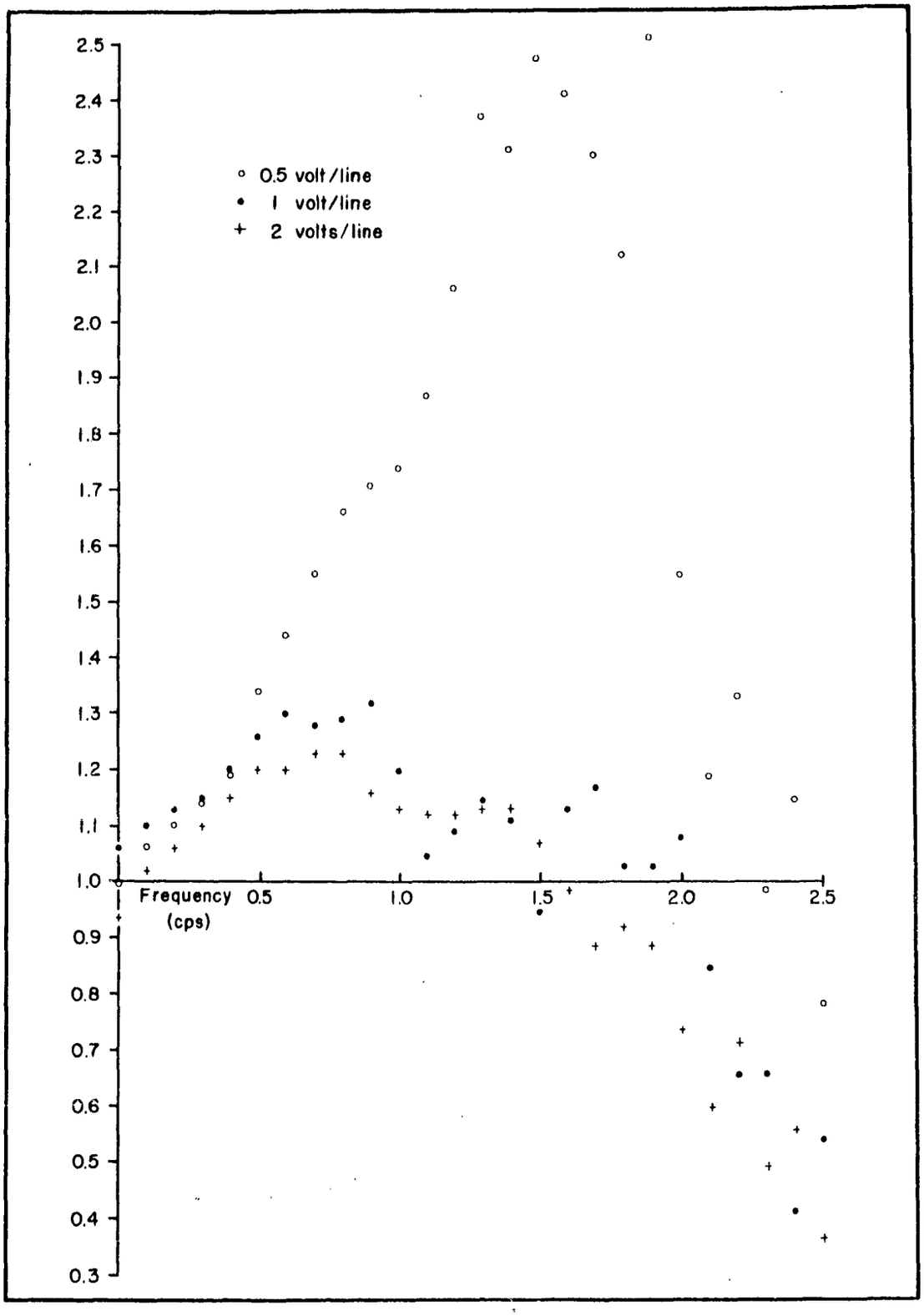

Figure 2.21 Dynamic Response Transfer Function

and some gain at the higher frequencies. This is in accord with a pattern which can occasionally be noted in the test records. Figure 2.22 shows an exaggerated schematic representation of the occurrence.

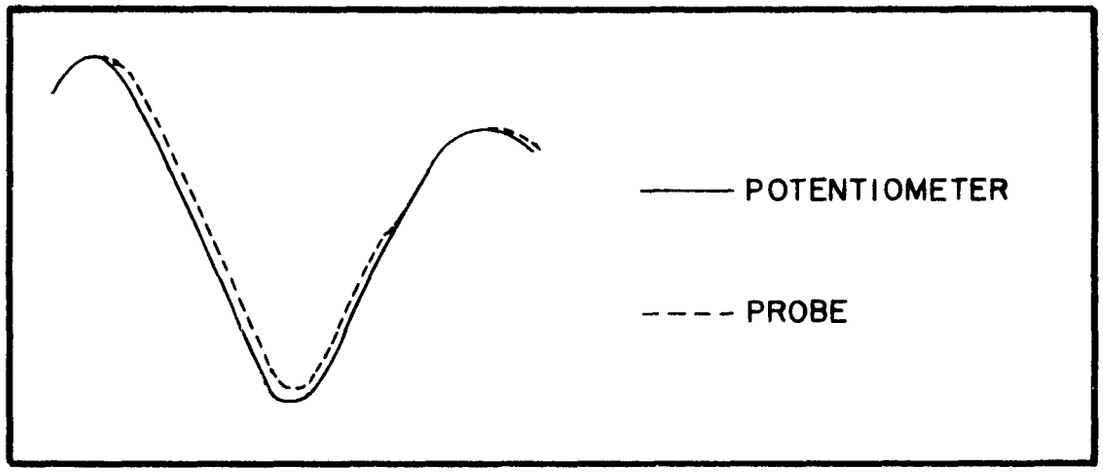

Figure 2.22 A Deformation Occurring in the Dynamic Response Exploration

An additional sequence of 60 abrupt withdrawals of the probe for the full range was made at each of the three sensitivities. At each sensitivity the time necessary for the probe to drain completely fell into two widely separated and quite consistent classes. This was noticed while the records were being made, and it was observed that the shorter drainage times occurred when a stray breeze struck the probe. These breezes were not strong enough to disturb the water surface in the tank, but they did break the film of water draining down the probe. It would seem that the drainage times given in table 2.4 must be longer than those to be expected in the field, where the winds are always at least 50 cm/sec while wave measurements are being made and where the water surface falls much more slowly.

If the system were a linear one, and if the tank conditions were a good approximation to the field conditions, there might be some virtue

Table 2.4 Mean Drainage Times for Abrupt Probe Withdrawals Through the Full Range

Sensitivity (volts/line)	Range (cm)	Time to Drain 90% (sec)	Time to Effective 100% (sec)
0.5	9.08	1.44	2.2
1	18.15	1.30	2.0
2	36.35	1.30	2.2

in using the transfer functions to correct the spectra taken in the field. For the reasons discussed earlier they are better considered as extreme bounds. Since rather wide statistical fluctuations are also present, any attempt to intuit suitable transfer functions would be the merest guesswork. The changes produced by the computed functions are certainly much more drastic than they should be. Consequently, it seems best to carry out the calculations using the records as they were taken and to present the results without modification. Evidently the instrument is apt to its task though not perfect, and each reader can make those modifications which from this exploration and his own experience seem suitable.

2.3 The Anemometers

The wind speed was measured at three heights during the July series, nominally at 61 cm, 122 cm, and 244 cm above mean water level. During the November series it was measured at four levels, nominally at 50 cm, 75 cm, 125 cm, and 225 cm above mean water level. In this report only the wind speed at 122 cm in July and 125 cm in November is considered.

The instruments used were commercially available, nondirectional, compensated, heated-thermocouple N-7 probes and model R-2 air meters made by Hastings-Raydist, Inc., Hampton, Virginia. Detailed information about them may be found in Gill (1954), Hastings (1949), Hastings and Wcislo (1951), and Hastings and Doyle (1956).

Figure 2.23 shows the structure of a single element of the N-7 probe. An alternating current heats very fine thermocouples supported

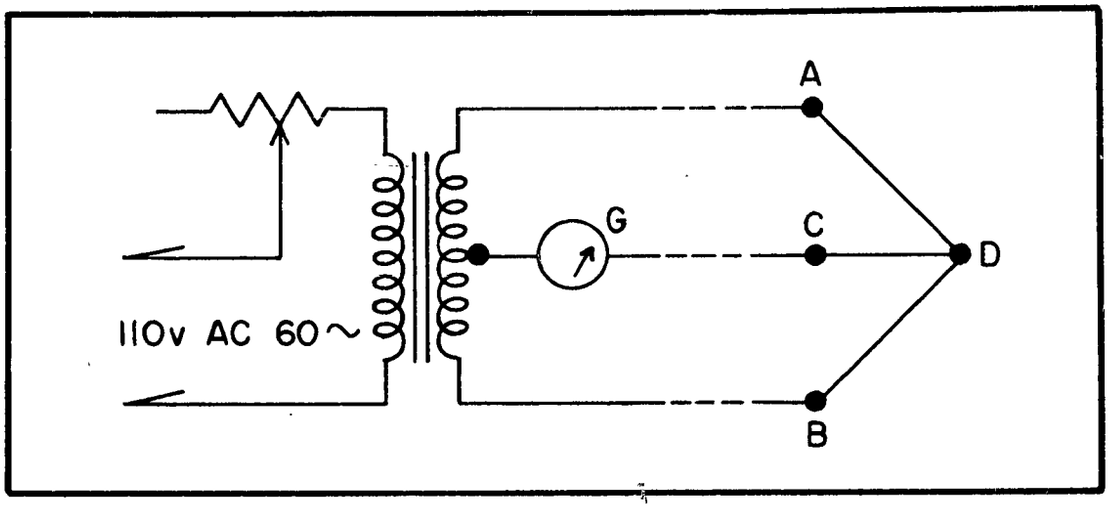

Figure 2.23 N-7 Probe Element

by wires between AD and BD, but not the one between CD. The resistance on AD equals that on BD, and the transformer is center tapped so that only the thermoelectric direct current flows through the millivoltmeter at G. Since AD and BD are in parallel, G registers the thermoelectric voltage for a single thermocouple. The unheated thermocouple CD provides a bucking voltage which cancels out voltages due to fluctuating air temperatures. Gill (1954) reports that laboratory tests showed perfect compensation over temperature fluctuations as great as 27 C. The basic unit may be combined as many times as you please to secure a stronger signal. The N-7 probe contains five units radially disposed.

The N-7 probes put out a nonlinear DC voltage ranging from 10 millivolts at 0 mph wind speed to 1.2 millivolts at 30 mph. Figure 2.24 is a copy of the calibration supplied by Hastings-Raydist. As showed on the face of the R-2 air meter, illustrated in figure 2.25, above 20 mph the scale is so compressed as to be nearly useless except for means.

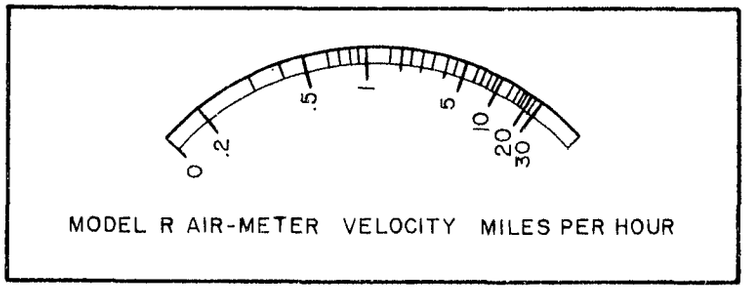

Figure 2.25 R-2 Air Meter Scale

Below 5 mph the scale is wide open and small differences are readily detectable, so that spectra may be computed.

Since the Brush oscillograph requires a 2-volt signal and the R-2 air meter provides a 10-millivolt signal, amplification is needed. It was decided to let a half-scale deflection on the air meter be displayed as a full-scale deflection on the oscillograph so that the gain required was 400. Two kinds of amplifiers were developed. The first was a vacuum tube device of which three were used. When a fourth anemometer was added to the stack after the July cruise, a transistorized amplifier was devised. The serial numbers of probes and air meters, the nominal level at which each was used, and the type of amplifier used with each are showed in table 2.5.

Mr. Edmund Schiemer, who assisted Dr. Willis C. Gore in developing the amplifiers, describes the vacuum tube amplifier, which was the first kind, as follows:

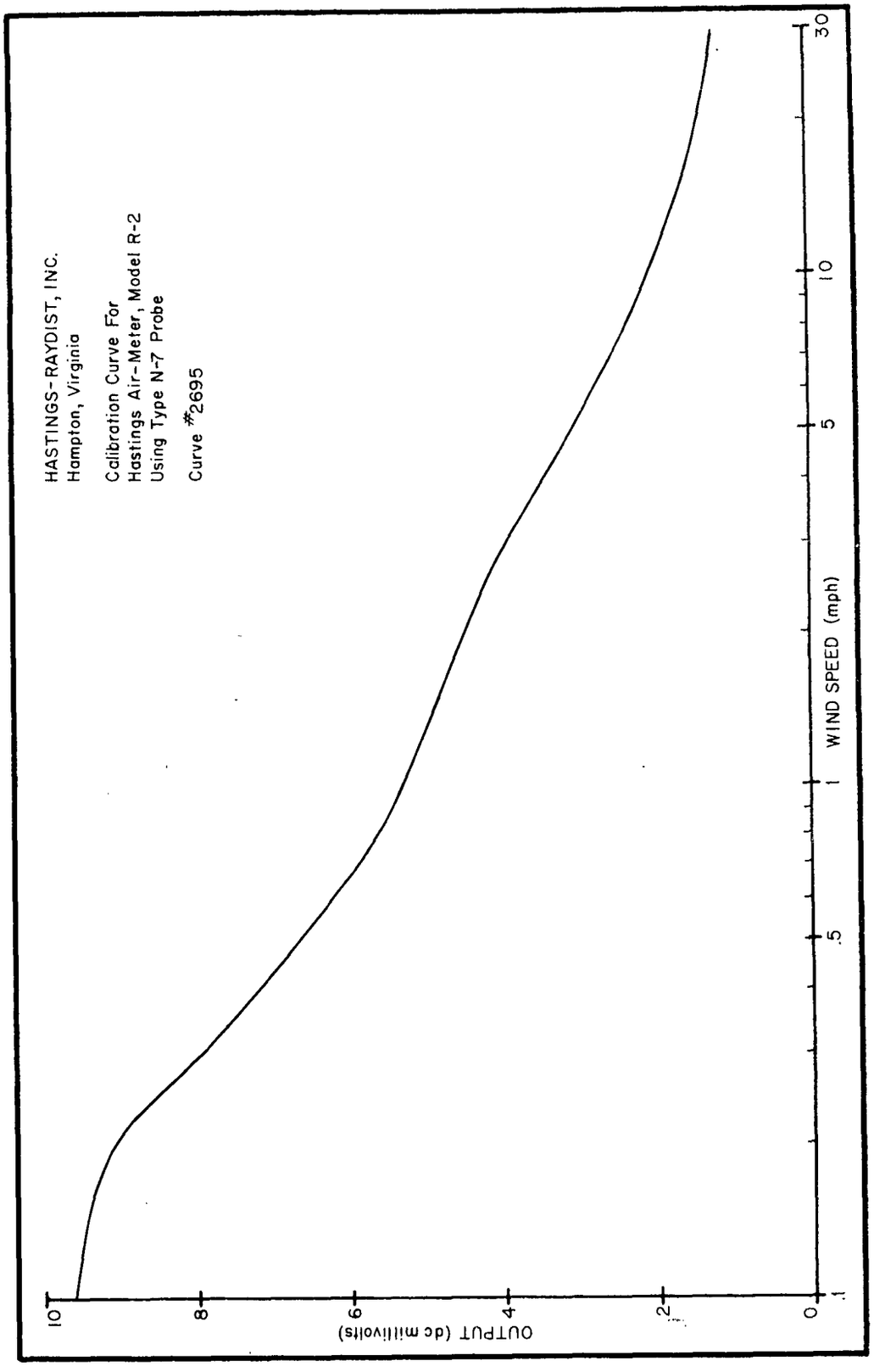

Figure 2.24 Hastings-Raydist Calibration Curve for the R-2 Air Meter

Table 2.5 The N-7 Probes, the Amplifiers Used with Each, and the Heights of the Probes Above the Water

N-7 Probe	R-2 Air Meter	Nominal Level (cm) July	Nominal Level (cm) November	Amplifier
291	39	244	225	Vacuum
287	33	122	125	Vacuum
305	40	61	75	Vacuum
316	65	-	50	Transistor

"The amplifier (table 2.6 and figure 2.26) consists of three triode amplifiers, R-C coupled, each having cathode degeneration, and a cathode follower output. The incoming 5-mv DC signal is first filtered to remove the 60-cycle heating power component, chopped, amplified, rectified, and finally filtered to remove the 60-cycle chopper component. The identical input and output filters were designed to block effectively any frequency of 60 cycles or over and to pass equally well frequencies in the range from 0 to 1.5 cycles. A single regulated power supply (table 2.7 and figure 2.27) energizes three amplifiers. The four air meters receive regulated 60-cycle power from a Sola CV 3 transformer."

The transistor amplifier (table 2.8 and figure 2.28) is described by its designer Dr. Gore as follows:

"The transistor amplifier for air meter No. 65 is a transistorized 'chopper' type amplifier, in which the signal to be amplified is 'chopped' or converted to an AC signal, amplified, inverted to form the original signal time structure and displayed on a meter or recorder.

"Transistors A and B form a square-wave oscillator (or multivibrator) whose outputs are shaped and amplified by transistors C and D. This square wave-chopping wave form is applied to transistor H, which converts the signal to an AC square wave form of frequency

Table 2.6 Parts List for the Vacuum Tube Amplifier

R_1	470 K, 0.5 W	R_{11}	1.5 K, 0.5 W	R_{21}	5 K, 0.5 W	C_5	20 μfd
R_2	51 K, 0.5 W	R_{12}	1 M, 0.5 W	R_{22}	51 K, 0.5 W	C_6	0.015 μfd
R_3	51 K, 0.5 W	R_{13}	2.2 K, 0.5 W	R_{23}	51 K, 0.5 W	C_7	0.1 μfd
R_4	51 K, 0.5 W	R_{14}	1.5 K, 0.5 W	R_{24}	51 K, 0.5 W	C_8	0.1 μfd
R_5	51 K, 0.5 W	R_{15}	1 M, 0.5 W	R_{25}	51 K, 0.5 W	C_9	1.0 μfd
R_6	220 K, 0.5 W	R_{16}	82 K, 0.5 W			C_{10}	0.25 μfd
R_7	10 K, 0.5 W	R_{17}	2.2 K, 0.5 W	C_1	0.25 μfd	C_{11}	0.25 μfd
R_8	220 K, 0.5 W	R_{18}	1.5 K, 0.5 W	C_2	0.25 μfd	C_{12}	0.25 μfd
R_9	1 M, 0.5 W	R_{19}	27 K, 1 W	C_3	0.25 μfd	C_{13}	0.25 μfd
R_{10}	2.2 K, 0.5 W	R_{20}	5.1 K, 0.5 W	C_4	0.25 μfd		
		V_1	12AX7		D_1 IN100		
		V_2	12AU7		D_2 IN100		

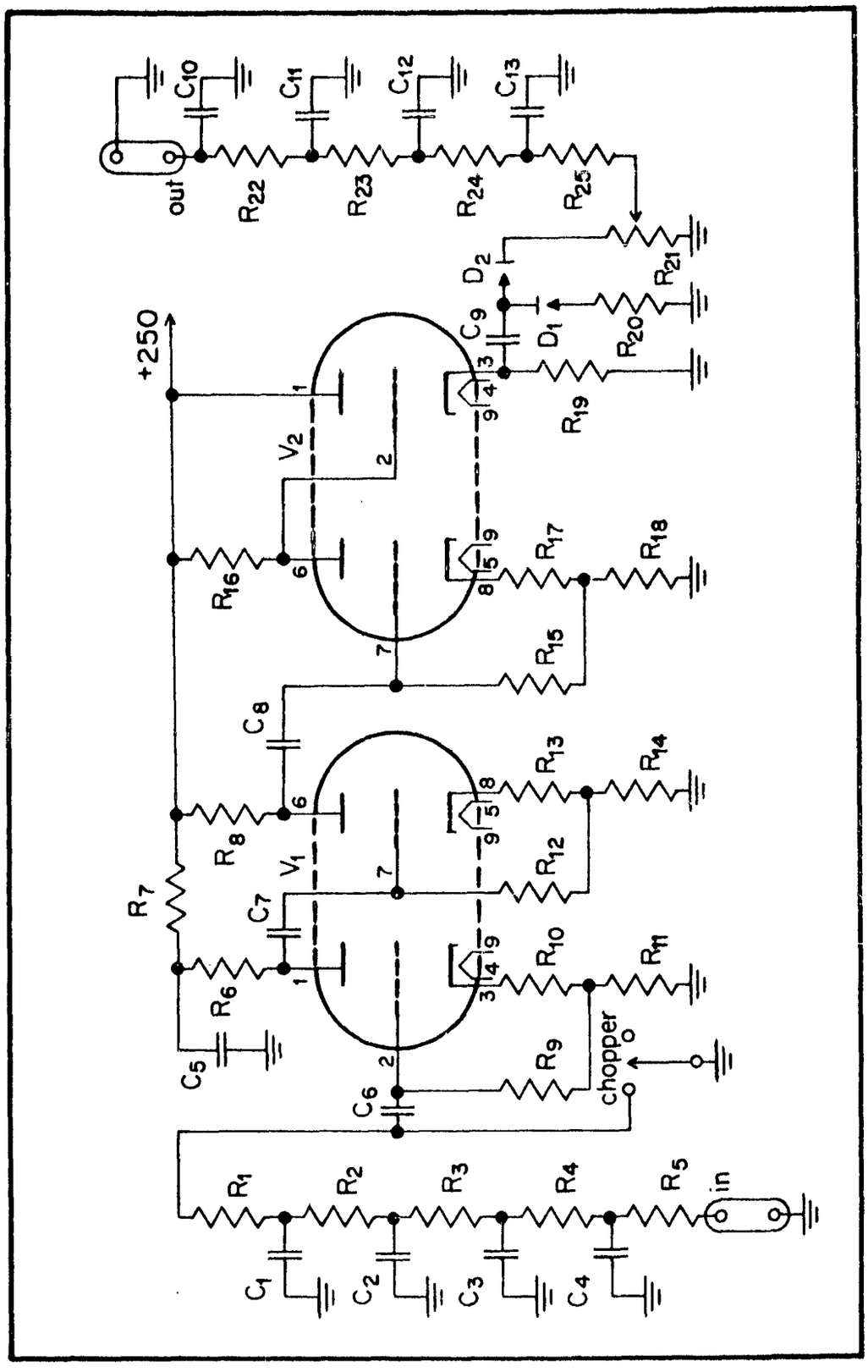

Figure 2.26 Circuit Diagram of the Vacuum Tube Amplifier

Table 2.7 Parts List for the Power Supply for the Anemometer Amplifiers

R_1	750 , 50 W, 10%	R_8	1.2 M, 0.5 W, 10%	C_1	40 μfd at 500 v	V_1	6AS7	T_1	Merit P-2834
R_2	150 K, 0.5 W, 10%	R_9	68 K, 1 W, 10%	C_2	40 μfd at 500 v	V_2	5U4	T_2	Sola 20-10-015
R_3	68 K, 1 W, 10%	R_{10}	220 K, 0.5 W, 10%	C_3	0.004 μfd	V_3	12AX7		
R_4	1 M, 0.5 W, 10%	R_{11}	150 K, 0.5 W, 10%	C_4	1.0 μfd	V_4	12AX7	S_1	DPST
R_5	1.2 M, 0.5 W, 10%	R_{12}	150 K, 0.5 W, 10%	C_5	40 μfd at 450 v	V_5	5651		
R_6	1 M, 0.5 W, 10%	R_{13}	25 K, 0.5 W, 10%			V_6	5651	L_1	Merit C-2974; 50Ω, 2 h at 200 ma
R_7	150 K, 0.5 W, 10%	R_{14}	75 K, 0.5 W, 10%						

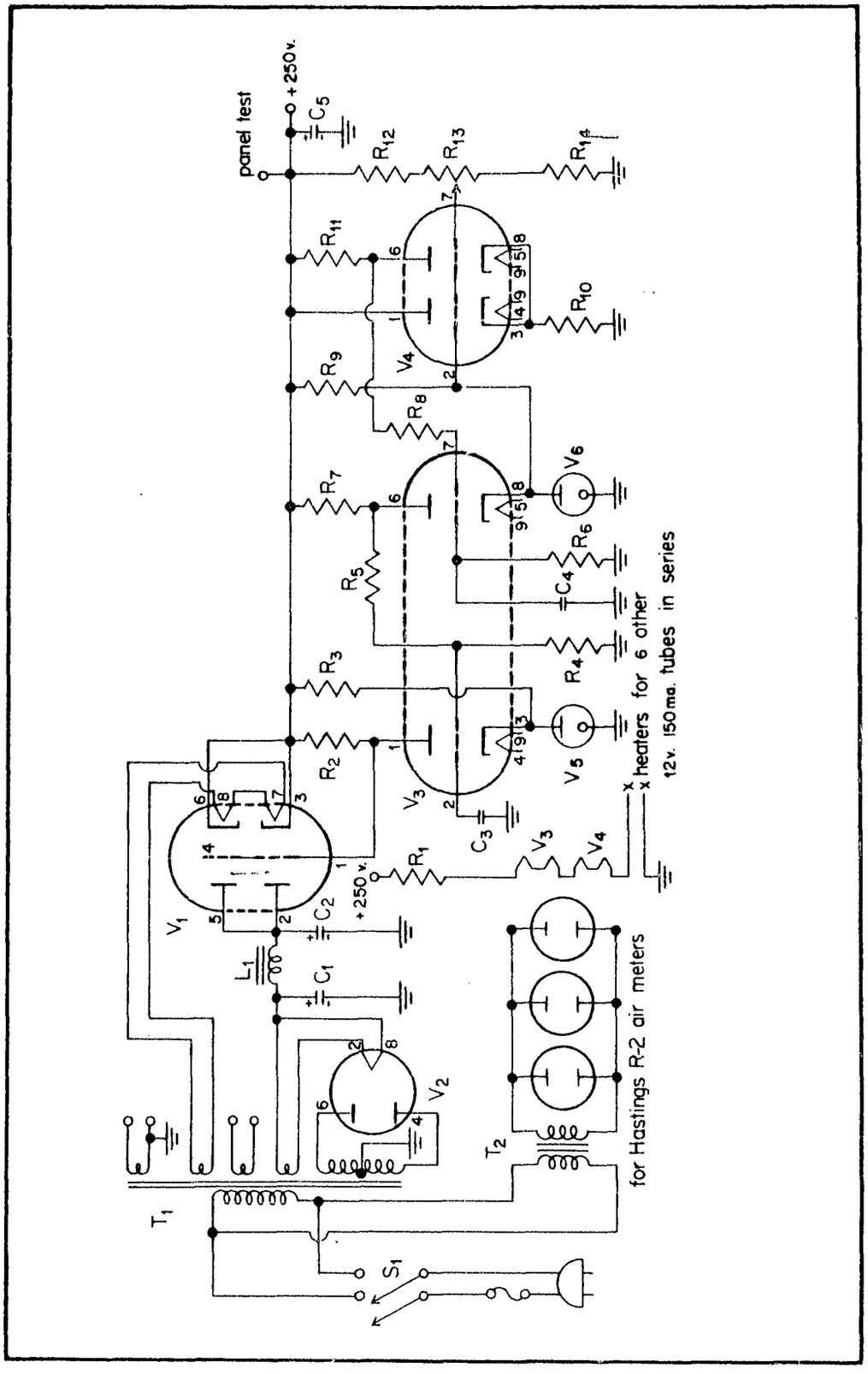

Figure 2.27 Circuit Diagram of the Power Supply for the Anemometer Amplifiers

Table 2.8 Parts List for the Transistor Amplifier

R_1	3.3 K								
R_2	3.3 K	R_{18}	680 K	C_1	0.01 μfd	C_{17}	0.25 μfd	TR_1	2N170
R_3	3.3 K	R_{19}	510 K	C_2	0.01 μfd	C_{18}	0.25 μfd	TR_2	2N170
R_4	3.3 K	R_{20}	4.7 K	C_3	100 μfd	C_{19}	8 μfd	TR_3	2N170
R_5	3.3 K	R_{21}	100 K	C_4	100 μfd	C_{20}	8 μfd	TR_4	2N170
R_6	10 K	R_{22}	1 K	C_5	100 μfd	C_{21}	8 μfd	TR_5	2N170
R_7	10 K	R_{23}	10Ω	C_6	100 μfd			TR_6	2N170
R_8	3.3 K	R_{24}	1 K	C_7	8 μfd			TR_7	2N168A
R_9	3.3 K	R_{25}	220 K	C_8	8 μfd			TR_8	2N168A
R_{10}	3.3 K	R_{26}	4.7 K	C_9	0.1 μfd			TR_9	2N170
R_{11}	130Ω	R_{27}	220 K	C_{10}	8 μfd			TR_{10}	2N170
R_{12}	130Ω	R_{28}	5.6 K	C_{11}	8 μfd	D_1	1N67		
R_{13}	130Ω	R_{29}	150 K	C_{12}	8 μfd	D_2	1N67	M_1	Brush Inst. Oscillograph and Amplifier
R_{14}	130Ω	R_{30}	51 K	C_{13}	8 μfd	D_3	1N67		
R_{15}	2.7 K	R_{31}	51 K	C_{14}	8 μfd	D_4	1N67		
R_{16}	1 K	R_{32}	51 K	C_{15}	0.25 μfd	D_5	1N67		
R_{17}	33 K	R_{33}	51 K	C_{16}	0.25 μfd	D_6	1N67		

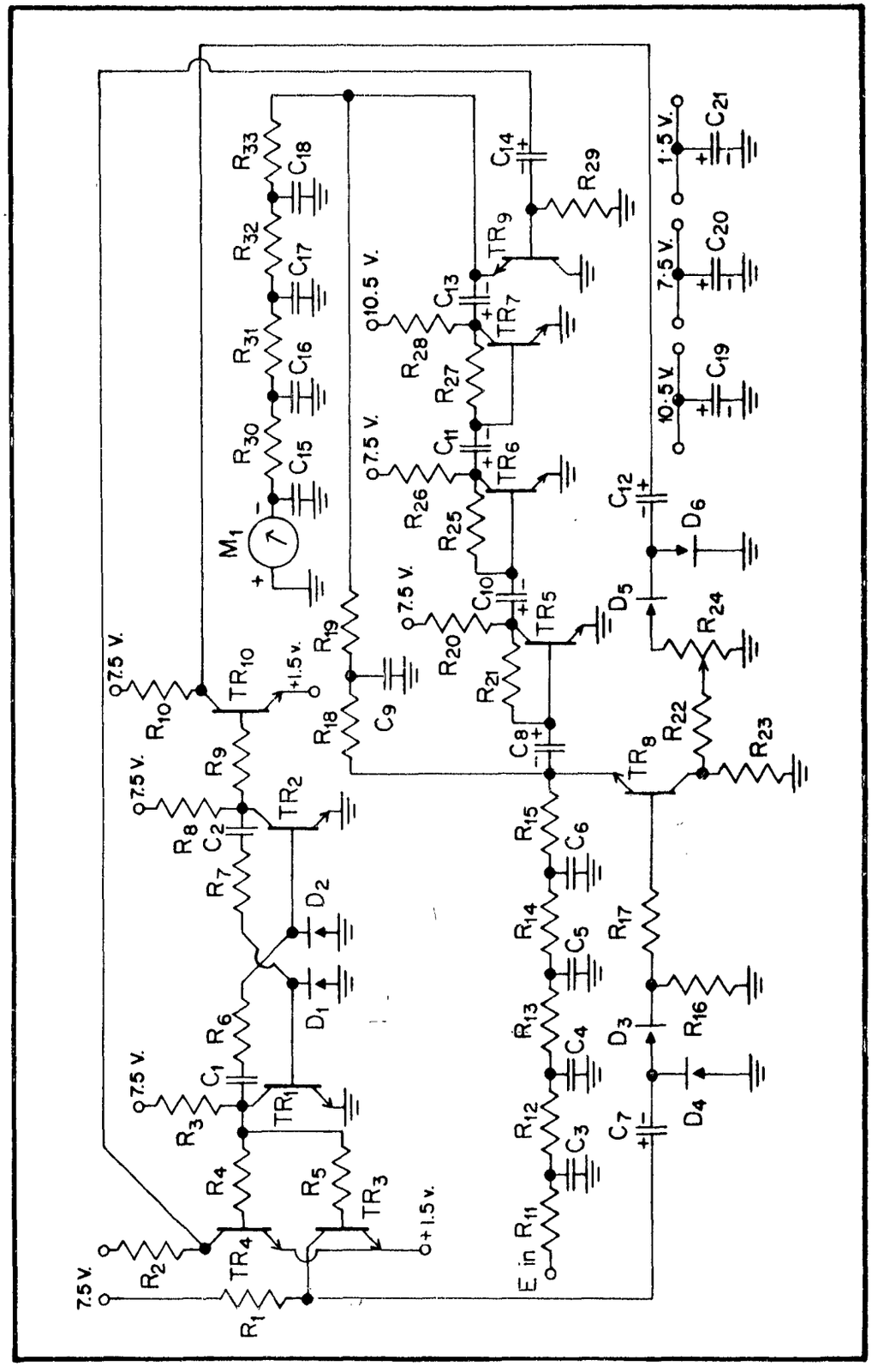

Figure 2.28 Circuit Diagram of the Transistor Amplifier

2,600 cps (set by the oscillator A and B). This square wave signal is amplified by transistors E, F, and G, and the resulting amplified square wave is inverted to the original signal by means of the synchronous chopper transistor K. The output of the transistor K is presented on the meter M and is fed back to the input to stabilize the gain and hence the performance of the amplifier."

During the trial July cruise it was found to be very difficult to position the anemometer signals at exactly the same point on the oscillograph paper for each record. A method of providing reference lines at the beginning of each record to scale the wind-speed traces was highly desirable. Reference lines were entered from time to time on the July records with a jury rig. Before undertaking the November cruise each air meter was modified to provide easy, rapid entry of reference lines on the oscillograph paper. Of this device Mr. Schiemer says:

"A 0- to 10-mv DC source was incorporated in the air meter using the speed-indicating meter as a reference (figure 2.29). The double-pole double-throw switch installed in the air meter cabinet removes the meter from the probe circuit and connects it to the 10-mv circuit, at the same time connecting the dry cell to the adjustable voltage divider. Thus any DC voltage corresponding to any wind speed may be applied to the meter and hence to the amplifier recorder system."

In the field, the N-7 probes were connected with the air meter by 350-foot lengths of number 12, 3-conductor, type S cable. The probes consist of a 1-13/16-inch-diameter head, 1-1/4 inches thick, mounted on a 3/8-inch-diameter stainless steel stem, 12 inches long, on which a protecting cover slides. The probes were secured by small hose clamps to the 2-foot support arms and were spaced from the bottom of the anemometer mast. Before each record was made, a skiff went out to the tower and the entire mast was raised or lowered until the bottom

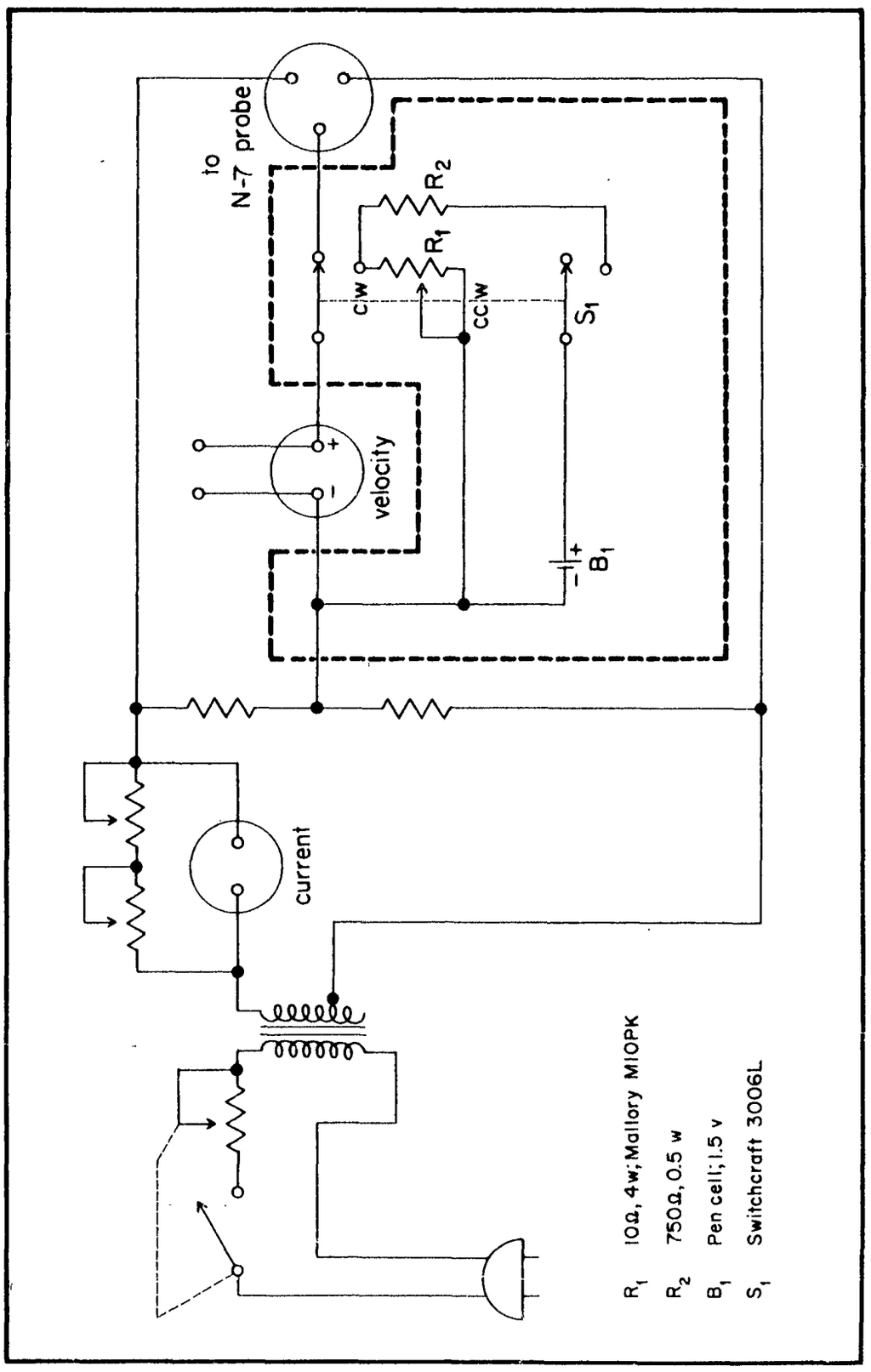

Figure 2.29 Circuit Diagram of the Reference Circuit Incorporated in the R-2 Air Meter

end was submerged about half the time. This gave a vertical adjustment of the anemometers to within a centimeter or two of their nominal height above mean water level. When the tide was unusually high a full adjustment was not always possible because the cross-arm clamp got in the way of an anemometer support arm. At these times, rather than alter the fixed spacing of the probes, the degree of immersion of the foot of the anemometer mast was estimated and a correction was applied.

It has been remarked that a fourth anemometer was added for the November cruise. The decision to do this was made when some preliminary reduction of the July data revealed wind profiles that were so widely divergent from the logarithmic profile that further details seemed imperative. Unfortunately, the additional anemometer only reinforces the suggestion of chaos in the lowest 2 meters. It has been suggested that a logarithmic profile would be more easily secured by reducing, rather than increasing, the number of anemometers--a suggestion which, while true, is not precisely to the point.

The inevitable first reaction to the bizarre profiles obtained in July was that the calibrations must be some way in error. The calibrations supplied by Hastings-Raydist with the instruments had been made with a simulated 350-foot lead between probe and air meter. An attempt was made to check these calibrations in a wind tunnel equipped with a very sensitive manometer. The attempt proved abortive because the manometer was relatively insensitive at less than 5 mph, while the R-2 air meter was relatively insensitive at more than 10 mph. At least no negative results occurred.

Being even more uneasy about the wind-speed results after the November cruise, we turned to Hastings-Raydist for help. They were most cordial in their assistance, offering us the use of their laboratory

and the services of their technicians and Research Director Dr. James M. Benson. We took advantage of this kindness to carry the anemometers, the cables, and the oscillograph to Hampton, Virginia, where we devoted 2 days to calibrating with all the components exactly as they had been used in the field with one exception. Probe number 287 had been damaged sometime between the end of the November cruise and the trip to Virginia; it was repaired by Hastings-Raydist in about half an hour and was tested with the others.

The testing setup consisted of a wind tunnel with an 8-inch-square working section, 19 inches long, in which the N-7 probes could be mounted. Wind speeds of 0 to 80 mph were available. For a standard, a Hastings-Raydist model TS 8 directional probe, which had been calibrated by the U.S. National Bureau of Standards, was also mounted in the working section of the wind tunnel. This standard was an order of magnitude more sensitive than the R-2 air meter. The wind speed was then adjusted to the series of values 1.00, 2.00, 4.00, 6.00, 8.00, 10.00, 12.00, 16.00, 20.00, 25.00, and 30.00 mph as showed by the standard, and the corresponding R-2 air meter values were read. After each series the N-7 probe was rotated 90° and the readings were repeated. This was done to eliminate possible effects of the wall on the geometry of the probe thermocouples. For the three probes which had not been injured this calibration confirmed the calibration sent with the instruments, and it may be assumed that the initial calibration for the damaged probe is equally valid. We were reassured that the results were accurate renditions of natural conditions. From the evidence collected during these calibrations we feel that the company's claim of an accuracy of 2% of full scale errs on the side of modesty and that the precision is probably quite a bit better.

The Hastings-Raydist N-7 probe with the modified R-2 air meter

seems to be a serviceable instrument for our uses. It has proved rugged enough to survive field conditions which would have destroyed the conventional hot-wire anemometer. There was no visible indication that the anemometers were affected by rain, from which they were to some extent sheltered by the form of the cap, or by salt spray, from which they were not protected at all. It was customary to sluice the probes under a cold water tap after returning from a cruise and before storing them. Besides being sturdy, the probe-air meter provides enough detail at less than 5 or 6 mph for spectra to be calculated. It is not so suitable for mean values at the higher wind speeds because of the computational labor to make and average many readings. However, in return for the labor one can get frequency distributions and moments as well as a mean value. If extensive use were to be made of the instrument, it might be advisable to build an electronic circuit to process the signal in the field into a mean and variance, reserving the option to record in detail at low wind speeds.

Dr. Benson of Hastings-Raydist has suggested that greater detail at higher wind speeds without appreciable increase in the noise level becomes possible by increasing the heating voltage to the thermocouples by a factor of five. He says that the probe is well able to take the increase without damage. We plan to follow this suggestion in future work. The instruments will, of course, have to be recalibrated at the higher voltage.

2.4 The Wind Vane

Wind direction was measured with a light split vane made of balsa wood. The details of its construction are showed in figures 2.30 and 2.31. The vane turns a small, low-torque (0.050 oz-in), linearity 0.2%, continuous-rotation potentiometer (figure 2.32). A 90° rotation of the

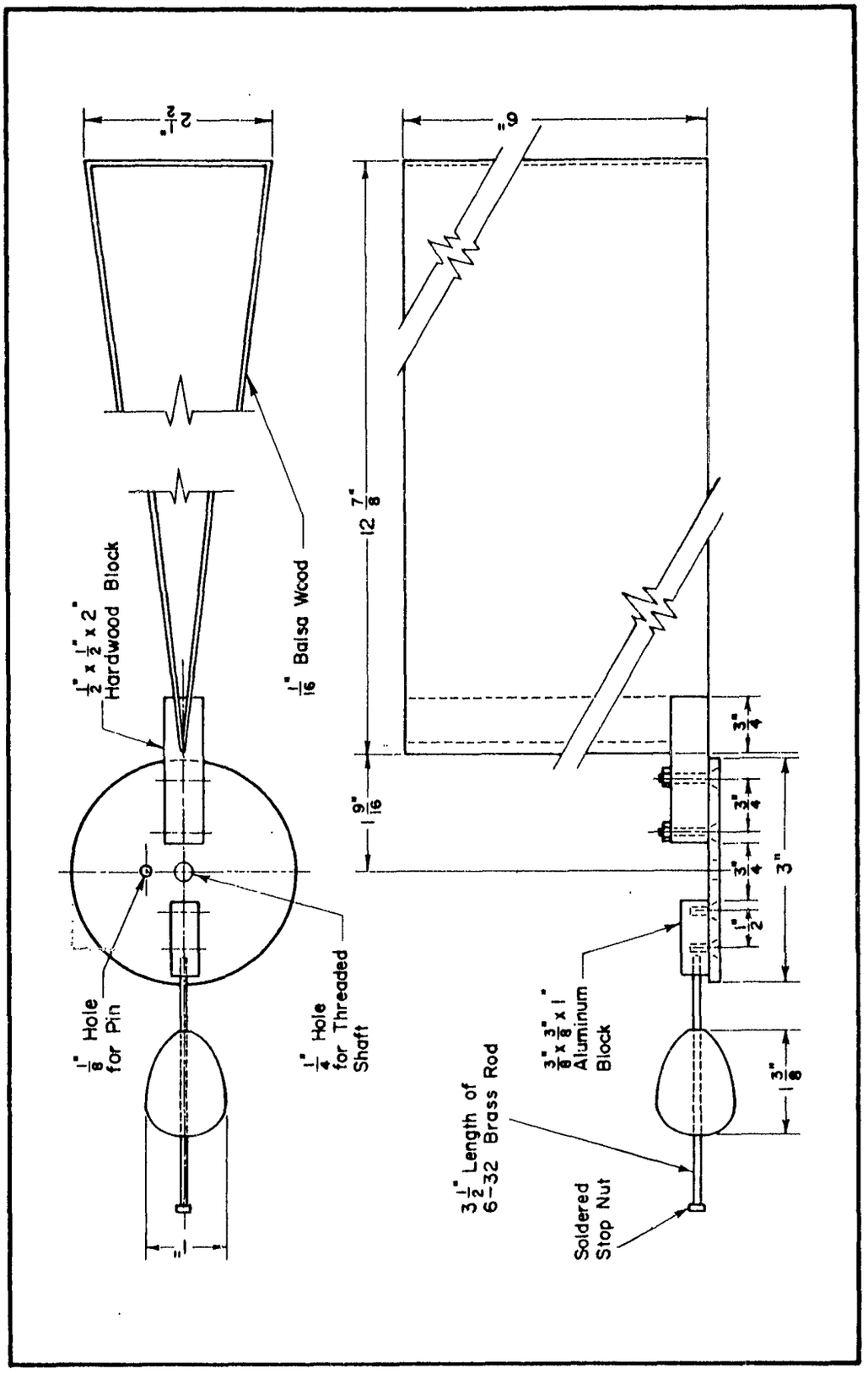

Figure 2.30 The Wind Vane

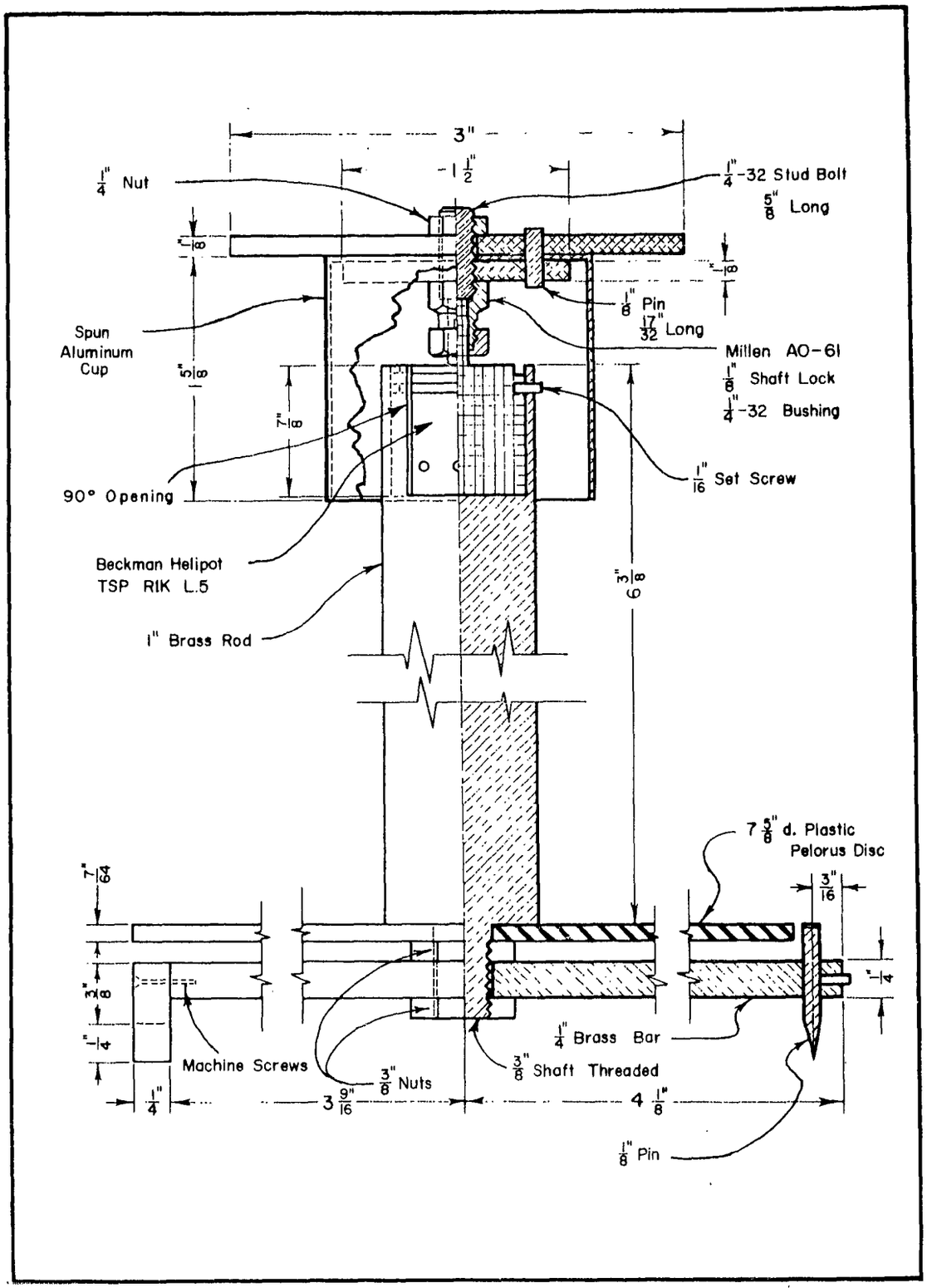

Figure 2.31 The Mounting of the Potentiometer and Pelorus

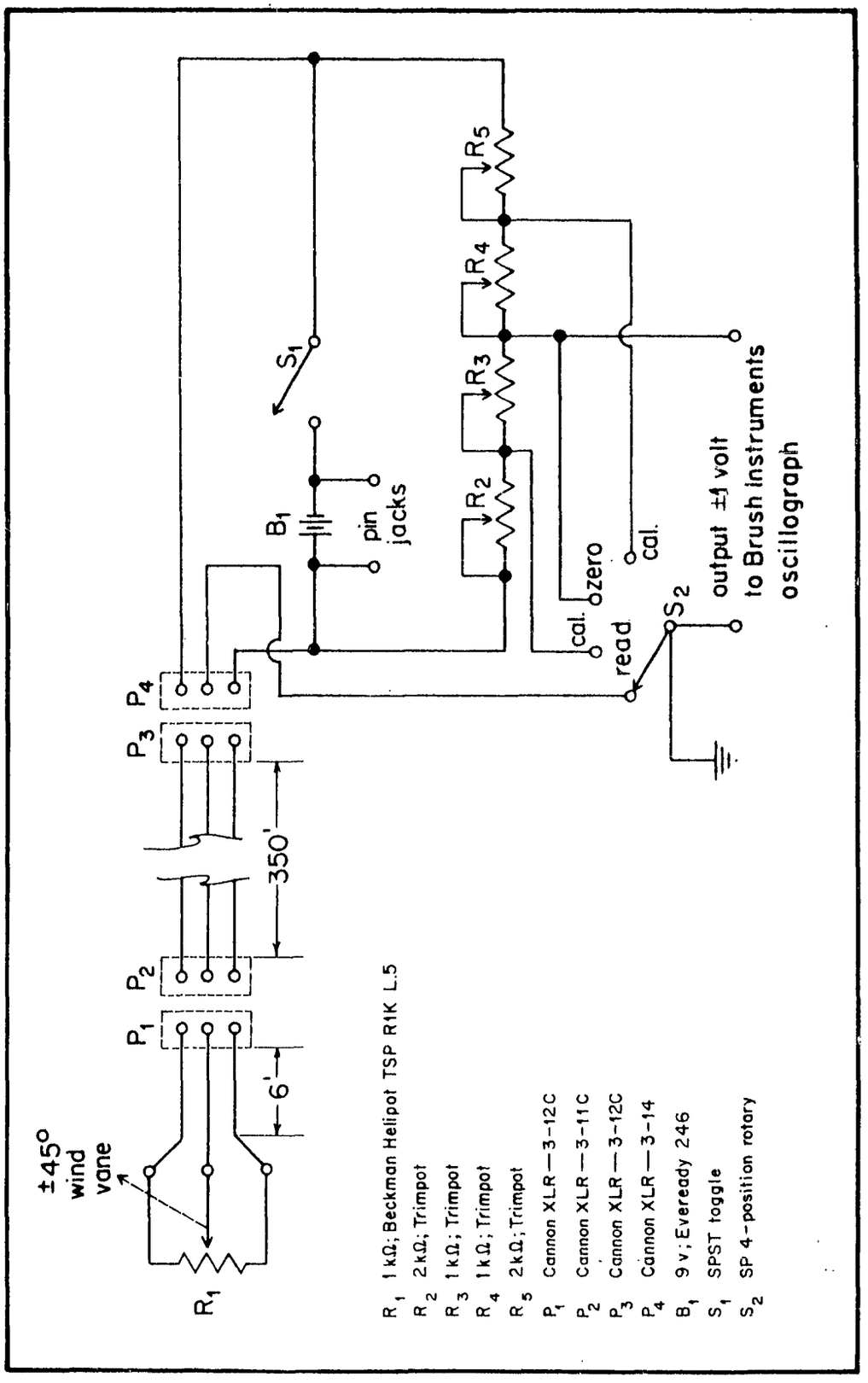

Figure 2.32 Circuit Diagram of the Wind Vane

vane produces at least the 2-volt signal required by the oscillograph by connecting a 9-volt battery across the potentiometer. The ±1-volt signal is taken off between the potentiometer contact and the center of a voltage divider in parallel with the potentiometer coil. The oscillograph has a zero offset large enough to make exact positioning of the potentiometer housing unnecessary, but the wind direction must not exceed ± 135° from the potentiometer zero setting.

As with the anemometers, provision for entering reference lines on the chart paper was made. Three values could be selected with one switch: -45°, 0°, and +45°. These were used for setting the oscillograph gain and zero adjustments. The voltages necessary to do this come from the voltage divider, which is made of four adjustable resistors.

In the field the zero of the instrument, which is located at a known position in relation to the pelorus disc, is set centrally toward the sector of usable wind. Its orientation is determined by taking the angle between the desired direction and some prominent landmark as measured from the location of the tower. The adjustable sight below the pelorus disc is locked at this angle, and a bearing is taken on the landmark while the wind vane is being mounted on its support arm. This bearing could be made after each vertical adjustment of the anemometer mast but it is simpler to mark a vertical reference line on the anemometer mast and another on the sleeve of the support clamp. By aligning these, the orientation of the wind vane can be maintained. During the July cruise the wind vane was set at 5 feet above mean water level and in November it was set at 6 feet.

Before each record was made, the switch was set at "calibrate," the zero was centered in the recording channel, and the gain was adjusted

so that ±45° corresponded to the outside lines of the recording channel. The switch was then turned to "read." If the wind direction was such that the trace remained within the channel, then the adjustment was satisfactory. If the trace fell outside the channel, the zero was repositioned without altering the gain adjustment.

The minimum wind speed necessary to move the vane may be very roughly estimated from the relationship

$L = C_L(1/2)\rho v^2 A$ using Kutta's value for a thin flat plate

$C_L = 2\pi \sin B$, as given in Binder (1955).

A brief calculation shows that for a wind of 1 meter per second and a deflection of 1° the restoring torque is 1.33×10^4 dyne-cm. Since 0.005 oz-in is 3.55×10^3 dyne-cm, the indication is that the vane is sufficiently sensitive. In practice the vane seemed to be following wind direction shifts of several degrees in a few tenths of a second.

To locate the zero position according to the pelorus, the wind vane was mounted in the 25-inch-square working section of a wind tunnel. A 10-minute record made on a Varian recorder partly at high and partly at low wind speeds showed that the pelorus zero corresponded to 4.1° on the instrument. There was a small erratic quiver about the mean which was more frequent at the high than at the low wind speed. Its range was about ±0.45°.

The wind direction values were read to the nearest degree every 0.1 second, and only means, variances, and frequency sorts were calculated. For these crude operations the wind vane seems to be adequate.

Figure 2.33 shows a typical section of a field record. The left-hand margin carries the 0.1-second timing pips. The heavy lines and

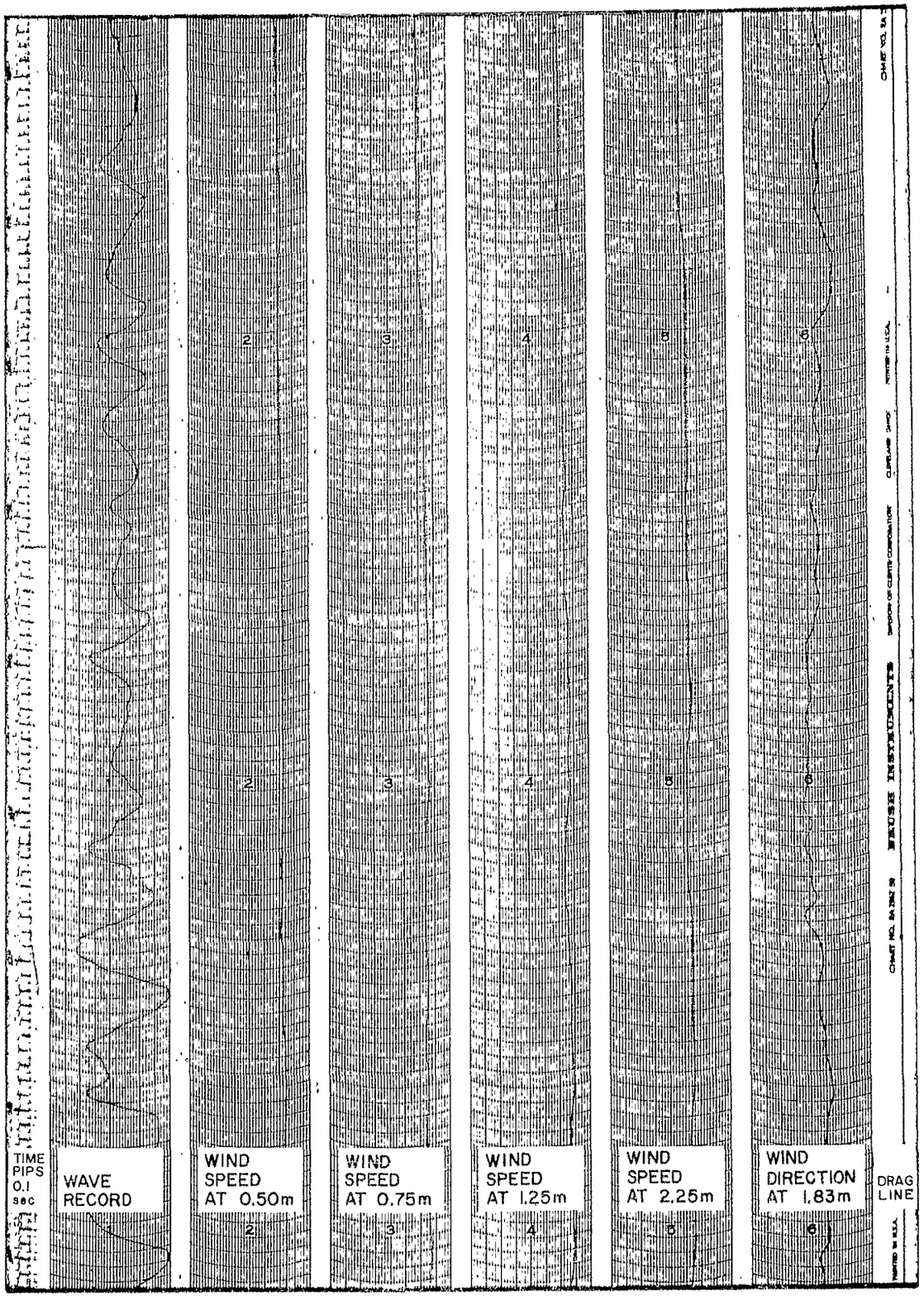

Figure 2.33 Section of a Typical Field Record

the numbers were entered by hand to make reading every 0.2 second easier and more certain. The time was judged by the fine tails beneath the heavy marks. The content of each channel is indicated on the figure. The right-hand margin shows the drag line used to judge paper creep. The chart paper is printed in light orange; the traces are black.

2.5 The Time-Lapse Camera

A time-lapse camera was mounted on the tower about 3 feet above mean water level and pointed directly downward (figure 2.3). It was hoped to get some idea of the nonlinearity of the process by determining the average fraction of the picture area covered by breaking processes for various wind speeds and fetches. The camera was a Keystone 16-mm A-12 Criterion Deluxe, Serial No. 540671, equipped with CINOR 1:1.9 F = 10 and Keystone-Elgeet 1 inch f = 1.9 lenses. At 3 feet using the 10-mm lens the field has an area of about one-third of a square meter. The time-lapse mechanism, which provides rates ranging from one frame every 1.5 seconds to one frame every 15 seconds, was made by Meteorology Research, Inc., Pasadena, California. It is battery operated and was originally designed for cloud studies. The only modification made was to add a switch on a 350-foot cable so that the camera could be turned on and off from the MAURY. Good quality cable was necessary; the lamp cord used at first soaked through and short-circuited within a day. The entire camera and mechanism was mounted on the tower and protected from rain by a plastic hood. Eastman Daylight Kodachrome film was used. For each record, at the time the wave probe and anemometer heights were adjusted a few frames were exposed showing a board with the date and record number. Pictures were made at the rate of one frame every 3 seconds concurrently with the 5-minute wave records.

No usable results were secured from the camera. The position of the mount brought the probe cables into the field. These cables generated numerous foam flecks that were impossible to distinguish from small breaking waves. The pictures, taken perpendicular to the water surface, were so lacking in definition that they were nearly impossible to read. Something might be done with this idea, but it would seem advisable, in addition to mounting the camera to give an unbroken upwind view, to provide strong artificial side lighting to heighten the relief, and to shoot at a fast enough rate so that individual wave features could be traced from frame to frame. This latter change would help to identify foam patches, floating leaves, and other extraneous objects.

2.6 The Thermometers

During the July cruise water temperatures were measured from the MAURY with a conventional bucket thermometer. The air temperatures were measured in a shaded upwind position on the MAURY's deck using one of the thermistor temperature-measuring devices constructed at the Chesapeake Bay Institute (figure 2.34).

During the November cruise more elaborate temperature measurements were made using three of the thermistor units. To adapt two of them for use in air, the Veco 32A1 thermistor probe was potted in Wood's alloy, thus increasing the response time (63%) in air to about four minutes and limiting the self-heating to a negligible value. Shields consisting of parallel plates blackened on the inside and coated with zinc oxide on the outside were placed above and below each sensing element (figure 2.35a,b). To avoid possible interference from the ship, these probes were supported on a mast attached to a life raft which was anchored about 50 feet to windward of the MAURY (figure 2.35c). Had

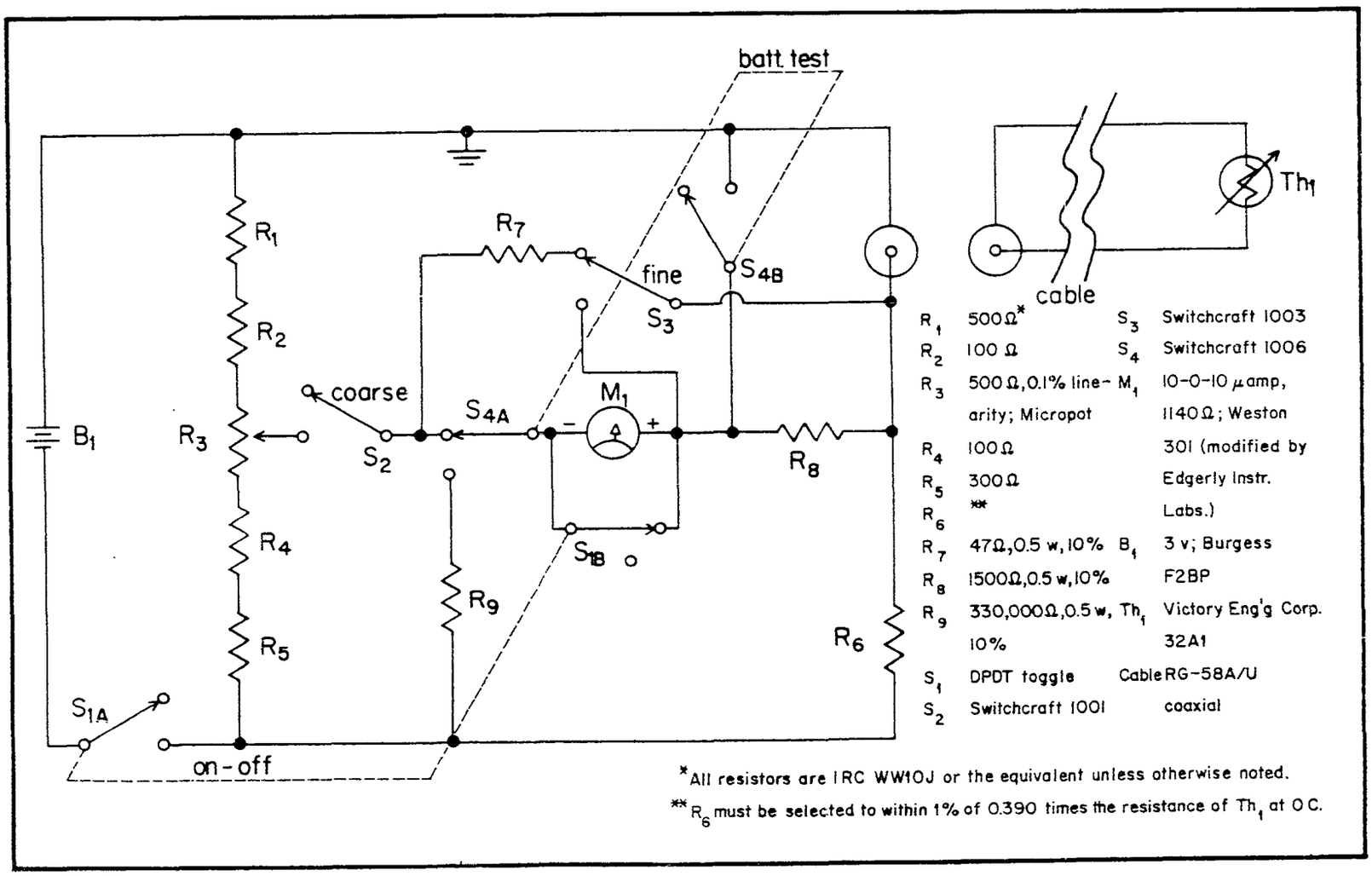

Figure 2.34 Circuit Diagram of the CBI Thermistor Bridge

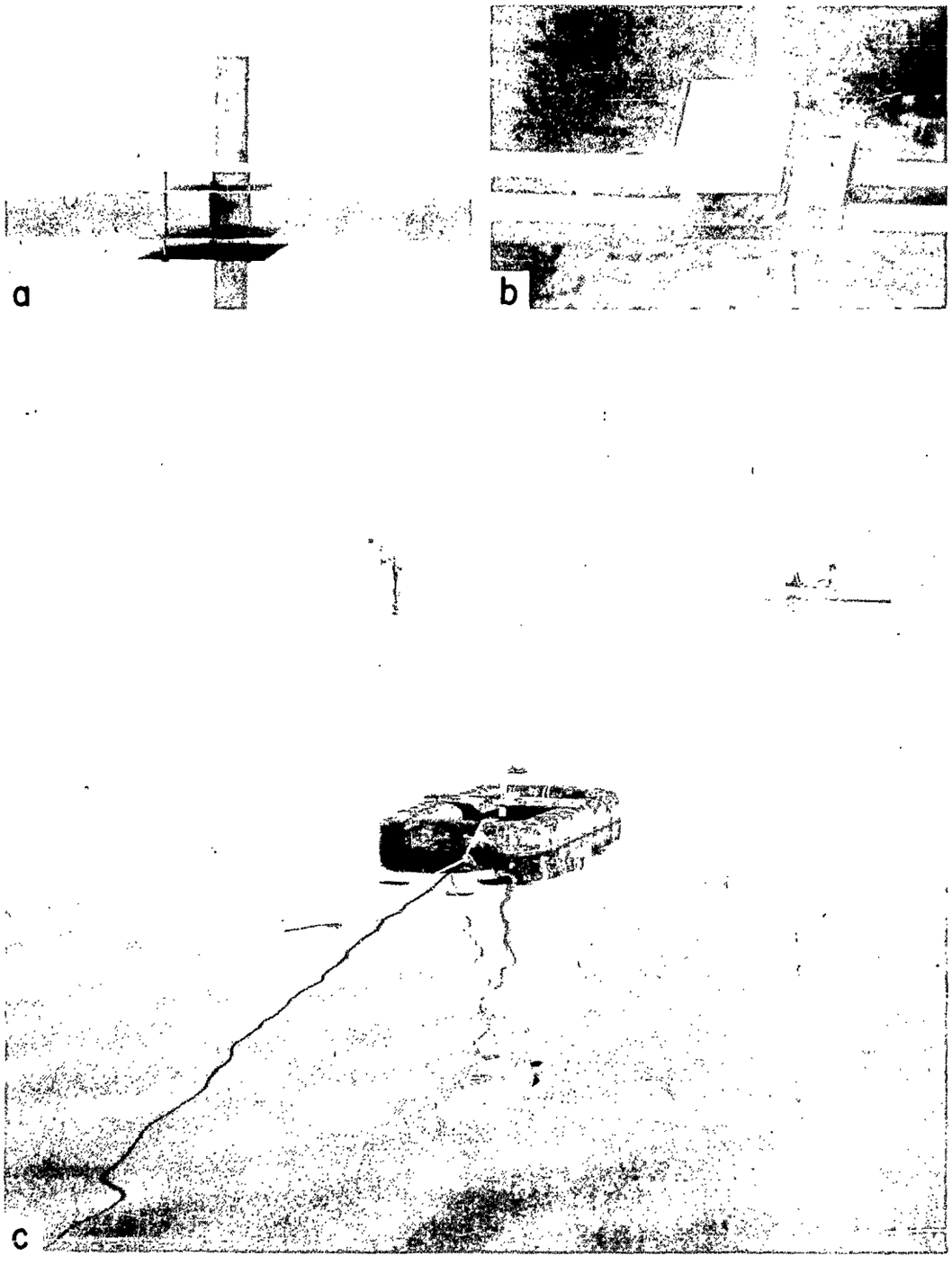

Figure 2.35 Thermistor Mounting and Shield

there been time to make up 350-foot cables and recalibrate the thermistors, they could have been mounted on the tower. The levels at which the probes were set corresponded to the highest (225 cm) and lowest (50 cm) anemometers.

The third thermistor was suspended an inch or two below the water surface by thrusting it through a 1-foot-square styrofoam float. Unfortunately, the shank of this thermistor had been broken. A jury rig held it together and a coating of silicone grease made it watertight, but the grease had to be renewed periodically. Surface temperatures were also taken with the bucket thermometer as before. When both thermistor and bucket temperatures are available, they differ systematically by about 0.14 C.

During the 5 minutes that a wave record was being made, each of the three thermistors (two when the broken one was not working) was read in turn, the cycle being repeated as many times as possible during the 5-minute interval. (Since all the oscillograph channels were already in use, these results had to be logged by hand.) Thus the temperatures reported are averages of from 9 to 17 values sampled at approximately equal intervals over a 5-minute period.

2.7 The Induction-Conductivity-Temperature-Indicator

To form some idea of the density structure of the water, salinity and water-temperature depth profiles were secured with the CBI-ICTI. This instrument is an induction-conductivity-temperature-indicator, and a description of it may be found in Esterson (1957). It is the standard field instrument of the Chesapeake Bay Institute for such work.

During the July cruise four lowerings were made from the deck of the MAURY. Unfortunately, the ICTI requires that the ship's generator be turned off, while the wave probe requires a continuous source of current. Since water level was our primary concern, the generator was kept running. Thus the July profiles must be considered qualitative at best. During the November cruise we were fortunate in having the cooperation of the R.V. LYDIA-LOUISE II which, with its own ICTI, made a series of eight stations in Round Bay. The station locations and identifications are showed in figure 1.2.

3.0 DATA REDUCTION AND COMPUTATION

3.1 Spectral Measurement

The preliminary plans for this study were guided by the considerations governing spectral calculations discussed by Tukey (1949). A more recent and much more complete treatment is given by Blackman and Tukey (1958). There is an excellent account of the problems involved in using spectral analysis for a band of frequencies rather than for the entire spectrum in Munk, Snodgrass, and Tucker (1959).

In any campaign to measure power spectra three things must be balanced: precision, resolution, and cutoff frequency. Each estimate of the power calculated from a finite record for a particular frequency is actually an estimate of the average power contained in a band centered at the nominal frequency. It is not a point estimate and, according to De Feriet (1954-1955), it never can be, if calculated from a finite piece of record.

The power estimates are evenly spaced on a frequency interval from zero to the Nyquist or folding frequency. The Nyquist frequency is the highest frequency about which the analysis provides information; it is the reciprocal of twice the sampling interval. However, power present in the record at frequencies above the Nyquist frequency is not simply discarded. It is reported erroneously (aliased) at frequencies lower than the Nyquist frequency. Thus in order to get a true concept of the spectrum, the sampling rate must be sufficiently rapid to insure that the record contains no appreciable power at frequencies higher

than the Nyquist frequency. One method is to build a low-pass filter into the sensing instrument and to sample at a rate which will make the Nyquist frequency coincide with the filter cutoff frequency. Another method, the one used in this study, is to estimate the natural cutoff frequency on physical grounds and to test the estimate by setting the Nyquist frequency considerably higher. Since we are studying wind-generated gravity waves, it seemed quite unlikely that oscillations with appreciable power as fast as 2 or 3 cps would be encountered. Thus a sampling interval of 0.1 second corresponding to a Nyquist frequency of 5 cps was chosen.

The next consideration was the resolution desired. Since there was little previous work to hint at the exact form of the spectrum to be encountered, it was felt that quite high resolution was desirable and a power estimate every 0.1 cps from 0 to 5 cps was selected. The auto-correlation function must then be computed to a maximum of 50 lags. Following the common rule of thumb that the maximum lag computed should never exceed 10% of the number of data points in the record, this gives a minimum record length of 500 sample points or 50 seconds.

To determine a good record length more precisely, we can calculate an estimate of the number of degrees of freedom for each power estimate. The power estimates upon repeated sampling have essentially a chi-square distribution with

$$k = \frac{2N'}{m} \text{ degrees of freedom, according to Tukey (1949),}$$

where $N' \equiv N - 3m/4$,

$N \equiv$ the number of data points in the record, and

$m \equiv$ the maximum lag from which the autocorrelation function is computed if the spectrum is substantially flat.

As N is increased, the number of degrees of freedom and consequently the precision of the estimate of the power increases. So also does the computational labor, and much more rapidly. Furthermore, an unequivocal interpretation of the results requires that the process be quasi-stationary. Thus, in measuring an uncontrolled phenomenon in the field, the apparent gain in precision resulting from very long records is often offset in unknown ways by the changing nature of the process measured. With a chi-square distribution there is a rapid gain in precision up to about 50 degrees of freedom. Beyond 50 degrees of freedom the return for increased record length is much more meager. Consequently, it was decided that any convenient record length yielding more than 50 degrees of freedom would be satisfactory. Solving the equation

$N = m(0.5k + 0.75)$ for N at $m = 50$ and $k = 50$ gives

$N = 1287.50$. Thus any record lasting more than 129 seconds will provide the required degrees of freedom per power estimate. On this basis a 2.5-minute record length was selected. Blackman and Tukey (1958) give a revised estimate of k,

$$k \approx \frac{2T'_n}{T_m}$$

where $T'_n \equiv T_n - T_m/3$,

$T_n \equiv$ the length of the record, and

$T_m \equiv$ the maximum lag. With $k = 50$ and $T_m = 50$ this revised estimate gives

$N = T_n = 1266.50$. With $T_n = 1500$ and $T_m = 50$ it gives $k \approx 60$.

Existing mathematical models for time series incorporate stationarity. Stationary random processes are processes whose statistical properties are time invariant. It is trivial that no geophysical process

can be stationary in the mathematical sense. For the geophysicist the equivalent property is that the statistics of the process change very little during the time that a record is made, whether during 5 minutes or 5 millenia. If this condition obtains, then the mathematical abstraction of stationarity will serve his turn. In order to get evidence on the quasi-stationarity of a 2.5-minute point record of waves, each field record was 5 minutes long. The first 2.5 minutes and the second 2.5 minutes could then be analyzed separately and some judgment formed.

The computations for the eight July records were made according to the scheme just outlined. It turned out that the Nyquist frequency had been set about twice as high as necessary. As can be seen in table 3.1,

Table 3.1 Comparison of the Power Contained Between 2.6 and 5.0 cps with the Total Power in the Spectra of the July Records

Record	Mean Wind at 122 cm	Power from 0.0 to 5.0 cps	Power from 2.6 to 5.0 cps	Relative Power from 2.6 to 5.0 cps
	(m/s)	(cm^2 x 0.2 sec)	(cm^2 x 0.2 sec)	(%)
009	4.66	0.841, 1*	0.240, -1*	0.28
010	5.20	0.896, 1	0.275, -1	0.31
011	5.37	0.108, 2	0.356, -1	0.33
012	4.77	0.851, 1	0.626, -1	0.74
017	4.12	0.328, 1	0.423, -1	1.29
018	3.63	0.411, 1	0.257, -1	0.63
027	4.87	0.387, 1	0.310, -1	0.80
028	4.41	0.381, 1	0.412, -1	1.08

*These numbers are expressed by a 3-digit number μ, $0.100 \leq \mu \leq 0.999$, followed by the power to which the factor 10 must be raised to position correctly the decimal point, e.g.,

$0.138, 2 \equiv 0.138 \times 10^{2} = 13.8,$

$0.709, -1 \equiv 0.709 \times 10^{-1} = 0.0709.$

the power contained at frequencies from 2.6 to 5.0 cps in two-thirds of the cases is less than 1% of the total power in the record. Consequently, it seems safe to set the Nyquist frequency at 2.5 cps by reading the records at an interval of 0.2 second. In using this reading interval, if the record length is maintained at 2.5 minutes, the maximum lag that must be computed to give an estimate at each 0.1 cps is 25. The degrees of freedom per estimate computed according to Blackman and Tukey (1958) will be about 59. All the results for the November records were calculated with these choices, materially reducing the labor involved.

3.2 Data Reduction

The physical problem of simply reading the records, before any calculation could start, was so unwieldy as to make ordinary reading by eye too formidable to consider. The eight test records from July totaled approximately 45 meters of chart paper carrying five traces which had to be read every 2.5 mm, a matter of 90,000 data points. The November sequence treated here consists of 16 records amounting to 60 meters of chart paper carrying six traces which had to be read every 5.0 mm, giving 72,000 data points. Some mechanical aid was obviously necessary.

We were fortunate in having at our disposal an OSCAR J oscillograph trace reader made by the Benson-Lehner Corporation, Los Angeles, California. This machine consists of a reading area which can hold oscillograph records up to 40 cm wide. The record is spooled on both sides of the machine and is reeled across the working area 50 cm at a time for reading. The reading device or head consists of two pieces: a cursor is scribed on clear plastic and lies across the oscillograph grid perpendicular to its length; on top of the cursor is a translucent overlay which moves laterally over the cursor. There are two controls

and a trigger switch on the base of the reading head. The left-hand control positions the cursor. When time pips have been entered on the chart paper, as in our case, positioning the cursor is very easy and rapid. The right-hand control moves the reading overlay over the cursor through about 3 inches. A new blank overlay is used for each record. The overlay control is attached to a digitizing potentiometer which distributes the digits from 000 to 999 evenly over the 3 inches of travel. To make a reading curve it is necessary to know only the values to be attached to the lines of the chart paper. The control is adjusted by trial and error until the OSCAR J gives the desired value for a particular line; then a point is penciled in on the overlay at the intersection of the line and the cursor. The process is repeated for the other chart lines until enough points have been entered to draw a smooth curve. The trace can then be digitized by aligning the reading curve drawn on the overlay with the intersection of the trace and the cursor. For a grid with six traces a single overlay can carry six reading curves and each may be different.

After the reading curves have been made, the OSCAR J is switched from "set" to "read," and the cursor is set at the first time position to be read. The reading curve is aligned on the intersection of the trace and cursor in the first channel and the trigger switch pressed. At this point several things happen. The digital value is displayed on a light bank; it is also typed out automatically by an attached typewriter; most important, it is punched on an IBM card. This IBM card has already been inserted in the keypunch and punched with the project and record identification. At the first depression of the trigger switch the ordinal number of the time slice is entered, then the measured value. The reading curve is then positioned for the second channel and the trigger switch pressed. The OSCAR J enters this measurement in another field on the same card, simultaneously displaying and typing it. This procedure is

repeated until all the channels have been read; then the card is ejected from the keypunch, a new card is drawn in and coded, and the time-slice number is automatically advanced by one. We have found that about 5,000 data points can be digitized in a normal working day. In emergencies production has been forced above 14,000 for a single day.

In reading the wave traces a linear reading curve was used that went from 100 to 900 over the 40-mm channel width. This means that the OSCAR J was asked to distinguish among 20 different trace positions within each millimeter. Inevitably noise was introduced. To form some idea of this noise an artificial record was made consisting of 11 straight line segments with slopes of 4, 2, 1, 0.5, 0.25, 0, -0.25, -0.5, -1, -2, and -4. Each of the segments was read 120 times with a 100-to-900 linear reading curve at each of nine positions evenly spaced across the chart paper. For each of the 99 resulting sets of 120 repeated readings the variance was computed. As it happened, reading at the edges of the channel seemed to be abnormally easy for the operator so the outside values were discarded. The seven remaining variances for each slope were then averaged. The average variance for the lines with steep slopes (4, -4) was about 0.0546 cm^2. From this value it decreased with shallower slopes to a low of 0.0119 cm^2 for the 0-slope line. The average of the average variances over all slopes was 0.0250 cm^2. It is interesting to compare this value with the values showed in table 3.1 which are total variances (0.0 to 5.0 cps) and variances associated with spectral frequencies from 2.6 to 5.0 cps. If we assume that the frequency does not affect the ease of reading, and it is hard to see that it would at the chart speed and reading intervals used, then perhaps the reading variance may be reasonably distributed evenly over all frequencies. Since 2.6 to 5.0 cps is half the spectral range, the average variance due to reading noise over this range would be about 0.0125 cm^2 x 0.2 second. Thus a sizable portion of the values showed in table 3.1 may be due to reading noise alone.

In handling such large amounts of data it is necessary to guard against gross error due to such factors as mechanical failure and operator fatigue. Simply scanning the hard copy from the typewriter or a printout of the finished cards proved to be unsatisfactory and consumed an inordinate amount of time. The solution finally adopted was two independent readings of each record. A roll of chart paper containing two consecutive records would be set up and digitized. The keypunch was programed to enter the results in the first half of each IBM card. The roll was then read again with the keypunch programed to enter the results in the second half of the same cards. The final result was thus a deck of IBM cards carrying identical identification and time-slice numbers in two places on each card, each followed by six fields containing the digitized data points in parallel. If the reading were perfect, the duplicate fields would be identical. Each deck of cards was then run through an IBM 650 which performed a number of operations. It first checked the identification and time-slice numbers to be sure that they were in fact identical and that the time-slice numbers were in sequence. It then found the differences between the parallel pairs of data points and with these differences computed the mean and k times the standard deviation of the differences for each channel, where k is any number selected. This information was then used in two ways. The IBM 650 flagged any difference in any channel which exceeded $k\sigma$, and the computed values and a table of the differences were printed out for each channel. With this information in hand, the records were put back on the OSCAR J, the flagged points carefully reread, and new cards made to replace the questionable ones. If very few flagged points occurred, then a new k smaller than the original was chosen, and the difference printouts were scanned for differences greater than the new limit. These points were checked and again new cards were made. The extent to which this reduction in gross reading error is carried depends upon the amount of effort that is available. We felt that a program that questioned about one point per hundred read was about right for us.

Upon completing this check of gross reading error, we put the clean decks through the IBM 650 which averaged the pairs of readings and rearranged these averages, punching 20 data points to a card and entering each channel on a separate deck. It is these averaged values rescaled to standard units which are given in appendix II* and which are the input data for all calculations.

Perhaps a word is in order about why nonstandard units, which we called "Oscars," were used instead of standard units. While familiarizing ourselves with the OSCAR J, we realized that the operator, contrary to our expectations, seemed to be able to read with greater precision when the digit density was high. To explore this phenomenon, a point on a straight line was read 120 times with each of 11 reading curves. The reading curves were linear and had digit densities of 1, 2, 4, 8, 16, 32, 64, 128, 256, 512, and 1,000 digits/mm. The standard deviations of each of these 11 attempts to read a single value were computed. The numerical values of these standard deviations did, of course, increase with digit density. However, when they were translated into millimeters of chart paper represented, they showed a sectional log-log decrease with digit density. Apparently an increase in the sensitivity of the reading curve permits the operator to make finer discriminations down to a standard deviation of about 0.1 mm at about 20 digits/mm. The operator's skill and judgment are apparently unable to take advantage of a further increase in the sensitivity. (The apparent increase in precision at 1,000 digits/mm is probably accounted for by the fact that only 1,000 digits are available on the OSCAR J.) Consequently, to take full advantage of the operator-cum-OSCAR J system, reading curves should, wherever possible, have a density of at least 20 digits/mm. The

*These data are stored on IBM cards at the Chesapeake Bay Institute. Any nonprofit research organization wishing to use these data may have duplicate decks at cost.

peculiarities of the reading system that led to this decision are clearly visible in figure 3.1.

If the standard unit in which a quantity is measured does not provide at least 20 digits/mm, then during the reading a nonstandard "Oscar" unit which does provide at least 20 digits/mm is used. We thus gain the realizable precision of the system. For final presentation these "Oscar" units are scaled to standard units.

3.3 Computer Programs

The computing for this study was done at New York University on their digital computers under the supervision of Mr. Emanuel Mehr; he developed all the programs used with the exception of the spectrum program which was already available. The inputs for all the programs were the averaged packed data on the sets of cards described earlier. The programs used are described briefly here:

1) The pair program takes two records and, channel by channel, computes the mean, standard deviation, and variance for each record separately, converting the final results to standard units. It then computes the same parameters for the two records combined and considered as a single record. This program is applied to all channels.

2) The frequency program makes a frequency sort of the data from any channel of a single record into six predetermined sort intervals. It gives the results as actual counts and as per cent frequency. It also combines records by pairs. This program was used for wind direction only.

3) The $\sigma/2$ frequency program takes the data for any channel from one

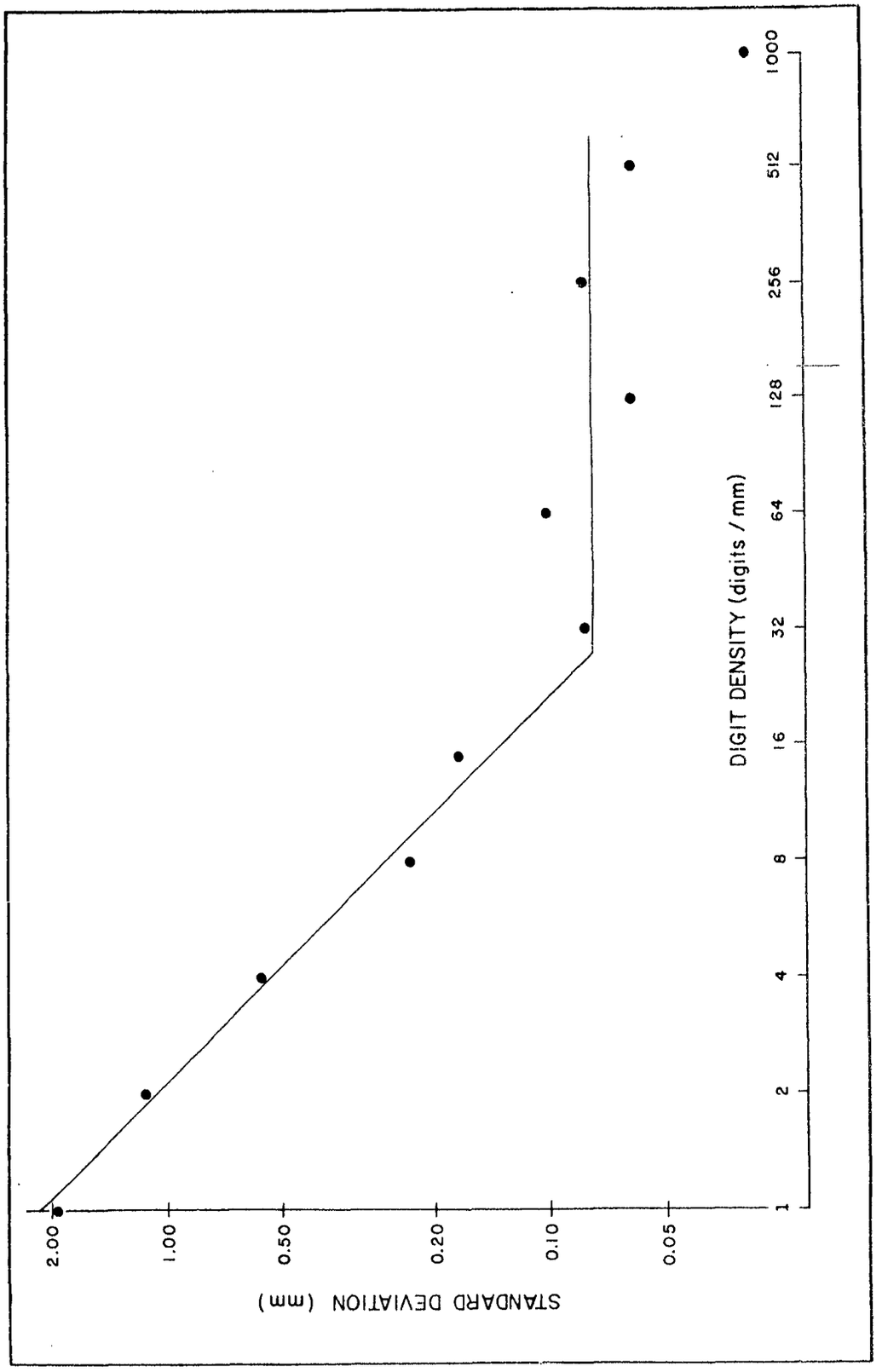

Figure 3.1 Digit Density vs. Standard Deviation of Repeated Readings with the OSCAR J

record and computes the mean and the standard deviation of the data. Then it sets up 18 sort intervals, each half the standard deviation wide, 9 on each side of the mean. Finally, it makes a frequency sort of the data into these intervals and gives its results both as actual counts and as per cent frequency. This program was applied to all channels.

4) The flip-flop program uses the sort intervals generated by the $\sigma/2$ frequency program. It locates the relative maxima and relative minima in the data and sorts them separately into these intervals. The results are reported both as actual counts and as per cent frequency. This program was applied to the wave records.

5) The spectrum program of New York University (ECU014) obtains spectra from empirical data by forming the autocorrelation function R_k, computing the Fourier cosine transform L_n, and forming weighted averages to get a smoothed function U_n. The computed relations follow.

$$R_k = \frac{1}{N-k} \sum_{i=1}^{N-k} x_i \, x_{i+k} \qquad k = 0,\ 1,\ 2, \ldots M'$$

$$L_0 = \frac{1}{M'} \left[\frac{1}{2} (R_0 + R_{M'}) + \sum_{k=1}^{M'-1} R_k \right]$$

$$L_n = \frac{2}{M'} \left\{ \frac{1}{2} \left[R_0 + (-1)^n R_{M'} \right] + \sum_{k=1}^{M'-1} R_k \cos \frac{\pi k n}{M'} \right\}$$

$$n = 1,\ 2,\ 3, \ldots M' - 1$$

$$L_{M'} = \frac{1}{M'} \left\{ \frac{1}{2} \left[R_0 + (-1)^{M'} R_{M'} \right] + \sum_{k=1}^{M'-1} (-1)^k R_k \right\}$$

$$U_n = \sum_{i=0}^{M'} a_{n,i} \, L_n \qquad n = 1,\ 2,\ 3, \ldots M' - 1$$

where $a_{n,n-1} = 0.23$

$a_{n,n} = 0.54$

$a_{n,n+1} = 0.23$

$a_{n,i} = 0$ for $i \neq n-1, n, n+1$

$N \leq 4000$

$M \leq 400$

$M' \leq M$

6) The cospectrum and quadrature spectrum program of New York University (ECU015) obtains cross-spectra from empirical data by forming the cross-correlation functions S_k^+ and S_k^-, computing the Fourier cosine transform C_n for S_k^+ and the Fourier sine transform Q_n for S_k^-, and taking weighted averages of C_n and Q_n to get smoothed functions UC_n and UQ_n. The relations are computed for the paired sequences of data $x_1, x_2, x_3, \ldots x_N; y_1, y_2, y_3, \ldots y_N$.

$$S_k^+ = \frac{1}{2(N-k)} \sum_{i=1}^{N-k} (x_i y_{i+k} + x_{i+k} y_i) \qquad k = 0, 1, 2, \ldots M'$$

$$S_k^- = \frac{1}{2(N-k)} \sum_{i=1}^{N-k} (x_i y_{i+k} - x_{i+k} y_i) \qquad k = 0, 1, 2, \ldots M'$$

$$C_0 = \frac{1}{M'} \left[\frac{1}{2} (S_0^+ + S_{M'}^+) + \sum_{k=1}^{M'-1} S_k^+ \right]$$

$$C_n = \frac{2}{M'} \left\{ \frac{1}{2} \left[S_0^+ + (-1)^n S_{M'}^+ \right] + \sum_{k=1}^{M'-1} S_k \cos \frac{\pi k n}{M'} \right\}$$

$$n = 1, 2, 3, \ldots M' - 1$$

$$C_{M'} = \frac{1}{M'} \left\{ \frac{1}{2} \left[S_0^+ + (-1)^{M'} S_{M'}^+ \right] + \sum_{k=1}^{M'-1} (-1)^k S_k^+ \right\}$$

$$Q_0 = 0$$

$$Q_n = \frac{2}{M'} \sum_{k=1}^{M'-1} S_k \sin \frac{\pi k n}{M'} \qquad n = 1, 2, 3, \ldots M' - 1$$

$$Q_{M'} = 0$$

$$UC_n = \sum_{i=0}^{M'} a_{n,i} C_n \qquad n = 1, 2, 3, \ldots M' - 1$$

$$UQ_n = \sum_{i=0}^{M'} a_{n,i} Q_n \qquad n = 1, 2, 3, \ldots M' - 1$$

where $a_{n,n-1} = 0.23$

$a_{n,n} = 0.54$

$a_{n,n+1} = 0.23$

$a_{n,i} = 0$ for $i \neq n - 1, n, n + 1$

$N \leq 4000$

$M \leq 400$

$M' \leq M$

7) The post spectrum program uses as its input the results of the spectrum program and the cospectrum and quadrature spectrum program. It changes the units expressed in "Oscars" to standard units, computes the degrees of freedom per estimate according to Blackman and Tukey (1958), and uses the corresponding factors given in that reference to compute the 10%, 50%, and 90% confidence limits for each spectral estimate. Whenever cospectra and quadrature spectra have been computed, it calculates the coherence, the phase shift, the transfer function, and the modulus; it also provides cospectra and quadrature spectra scaled by one of the spectra. The post spectrum program was used on all data for which spectra were calculated.

8) The data-edit program takes the primary data, converts them to standard units, and tabulates them. While doing so it also computes the first four moments about the mean, the mean, the standard deviation, the skewness, and the kurtosis. (These momental operations are also available separately as an IBM 650 program.) This program was used with all the data.

4.0 THE FIELD EXPERIENCE

4.1 Operating Conditions

The field procedure was to select a likely position for the probes, set them up, and then just wait until the wind blew from the right direction. Once a wind system and wave system were established, 5-minute records were taken every half hour as long as conditions held. This is a rather tedious procedure, but it does have the advantage that at the time a record is started the previous conditions are known and considered satisfactory.

The R.V. MAURY served as a floating laboratory and living quarters during the operation. It has bunks for seven people and requires a crew of three: captain, deckhand, and cook. A senior scientist, an electrical engineer, and a technician made up the complement. The laboratory and sleeping and eating facilities were adequate. The chief difficulty arose from the fact that the MAURY is quite small (68 feet). As a result there is no ward room where the crew can be comfortable when neither working nor sleeping. The "wait it out" technique inevitably entails long periods when there is nothing to be done. This was met to some extent by using the skiff for recreational excursions and SCUBA diving and by giving part of the crew a turn ashore when the wind was persistently in the wrong quarter. Even with these palliatives 5 days was long enough to operate in these cramped quarters without marked deterioration in efficiency and civility.

It proved impossible to keep a continuous watch on conditions with

only one man aboard thoroughly versed in the project's design. One sequence of running every half hour for a 12-hour period completely exhausted the crew. If a 24-hour watch were to be kept, it would be necessary to have at least two complete crews, each composed of a man capable of making the scientific decisions, a technician, and a deck hand. An electrical engineer on 24-hour call to maintain the instruments, a cook, and the captain would still be necessary. We need two more men than the MAURY can accomodate; even then we have only enough for watch and watch, a very exhausting schedule which cannot be maintained with efficiency for any length of time.

Two cruises were made during 1958, one in July which was largely devoted to the instruments, and one in November. The positions occupied during these two cruises are shown in figure 1.2. The July cruise lasted from 15 July through 24 July, 9 days, during which 16 successful runs providing 32 records were made. The November cruise lasted from 4 November through 9 November, 5 days, during which 48 successful runs providing 94 records were made. It would be incorrect to assume that the July cruise encountered unusable conditions for a greater part of its time than did the November cruise. In July much of the time was spent in debugging the instruments and learning how to operate them. For instance, 3 days in July were required to learn how to set the tower and to improve the voltage regulation.

The November cruise can be considered much more typical. The MAURY left the field laboratory about 0700 on 4 November. By mid-afternoon of the same day she was on station with the instruments ready to operate. The wind was adverse during both 4 and 5 November. The wind shifted to a usable direction during the night of 5-6 November and the first run was made at 0800, 6 November. Eighteen runs, 36 records, were made on 6 November, the last at 1630. Actually the wind continued

all night but our personnel were too tired to continue work. Work was resumed at 0825 on 7 November and continued until 1928. By 1950 there was a flat calm. On 8 November there was no usable wind. On 9 November recording began at 0745 and continued until 1152. At 1220 it was decided to discontinue because of general fatigue and excessive interference from week-end power boaters. The MAURY broke station and returned to the field laboratory at about 1600. Thus out of approximately 114 hours during which the instruments were set and functioning, there were about 46 hours of usable wind, i.e., about 40% of the time the wind lay in the sector from 251° to 340° T.

The numbering system adopted for records makes any odd-numbered record the first 2.5 minutes of a run, while the succeeding even number is the second 2.5 minutes of the same run. Table 4.1 lists the records used in this study.

Table 4.1 A List of the Records Included in This Report

Record Number	Date	Time Run Began (EST)	Weather
009 - 010	19 July 1958	0920	sunny, light haze
011 - 012	19 July 1958	1200	haze
017 - 018	19 July 1958	1645	sunny, light haze
027 - 028	23 July 1958	1529	rain
067 - 068	7 Nov 1958	0825	sunny, clear
069 - 070	7 Nov 1958	0929	sunny, clear
075 - 076	7 Nov 1958	1100	sunny, clear
081 - 082	7 Nov 1958	1230	sunny, clear
083 - 084	7 Nov 1958	1300	sunny, clear
085 - 086	7 Nov 1958	1330	sunny, clear
087 - 088	7 Nov 1958	1401	sunny, clear
093 - 094	7 Nov 1958	1530	sunny, clear

The two cruises differed quite markedly in weather characteristics. Perhaps the most obvious difference was in temperature. The temperatures during the July cruise were in the eighties while during November they were in the low fifties. During the July cruise the winds were light and rather variable. In November they tended to set in more strongly and blow for considerable periods in the same direction. There were some showers during the July cruise.

4.2 Temperature and Salinity

The temperature-salinity structure in Round Bay showed marked differences between July and November. Figure 4.1 shows the variation in salinity and temperature with depth, as measured with the ICTI from the MAURY at hourly intervals during the morning of 17 July 1958. They show a water column quite uniform from top to bottom with a temperature about 25 to 26 C and a salinity about 5 to 6‰. The bottom temperature of 21.8 C appearing at 1000 EST may well be an intrusion of cold water associated with the tide. Air temperatures were generally warmer than the water. Figure 4.2, showing the variation of temperature and salinity with depth on the late afternoon of 7 November 1958, presents a very different picture. The water is more saline and the temperature is much lower, although the air was 2 to 3 C colder than the water. Furthermore, the water column is no longer uniform, being both slightly warmer and considerably more saline on the bottom than it is on the top. There remains, however, an upper layer of 5 to 10 feet which is still uniform. Station locations are identified in figure 1.2. Tables 4.2 and 4.3 contain the values plotted in figures 4.1 and 4.2.

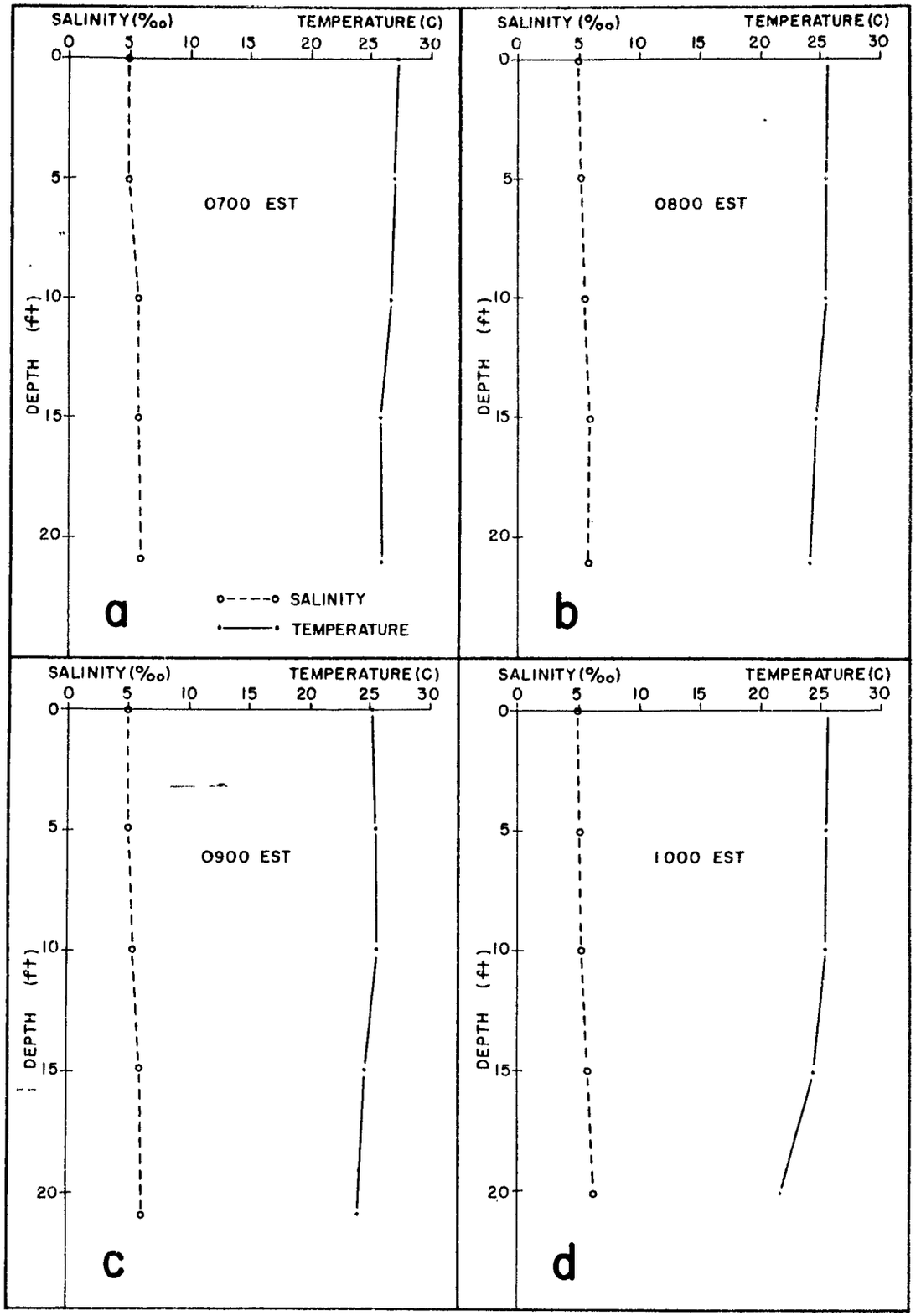

Figure 4.1 ICTI Profiles Measured from the MAURY in July

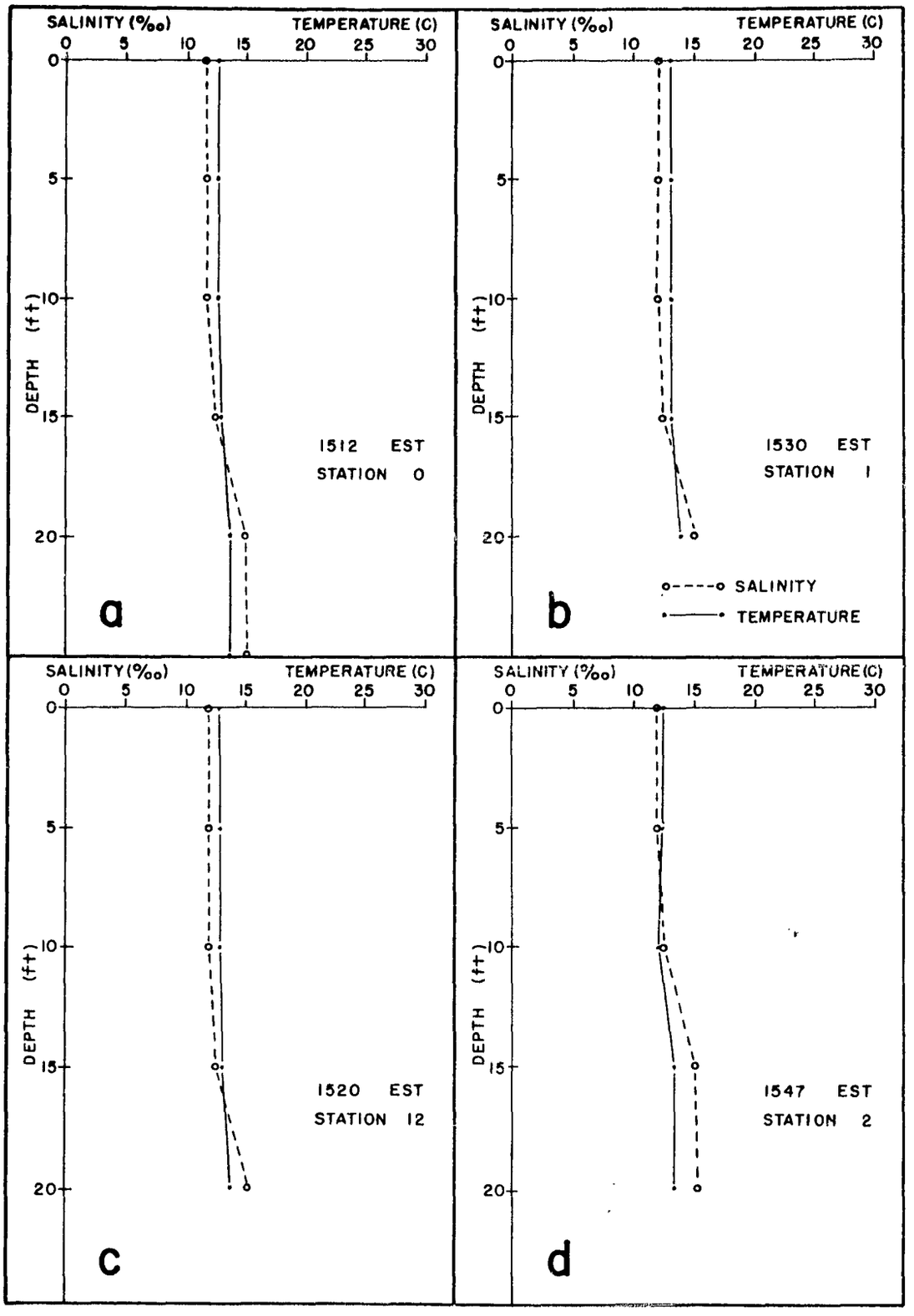

Figure 4.2 ICTI Profiles Measured from the LYDIA-LOUISE II in November (a--d)

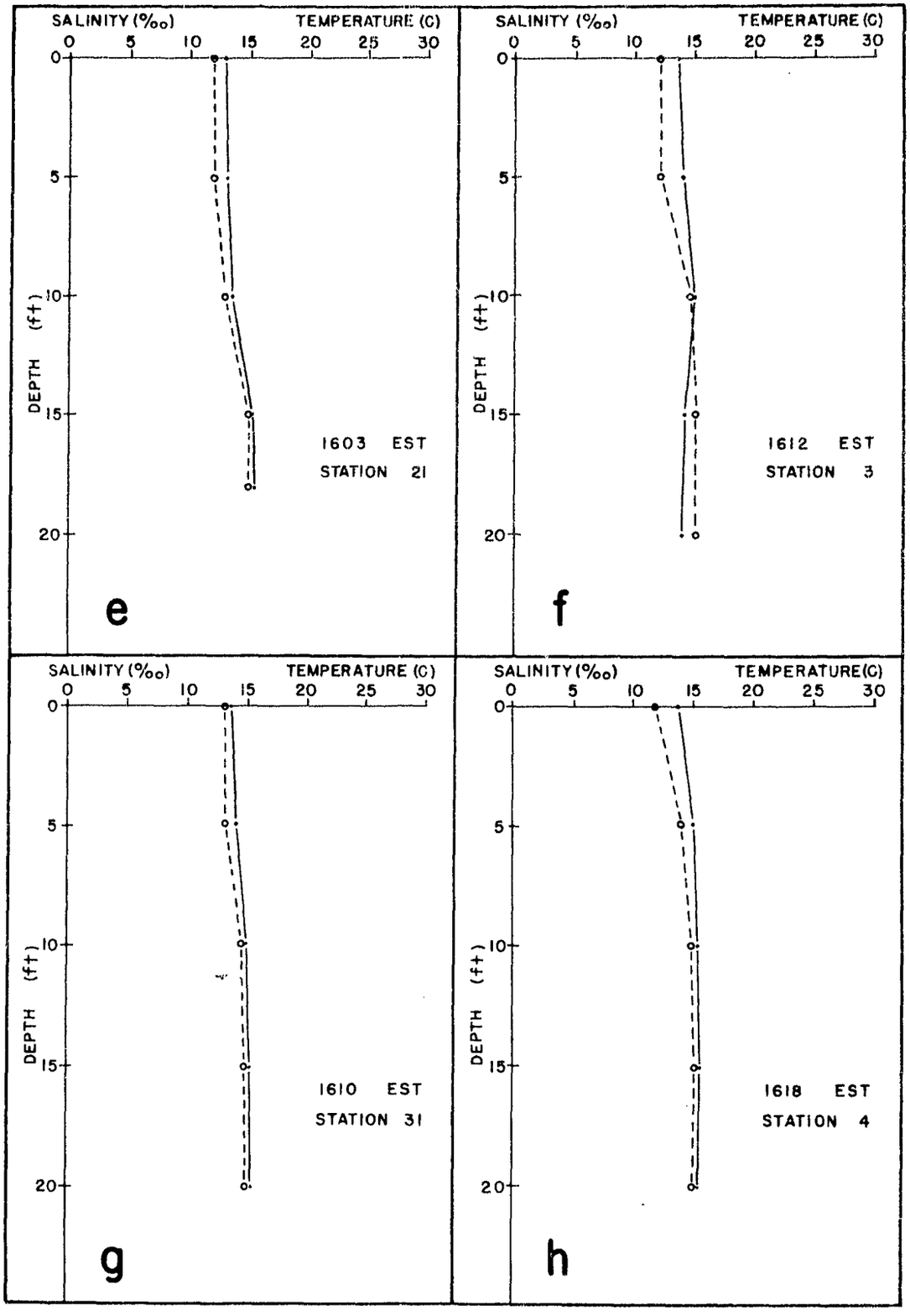

Figure 4.2 ICTI Profiles Measured from the LYDIA-LOUISE II in November (e--h)

Table 4.2 ICTI Measurements from the MAURY in July

Depth (ft)	Salinity (‰)	Temperature (C)	Depth (ft)	Salinity (‰)	Temperature (C)
a 0700 EST			b 0800 EST		
0	4.83	27.34	0	4.96	25.66
5	4.92	27.29	5	5.23	25.63
10	5.55	26.78	10	5.54	25.52
15	5.68	25.82	15	6.00	24.72
21	5.95	26.04	21	6.02	24.45
c 0900 EST			d 1000 EST		
0	5.05	25.56	0	5.05	25.58
5	5.23	25.61	5	5.07	25.60
10	5.45	25.58	10	5.43	25.60
15	5.99	24.89	15	5.97	24.67
21	6.13	24.09	20	6.44	21.85

Table 4.3 ICTI Measurements from the LYDIA-LOUISE II in November

Depth (ft)	Salinity (‰)	Temperature (C)
a Station 0; 1512 EST		
0	11.73	12.73
5	11.73	12.73
10	11.74	12.74
15	12.48	13.06
20	15.03	13.74
25	15.16	13.71
b Station 1; 1530 EST		
0	12.03	13.24
5	12.05	13.24
10	12.03	13.26
15	12.45	13.26
20	14.98	13.95
c Station 12; 1520 EST		
0	11.89	12.78
5	11.91	12.79
10	11.87	12.81
15	12.50	13.04
20	15.21	13.76
d Station 2; 1547 EST		
0	12.02	12.20
5	12.02	12.32
10	13.91	12.16
15	15.05	13.40
20	15.28	13.24
e Station 21; 1603 EST		
0	11.82	12.90
5	12.09	13.16
10	13.03	13.62
15	14.92	15.08
18	15.14	15.32
f Station 3; 1612 EST		
0	11.89	13.56
5	12.25	13.79
10	14.67	14.94
15	14.96	14.21
20	14.96	14.00
g Station 31; 1610 EST		
0	13.04	13.72
5	13.30	14.02
10	14.60	14.84
15	14.96	15.08
20	15.07	15.06
h Station 4; 1618 EST		
0	11.80	13.66
5	13.78	14.96
10	15.14	15.46
15	15.16	15.47
20	15.17	15.48

5.0 THE DENSITY FUNCTION OF THE WATER SURFACE

5.1 The Frequency Distribution

The sea surface has been taken as Gaussian to a good approximation in much recent work, e.g., Pierson (1955), Pierson, Neumann, and James (1955), and St. Denis and Pierson (1953), among others. The assumption has been highly successful for the purposes to which it has been put, i.e., purposes for which the high-frequency clutter on the sea surface is unimportant. For example, in considering the motion of a ship the ripples on the larger waves make no difference to the ship; it effectively averages them out over its length.

A recent paper by MacKay (1959) makes a detailed and exhaustive study of 16 wave records made with bottom pressure recorders. Each record was approximately an hour long and was read every 7.5 seconds. The statistical processing was unusually thorough and careful. After linear trend had been eliminated, the interval of independence was determined. Univariate normality was tested using Student's t, chi-square, Kolmogorov-Smirnov, and Cramér-Von Mises statistics; these univariate statistics were, in turn, analyzed jointly using chi-square. Joint normality was tested using Student's t, chi-square, Fisher-Geary, and Hotelling's T^2; these multivariate statistics were compared, mainly by chi-square. MacKay says, "One record...out of the sixteen analyzed showed some evidence of non-normality. Out of sixteen records, one might expect some such outcome. Joint analysis of the sixteen records gives no indication of non-normality, either univariate or multivariate. It appears, therefore, that the digital observations were actually samples

from stationary Gaussian stochastic processes (after elimination of linear trends).

"If any non-normality is present, it can presumably be detected only by studying observations spaced closer together in time."

The Gaussian nature of the underlying form of the process for the sea surface must be considered well established. That it cannot be strictly Gaussian is obvious for at least two reasons. The process is limited by breaking so that indefinitely high waves are not just highly unlikely; they are physically impossible. More important, however, is the fact that the wave motion must satisfy the nonlinear Bernoulli equation and the free-surface boundary conditions. The modification of the Gaussian structure must occur in the high-frequency components. MacKay's data cannot provide information about these. His records are bottom pressure records on which the hydrostatic effect has already operated to filter out the small, high-frequency components.

A consideration of the modifications made by the high-frequency components in the underlying quasi-Gaussian structure of the sea surface may be of no interest in many engineering and forecasting applications. High-frequency components can take on a vital importance in such problems as sea-return in radar, and they become crucial in the development of adequate models to explain the transfer of energy from wind to waves and the mechanism by which energy is transferred from frequency to frequency in building up a sea. It is hoped that the records analyzed in this paper will provide some guidance in constructing a theory of wave generation.

The records discussed here are surface records not subject to hydrostatic filtering. Surface records are much harder to make than

bottom pressure records and far fewer of them exist. Furthermore, the records discussed here have been digitized at intervals of 0.1 and 0.2 second, which gives a much higher resolution than the 7.5 seconds used by MacKay. It can be expected that they will show some deviation from the Gaussian. The question is how and how much. Our records may be thought of as coming from growing seas arrested at an early stage of their growth. The presence of a windward shore permits the sea to become only partially developed, after which it becomes quasi-stationary in this embryonic form, the stage of the development being controlled by the fetch. In effect, we are interested in a transient state of the open sea whose statistics become accessible because the transient state has been arrested by the fetch limitation.

Frequency sorts were made for each record in intervals of half the standard deviation symmetrically spaced about the mean. Table 5.1 and figure 5.1, plotted on probability paper, are examples of the results for the 24 records. The complete set appears in tables AIII 1.01 to AIII 1.24 and figures AIII 1.01 to AIII 1.24. The ordinates are per cent cumulative frequency and the abcissas are in units of the standard deviation. The line entered is the corresponding Gaussian. From these plots it would appear that the water-level records are substantially Gaussian except for a slight skewing toward high values. This skewing is compatible with the observed fact that surface waves are not symmetrical but have relatively longer and flatter troughs and sharper and more peaked crests. However, these plots must be taken with some caution. It has been our experience that the scale distortion occurring on probability paper leads to a substantially Gaussian appearance for widely differing frequency distributions.

The chi-square distribution offers a ready test of the extent of agreement with the Gaussian. Table 5.2 shows the values of chi-square

Table 5.1 An Example of the Tabulated Frequency Sorts

Sort Interval			
From	To	Frequency (Count)	Frequency (%)
-3.0	-2.5	1	0.13
-2.5	-2.0	14	1.87
-2.0	-1.5	37	4.93
-1.5	-1.0	65	8.67
-1.0	-0.5	100	13.33
-0.5	0.0	171	22.80
0.0	0.5	163	21.73
0.5	1.0	82	10.93
1.0	1.5	58	7.73
1.5	2.0	37	4.93
2.0	2.5	14	1.87
2.5	3.0	8	1.07

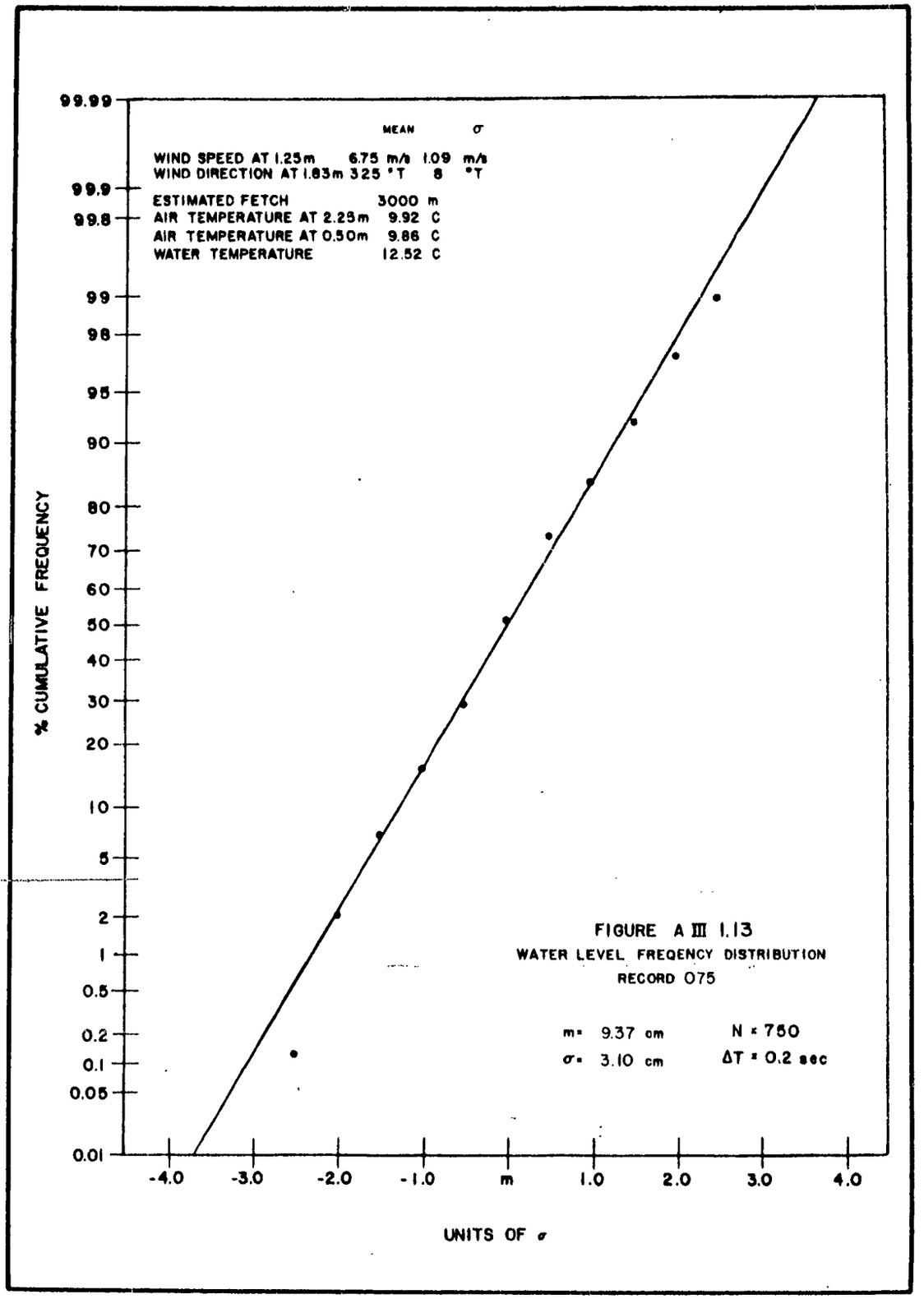

Figure 5.1 An Example of the Plotted Frequency Sorts

Table 5.2 Values of Chi-Square Calculated on the Assumption That the Underlying Distribution is Gaussian

July			November		
Record	Chi-Square	p on 11 df	Record	Chi-Square	p on 11 df
009	42.811	<0.001	067	4.339	0.957
010	32.028	<0.001	068	23.275	0.017
011	52.654	<0.001	069	10.160	0.517
012	30.399	0.002	070	10.670	0.474
017	38.999	<0.001	075	25.963	0.008
018	54.117	<0.001	076	13.690	0.254
027	60.271	<0.001	081	13.672	0.255
028	51.328	<0.001	082	7.746	0.735
			083	20.339	0.043
			084	7.935	0.718
			085	15.671	0.161
			086	16.844	0.116
			087	18.503	0.074
			088	21.544	0.031
			093	26.541	0.008
			094	23.971	0.014

and the associated probabilities for each record calculated on the assumption that they are random samples from a Gaussian process. It is evident that with the exception of record 067 these records do not correspond particularly well to the Gaussian. However, what is most striking is that the records made in July and those made in November form two different sets. This might well be expected on physical grounds. Tables 5.3 and 5.4 show the results of the pair program. Tables 5.5 and 5.6 show the air-sea temperature differences. Tables 5.7 and 5.8 show the frequency sorts for wind direction. The estimated fetches were obtained by using as a weighting factor the fraction of time the recorded wind direction lay in each fetch sector (figures 1.3 and 1.4) and averaging over the sector lengths. Table 5.9 shows the means for July and November.

Table 5.9 Mean Physical Parameters for the July and November Records

	July	November
Mean anemometer height (m)	1.21	1.25
Mean wind speed (m/sec)	4.63	7.05
Mean air temperature (C)	27.64	--
Mean air temperature at 2.25 m (C)	--	10.45
Mean air temperature at 0.50 m (C)	--	10.22
Mean water temperature (C)	26.68	12.65
Mean estimated fetch (m)	2100	2800

The physical parameters were measured while the wave records were being made; they represent conditions at the time and place where each wave record was measured. They do not describe conditions at the times and places where the measured waves were generated. Of the wind speeds, July's largest is smaller than November's smallest.

Table 5.3 Results of the Pair Program for the July Records

Record	No. of Points	Water Level		Wind Speed		Wind Direction	
		Mean (cm)	σ (cm)	Mean (m/s)	σ (m/s)	Mean (°T)	σ (°T)
009	1549	8.94	2.92	4.66	0.55	285.12	8.45
010	1406	8.77	3.00	5.20	0.45	287.72	7.40
009-010	2955	8.86	2.96	4.92	0.58	286.36	8.08
011	1509	8.93	3.29	5.37	0.42	287.07	7.17
012	1337	8.75	2.92	4.77	0.57	289.43	9.73
011-012	2846	8.85	3.12	5.09	0.58	288.18	8.56
017	1473	11.12	1.82	4.12	0.41	277.95	9.54
018	1411	11.21	2.04	3.63	0.32	275.28	10.17
017-018	2884	11.17	1.93	3.88	0.45	276.64	9.95
027	1527	10.11	1.97	4.87	0.53	315.83	6.00
028	1574	9.90	1.77	4.41	0.47	312.89	7.55
027-028	3101	10.00	1.87	4.64	0.56	314.34	7.00

Table 5.4 Results of the Pair Program for the November Records

Record	No. of Points	Water Level		Wind Speed		Wind Direction	
		Mean (cm)	σ (cm)	Mean (m/s)	σ (m/s)	Mean (°T)	σ (°T)
067	750	7.74	2.23	5.47	0.86	302.91	7.54
068	850	7.29	2.35	6.80	0.85	309.95	4.53
067-068	1600	7.50	2.31	6.18	1.09	306.65	7.07
069	750	11.32	2.77	5.57	1.02	306.28	8.21
070	880	11.78	2.69	5.64	0.93	316.51	5.91
069-070	1630	11.57	2.74	5.61	0.98	311.80	8.71
075	750	9.37	3.10	6.30	0.73	330.35	5.95
076	850	9.81	2.71	7.14	1.19	319.37	6.50
075-076	1600	9.60	2.91	6.75	1.09	324.52	8.31
081	750	11.75	1.85	7.27	1.05	330.81	5.98
082	888	11.90	1.90	6.36	1.10	321.18	7.26
081-082	1638	11.83	1.89	6.78	1.17	325.59	8.25
083	750	11.75	2.75	7.83	1.29	306.43	9.48
084	566	12.18	2.57	7.70	0.93	323.42	5.80
083-084	1316	11.93	2.69	7.77	1.16	313.74	11.69
085	750	10.42	2.81	8.34	1.31	301.92	8.77
086	870	10.34	2.77	7.46	1.14	313.44	5.65
085-086	1620	10.38	2.79	7.87	1.31	308.11	9.26
087	750	10.36	1.85	7.51	1.42	304.41	8.77
088	870	10.17	2.01	6.96	1.42	299.76	6.04
087-088	1620	10.26	1.95	7.21	1.45	301.91	7.79
093	750	10.55	3.05	8.20	0.83	306.43	5.23
094	860	10.13	3.36	8.21	1.12	303.68	6.81
093-094	1610	10.33	3.23	8.20	1.00	304.96	6.28

Table 5.5 Air and Water Temperatures Measured in July

Record	Air Temperature (C)	Water Temperature (C)
009-010	27.45	26.18
011-012	28.98	26.62
017-018	29.51	27.55
027-028	24.64	26.38

Table 5.6 Air and Water Temperatures Measured in November

Record	Air Temperature at 2.25 m (C)	Air Temperature at 0.50 m (C)	Water Temperature (C)
067-068	9.25	9.88	12.46*
069-070	9.78	9.52	12.45*
075-076	9.92	9.86	12.52
081-082	10.42	10.46	12.69
083-084	10.76	10.61	12.72
085-086	10.53	8.99	12.70
087-088	10.89	10.56	12.79
093-094	12.02	11.86	12.87

*Corrected bucket-thermometer temperatures.

Table 5.7 The Results of the Frequency Program and the Estimated Fetches for July

Record	No. of Points	Frequency 240-248(°T) (cnt)	(%)	249-271(°T) (cnt)	(%)	272-286(°T) (cnt)	(%)	287-291(°T) (cnt)	(%)	292-303(°T) (cnt)	(%)	Est'd Fetch (m)
009	1549	-	-	102	6.58	773	49.90	317	20.46	348	22.47	
010	1406	-	-	9	0.64	648	46.09	345	24.54	375	26.67	
009-010	2955	-	-	111	3.76	1421	48.09	662	22.40	723	24.47	
011	1509	-	-	31	2.05	693	45.92	420	27.83	350	23.19	
012	1337	-	-	58	4.34	370	27.67	365	27.30	455	34.03	
011-012	2846	-	-	89	3.12	1063	37.35	785	27.58	805	28.29	
017	1473	-	-	359	24.37	822	55.80	202	13.71	89	6.04	
018	1411	27	1.91	295	20.91	994	70.45	93	6.59	2	0.14	
017-018	2884	27	0.93	654	22.68	1816	62.97	295	10.23	91	3.16	
027	1527	-	-	-	-	-	-	-	-	21	1.38	
028	1572	-	-	-	-	-	-	-	-	172	10.94	
027-028	3099	-	-	-	-	-	-	-	-	193	6.23	
		304-314(°T) (cnt)	(%)	315-319(°T) (cnt)	(%)	320-323(°T) (cnt)	(%)	324-330(°T) (cnt)	(%)	331-360(°T) (cnt)	(%)	
009		9	0.58	-	-	-	-	-	-	-	-	2039
010		27	1.92	2	0.14	-	-	-	-	-	-	2113
009-010		36	1.22	2	0.07	-	-	-	-	-	-	2076
011		15	0.99	-	-	-	-	-	-	-	-	2076
012		81	6.06	8	0.60	-	-	-	-	-	-	2242
011-012		96	3.39	8	0.28	-	-	-	-	-	-	2150
017		1	0.07	-	-	-	-	-	-	-	-	1779
018		-	-	-	-	-	-	-	-	-	-	1686
017-018		1	0.03	-	-	-	-	-	-	-	-	1742
027		612	40.08	418	27.37	312	20.43	158	10.35	6	0.39	2242
028		739	47.01	290	18.45	224	14.25	137	8.72	10	0.64	2354
027-028		1351	43.59	708	22.85	536	17.30	295	9.52	16	0.52	2298

Table 5.8 The Results of the Frequency Program and the Estimated Fetches for November

Record	No. of Points	Frequency 252-281(°T) (cnt)	(%)	282-292(°T) (cnt)	(%)	293-308(°T) (cnt)	(%)	309-314(°T) (cnt)	(%)	315-328(°T) (cnt)	(%)	329-339(°T) (cnt)	(%)	Est'd Fetch (m)
067	750	-	-	51	6.80	553	73.73	82	10.93	63	8.40	1	0.13	2291
068	850	-	-	-	-	323	38.00	365	42.94	162	19.06	-	-	2967
067-068	1600	-	-	51	3.19	876	54.75	447	27.94	225	14.06	1	0.06	2650
069	750	-	-	68	9.07	338	45.07	237	31.60	107	14.27	-	-	2691
070	880	-	-	-	-	84	9.55	236	26.82	549	62.39	11	1.25	3189
069-070	1630	-	-	68	4.17	422	25.89	473	29.02	656	40.25	11	0.67	2960
075	750	-	-	-	-	3	0.40	12	1.60	218	29.07	517	68.93	2900
076	850	-	-	-	-	50	5.88	136	16.00	606	71.29	58	6.82	3149
075-076	1600	-	-	-	-	53	3.31	148	9.25	824	51.50	575	35.94	3032
081	750	-	-	-	-	1	0.13	13	1.73	192	25.60	544	72.53	2889
082	888	-	-	-	-	40	4.50	146	16.44	546	61.49	156	17.57	3126
081-082	1638	-	-	-	-	41	2.50	159	9.71	738	45.05	700	42.74	3019
083	750	-	-	6	0.80	519	69.20	45	6.00	171	22.80	9	1.20	2398
084	566	-	-	-	-	-	-	41	7.24	429	75.80	96	16.96	3128
083-084	1316	-	-	6	0.46	519	39.44	86	6.53	600	45.59	105	7.97	2711
085	750	5	0.67	117	15.60	450	60.00	124	16.53	54	7.20	-	-	2337
086	870	-	-	-	-	165	18.97	326	37.47	377	43.33	2	0.23	3147
085-086	1620	5	0.31	117	7.22	615	37.96	450	27.78	431	26.60	2	0.12	2771
087	750	1	0.13	83	11.07	385	51.53	200	26.67	80	10.67	1	0.13	2567
088	870	-	-	98	11.26	695	79.89	69	7.93	8	0.92	-	-	2139
087-088	1620	1	0.06	181	11.17	1080	66.67	269	16.60	88	5.43	1	0.06	2335
093	750	-	-	1	0.13	515	68.67	168	22.40	66	8.80	-	-	2509
094	860	-	-	52	6.05	592	68.84	183	21.28	33	3.84	-	-	2545
093-094	1610	-	-	53	3.29	1107	68.76	351	21.80	99	6.15	-	-	2459

For the fetches, the greatest estimated fetch for a July record is equal to the smallest estimated fetch for the November records. Furthermore, 3 of the 4 air-sea temperature differences in July were stable, while in November all 16 were unstable. These are two physically different regimes. Table 5.2 shows that the November regime with its higher winds, longer fetches, and unstable air-sea temperature is markedly more Gaussian than the July regime.

5.2 The Moments and the Gram-Charlier A-Series

The second, third, and fourth moments for each distribution were computed from the ungrouped data in the course of the data-edit program. The momental skewness and the kurtosis were also computed. Table 5.10 shows these values. The averages of the absolute values of the skewness are 0.165 for July and 0.057 for November. The averages of the absolute values of the kurtosis are 0.097 for July and 0.096 for November. The difference between July and November can be seen in the skewness but not in the kurtosis.*

To form an idea of the way our distributions depart from the Gaussian, we may use the Gram-Charlier A-series. It gives an empirical fit to a frequency distribution expressed as a Gaussian

*It was the author's first inclination to call these values of skewness and kurtosis small. A little further thought led him to the realization that so much of his experience had been gained from the Gaussian distribution that he had no real basis for the judgment. In casting about for something with which to make a comparison, it was decided to find the Poisson distributions for which skewness or kurtosis was less than 0.1. The Poisson distribution is a likely one for comparison since it is skewed to the right and tends to the Gaussian for large values of the mean. It was something of a shock to discover that the skewness is less than one-tenth when the mean is 25 and that the kurtosis is less than one-tenth when the mean is 5. Five is not large, and 25 is not particularly impressive either.

Table 5.10 The Moments, Skewness, and Kurtosis of the Wave Records

Record	μ_2 (cm^2)	μ_3 (cm^3)	μ_4 (cm^4)	Skewness	Kurtosis
009	0.845,1	0.844, 1	0.221,3	0.172	0.046
010	0.894,1	0.763, 1	0.237,3	0.143	-0.015
011	0.108,2	0.667, 1	0.318,3	0.096	-0.125
012	0.845,1	0.893, 1	0.229,3	0.182	0.101
017	0.330,1	0.210, 1	0.337,2	0.175	0.050
018	0.412,1	0.365, 1	0.571,2	0.219	0.183
027	0.387,1	0.241, 1	0.391,2	0.158	-0.196
028	0.313,1	0.198, 1	0.306,2	0.178	0.059
067	0.499,1	0.182, 1	0.742,2	0.082	-0.007
068	0.557,1	0.227, 1	0.946,2	0.087	0.025
069	0.771,1	0.294, 1	0.203,3	0.069	0.207
070	0.725,1	0.105, 1	0.163,3	0.027	0.045
075	0.965,1	0.607, 1	0.287,3	0.101	0.043
076	0.737,1	0.370, 1	0.160,3	0.092	-0.031
081	0.346,1	0.371, 0	0.343,2	0.029	-0.065
082	0.364,1	0.465, 0	0.366,2	0.034	-0.116
083	0.757,1	-0.870,-1	0.160,3	-0.002	-0.101
084	0.664,1	0.151, 1	0.134,3	0.044	0.024
085	0.791,1	-0.235, 0	0.160,3	-0.005	-0.224
086	0.772,1	0.458, 0	0.170,3	0.011	-0.078
087	0.345,1	-0.618,-1	0.397,2	0.005	0.165
088	0.406,1	-0.749, 0	0.544,2	-0.046	0.150
093	0.934,1	0.819, 1	0.299,3	0.144	0.216
094	0.113,2	0.103, 2	0.395,3	0.136	0.023

distribution plus an infinite series of correction terms based on the sample moments. Smart (1958) gives it in the form

$$F(x) = \left[1 + \sum_{n=3} (-1)^n \frac{A_n}{\sigma^n n!} H_n(t)\right] f(x)$$

where $t \equiv \frac{x - \bar{x}}{\sigma}$,

$f(x) \equiv \frac{1}{\sigma\sqrt{2\pi}} \exp\left\{-\frac{(x - \bar{x})^2}{2\sigma^2}\right\}$, the Gaussian,

$\sigma \equiv$ the standard deviation,

$A_n \equiv$ polynomials in the moments of the distribution, and

$H_n(t) \equiv$ Hermite's polynomials. If the Gram-Charlier A-series is approximated by its first three terms, it takes the form

Sample distribution = [1 + a correction dependent upon skewness + a correction dependent upon kurtosis] × the Gaussian.

Specifically, when the argument of the Gaussian is expressed in units of the standard deviation and the mean is set at zero,

$$F(t) = \left[1 + \text{skewness} \times \frac{t^3 - 3t}{3} + \text{kurtosis} \times \frac{t^4 - 6t - 3}{12}\right] f(t)$$

where $\text{skewness} = \frac{\mu_3}{2\sigma^3}$, and

$\text{kurtosis} = \frac{\mu_4 - 3\mu_2^2}{2\mu_2^2}$. The sum of the second and third terms within the bracket gives the per cent correction to be applied against the Gaussian. Tables AIII 2.01 to AIII 2.24 show these values for each of the records. They are quite large even for small values of skewness and kurtosis. As an example, record 070, for which skewness is 0.027 and kurtosis is 0.04, has corrections of -1.20% at $-\sigma$ and 4.80% at $+\sigma$. The average absolute corrections for all 24 records are 10.33% at $+\sigma$ and 8.00% at $-\sigma$. Corrections in the tails exceeding 200% are not

uncommon. Figures AIII 2.01 to AIII 2.24 show the Gaussian, the Gram-Charlier 3-term fits, and the sample frequencies for each record.

Since we are dealing with two fairly consistent and well-separated physical regimes, and since each record has been sorted according to its own mean and standard deviation, we may group the records into two sets for further study. The July records have 11,786 measures, while the November records have 12,634. The skewness and kurtosis for each set were computed from the formula for grouped data, and Sheppard's corrections were applied to get table 5.11. The 3-term Gram-Charlier

Table 5.11 The Skewness and Kurtosis for the Grouped July and November Records

	Skewness	Kurtosis
July	0.168	0.010
November	0.045	0.029

fits to these distributions are showed in tables 5.12 and 5.13 and figures 5.2 and 5.3. Both demonstrate the characteristic raising of the positive tail, the depression of the negative tail, and the shift of the mode toward the negative side. The effect is much more pronounced for July than for November.

For comparison with the values of chi-square computed for the Gaussian as showed in table 5.2, table 5.14 gives the values of chi-square computed for the Gram-Charlier fits. These latter values are generally better, although the probabilities are sometimes worse than those for the Gaussian since only nine degrees of freedom (df) were used, two more parameters having been used in calculating the Gram-Charlier fits. Chi-square was also computed for the grouped July and November series with the results showed in table 5.15. The Gaussian

Table 5.12 Gram-Charlier Skewness and Kurtosis Corrections to the Gaussian for the Grouped July Records

t (σ)	Correction for -t (%)	Correction for +t (%)	t (σ)	Correction for -t (%)	Correction for +t (%)
0.0	- 0.25	- 0.25			
0.1	1.42	- 1.92	2.1	- 17.41	15.75
0.2	3.04	- 3.58	2.2	- 23.39	21.95
0.3	4.60	- 5.18	2.3	- 30.06	28.94
0.4	6.03	- 6.69	2.4	- 37.46	36.72
0.5	7.33	- 8.07	2.5	- 45.62	45.38
0.6	8.45	- 9.29	2.6	- 54.57	54.93
0.7	9.36	- 10.32	2.7	- 64.33	65.39
0.8	10.03	- 11.11	2.8	- 74.94	76.84
0.9	10.44	- 11.64	2.9	- 86.42	89.30
1.0	10.53	- 11.87	3.0	- 98.80	102.80
1.1	10.30	- 11.76	3.1	-112.11	117.39
1.2	9.68	- 11.28	3.2	-126.37	133.11
1.3	8.68	- 10.40	3.3	-141.62	150.00
1.4	7.24	- 9.06	3.4	-157.87	168.09
1.5	5.35	- 7.25	3.5	-175.17	187.43
1.6	2.96	- 4.92	3.6	-193.52	208.06
1.7	0.05	- 2.05	3.7	-212.98	230.02
1.8	- 3.42	1.42	3.8	-233.53	253.35
1.9	- 7.46	5.52	3.9	-255.25	278.09
2.0	-12.12	10.28	4.0	-278.12	304.28

Table 5.13 Gram-Charlier Skewness and Kurtosis Corrections to the Gaussian for the Grouped November Records

t (σ)	Correction for -t (%)	Correction for +t (%)	t (σ)	Correction for -t (%)	Correction for +t (%)
0.0	-0.73	-0.73			
0.1	-0.29	-1.19	2.1	- 6.86	2.02
0.2	0.11	-1.67	2.2	- 8.15	3.99
0.3	0.46	-2.16	2.3	- 9.53	6.27
0.4	0.75	-2.65	2.4	-11.00	8.88
0.5	0.97	-3.11	2.5	-12.54	11.84
0.6	1.16	-3.60	2.6	-14.14	15.18
0.7	1.26	-4.02	2.7	-15.80	18.92
0.8	1.28	-4.38	2.8	-17.56	23.08
0.9	1.22	-4.70	2.9	-19.36	27.70
1.0	1.07	-4.93	3.0	-21.20	32.80
1.1	0.82	-5.08	3.1	-23.08	38.40
1.2	0.50	-5.12	3.2	-24.98	44.52
1.3	0.06	-5.04	3.3	-26.92	51.20
1.4	-0.46	-4.82	3.4	-28.85	58.47
1.5	-1.07	-4.45	3.5	-30.78	66.34
1.6	-1.78	-3.92	3.6	-32.71	74.85
1.7	-2.62	-3.18	3.7	-34.61	84.05
1.8	-3.52	-2.22	3.8	-36.48	93.94
1.9	-4.55	-1.07	3.9	-38.30	104.56
2.0	-5.66	0.34	4.0	-40.06	115.94

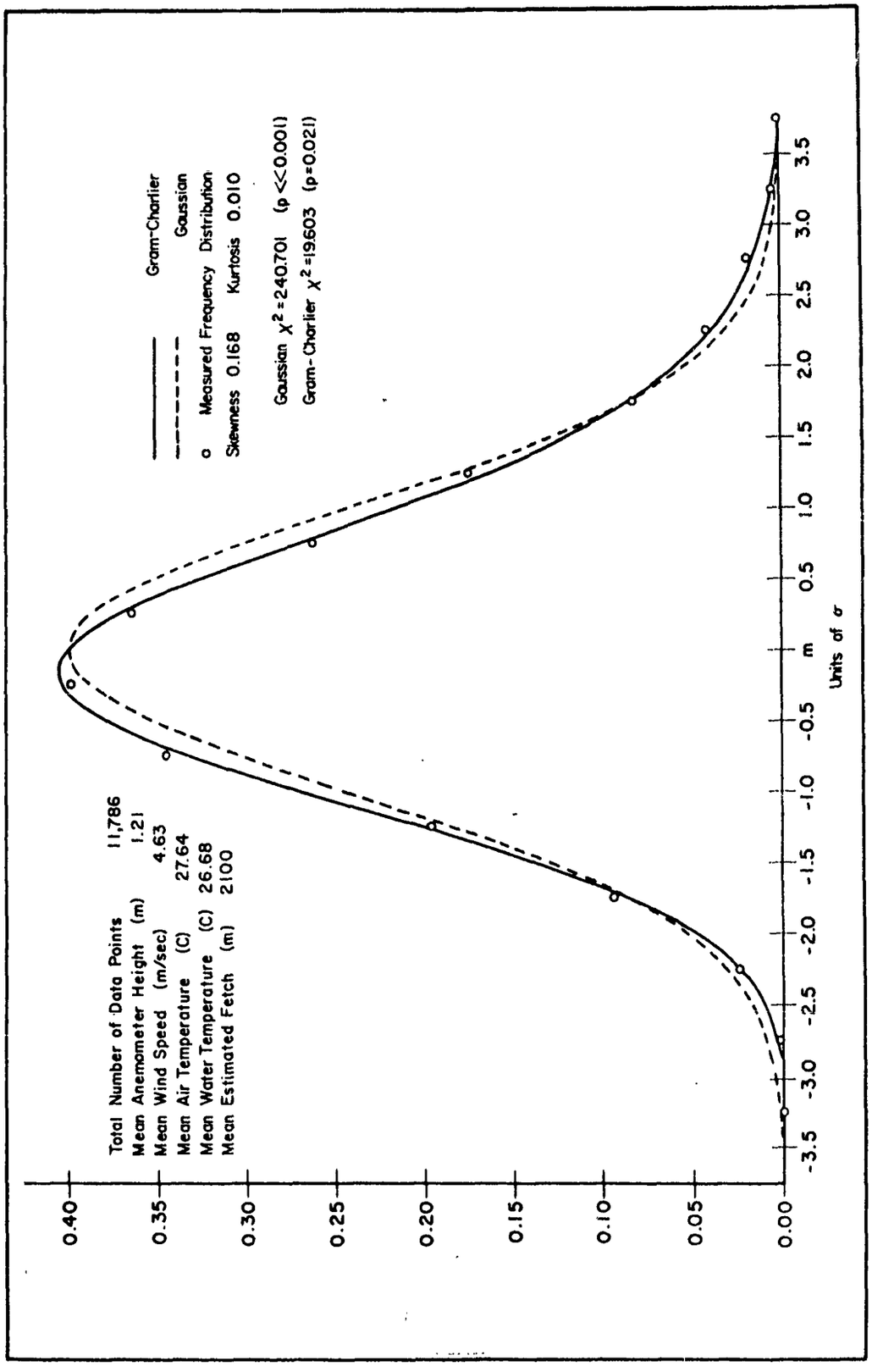

Figure 5.2 Gram-Charlier Fit for the Grouped July Records

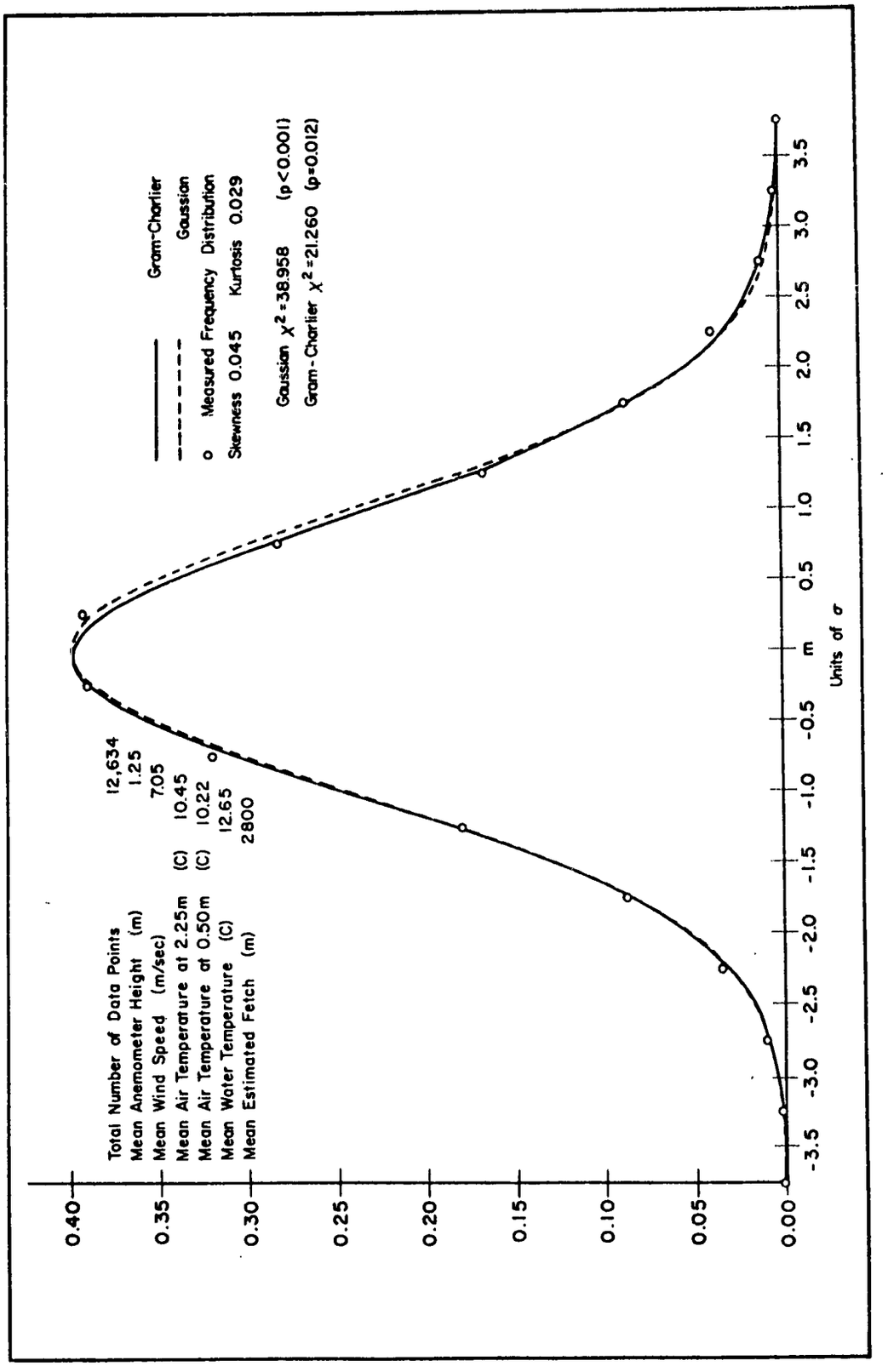

Figure 5.3 Gram-Charlier Fit for the Grouped November Records

Table 5.14 Values of Chi-Square Calculated on the Assumption That the Underlying Distributions May be Described by the Three-Term Gram-Charlier Fits

July			November		
Record	Chi-Square	p on 9 df	Record	Chi-Square	p on 9 df
009	9.531	0.394	067	2.766	0.971
010	11.572	0.242	068	25.590	0.004
011	42.303	<0.001	069	19.838	0.019
012	12.076	0.210	070	10.591	0.306
017	7.466	0.590	075	20.754	0.015
018	35.458	<0.001	076	10.718	0.296
027	34.562	<0.001	081	13.436	0.151
028	16.558	0.058	082	8.922	0.450
			083	19.629	0.021
			084	6.781	0.660
			085	17.761	0.041
			086	17.553	0.043
			087	16.870	0.051
			088	22.305	0.009
			093	29.185	<0.001
			094	9.482	0.402

Table 5.15 Values of Chi-Square for the Grouped July and November Records on Both the Gaussian and the Gram-Charlier Assumptions

	Gaussian Chi-Square	p on 11 df	Gram-Charlier Chi-Square	p on 9 df
July	240.701	$\ll 0.001$	19.603	0.021
November	38.958	< 0.001	21.260	0.012

is obviously not a good fit to either one; the Gram-Charlier 3-term fit, while not handsome, is better by orders of magnitude as measured by the associated probability.

In the light of these results there are applications where the Gaussian assumption may be very good in spite of the distortion. For example, if one is interested in the absolute departures from mean water level, the distribution is folded on itself around the mean. The deficiency in the negative tail will be offset by the excess in the positive tail, and the resulting distribution could be expected to be very close to one derived from an exact Gaussian.

For other uses the assumption may be entirely untenable. Any time we assume that a process is nearly Gaussian, we are requiring, in effect, that the third moment be small in comparison with the second and fourth moments, when they have all been scaled by some suitable length, since all odd moments of the Gaussian are zero. If this requirement enters our analysis, either explicitly or implicitly, trouble may result. As a scaling length we have chosen the wave length corresponding to the frequency at which the maximum energy occurs in each record. The Gaussian assumption requires both

$$\frac{\mu_3}{L^2} \Big/ \frac{\mu_2}{L} \ll 1 \text{ and}$$

$\frac{\mu_3}{L^2} \Big/ \frac{\mu_4}{L^3} \ll 1$. Table 5.16 shows the values of these ratios for each of the records. The absolute values of the first ratio are of the order of a few thousandths at most and thus may be considered satisfactory. In contrast, the absolute values of the second ratio range from 0.236 to 20.6, so that any model which requires small odd moments of the Gaussian will be inapplicable to our records. In view of our results it seems conclusive that the process represented by these records is so non-Gaussian that a naive use of the Gaussian assumption is hazardous. It seems probable that this conclusion holds in general for any problem concerned with the high-frequency components.

Table 5.16 Comparison of Moments

Record	$\frac{\mu_3}{L^2} / \frac{\mu_2}{L}$	$\frac{\mu_3}{L^2} / \frac{\mu_4}{L^3}$
009	0.230, -2	0.166, 2
010	0.197, -2	0.140, 2
011	0.143, -2	0.910, 1
012	0.245, -2	0.169, 2
017	0.200, -2	0.198, 2
018	0.363, -2	0.156, 2
027	0.196, -2	0.196, 2
028	0.199, -2	0.206, 2
067	0.115, -2	0.780, 1
068	0.128, -2	0.764, 1
069	0.879, -3	0.629, 1
070	0.334, -3	0.279, 1
075	0.145, -2	0.915, 1
076	0.116, -2	0.100, 2
081	0.247, -3	0.468, 1
082	0.402, -3	0.404, 1
083	-0.265, -4	-0.236, 0
084	0.524, -3	0.490, 1
085	-0.685, -4	-0.637, 0
086	0.137, -3	0.117, 1
087	-0.734, -4	-0.380, 0
088	-0.578, -3	-0.440, 1
093	0.202, -2	0.119, 2
094	0.210, -2	0.113, 2

6.0 SPECTRAL ANALYSIS OF THE WATER SURFACE

6.1 Preliminary Inspection

The digital method of computing spectra produces autocovariance functions as a by-product.* These functions were scaled to one at t = 0 and are showed in figures AIV 1.01 to AIV 1.24 and tables AIV 1.01 to AIV 1.24 in appendix IV. Figure 6.1 uses record 075 as an example. It has a quite regular oscillation with a frequency about 0.6 cps and a rather slow decay.

The power spectrum for the same record is showed in figure 6.2. It is quite characteristic of the complete set showed in figures AIV 2.01.0 to AIV 2.24.0 and tables AIV 2.01 to AIV 2.24. It has a sharp spike on an interval about 0.5 cps wide. It falls away steeply toward lower frequencies and not quite so steeply toward higher frequencies. There is a slight increase in power near twice the frequency at which the maximum power occurs, which interrupts the smooth fall of the spectrum. By f = 2.5 cps the power is well down in the noise. There is a slight rise in power between 0.0 and 0.2 cps. All the November records except 087, figure AIV 2.21.0, show this feature. Record 087 has instead a second peak at 0.2 cps which is more than four times as great as the peak at 0.7 cps. Record 088, figure AIV 2.22.0, the second half of the same run, shows nothing of the sort. It is possible that a motor boat wake ran by undetected while record 087 was being made. At a later

*Bendat (1958) defines the autocovariance function as an autocorrelation function computed with mean differences instead of with raw data. In our computations the inputs to the computer were mean differences.

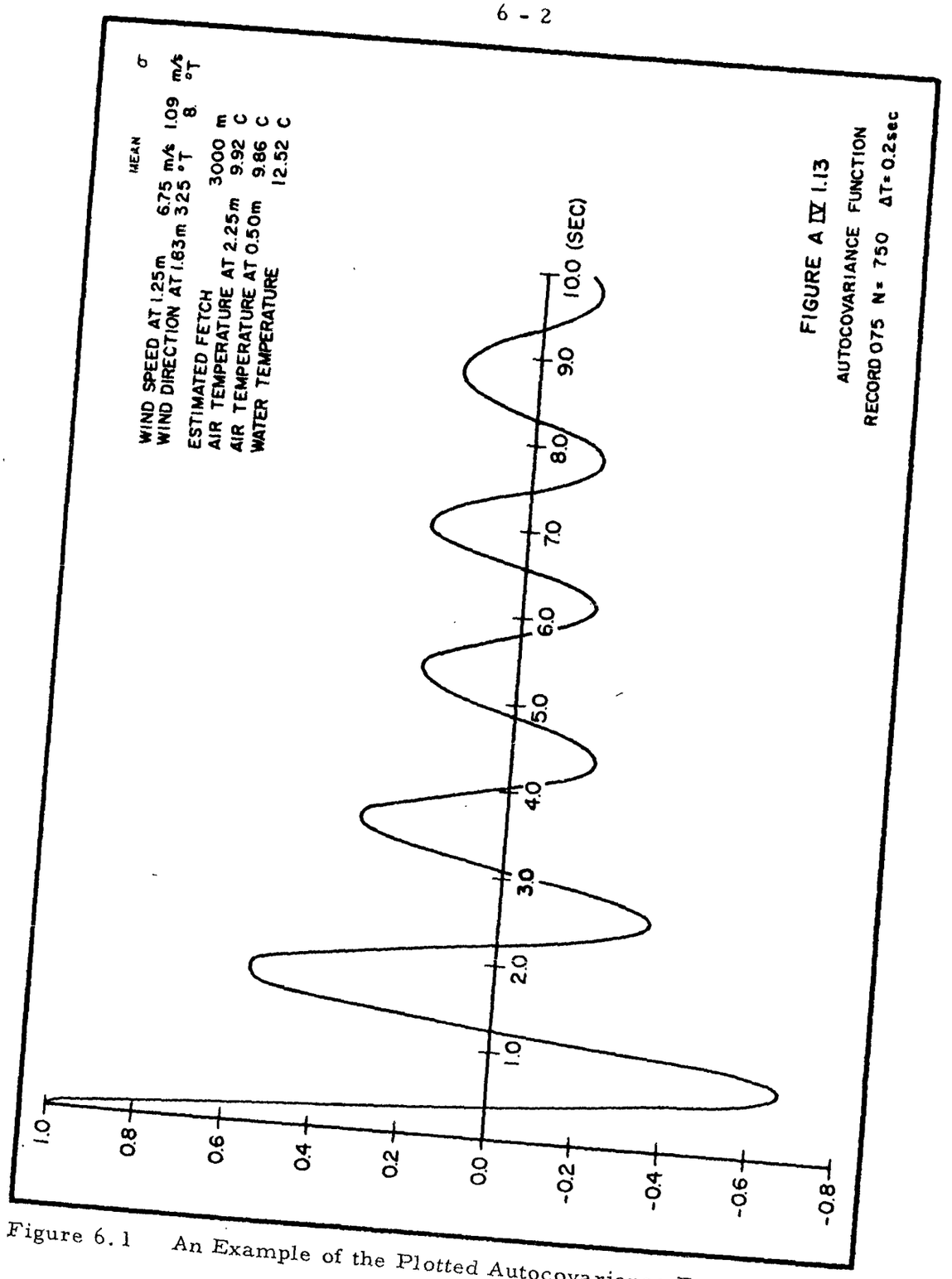

Figure 6.1 An Example of the Plotted Autocovariance Functions

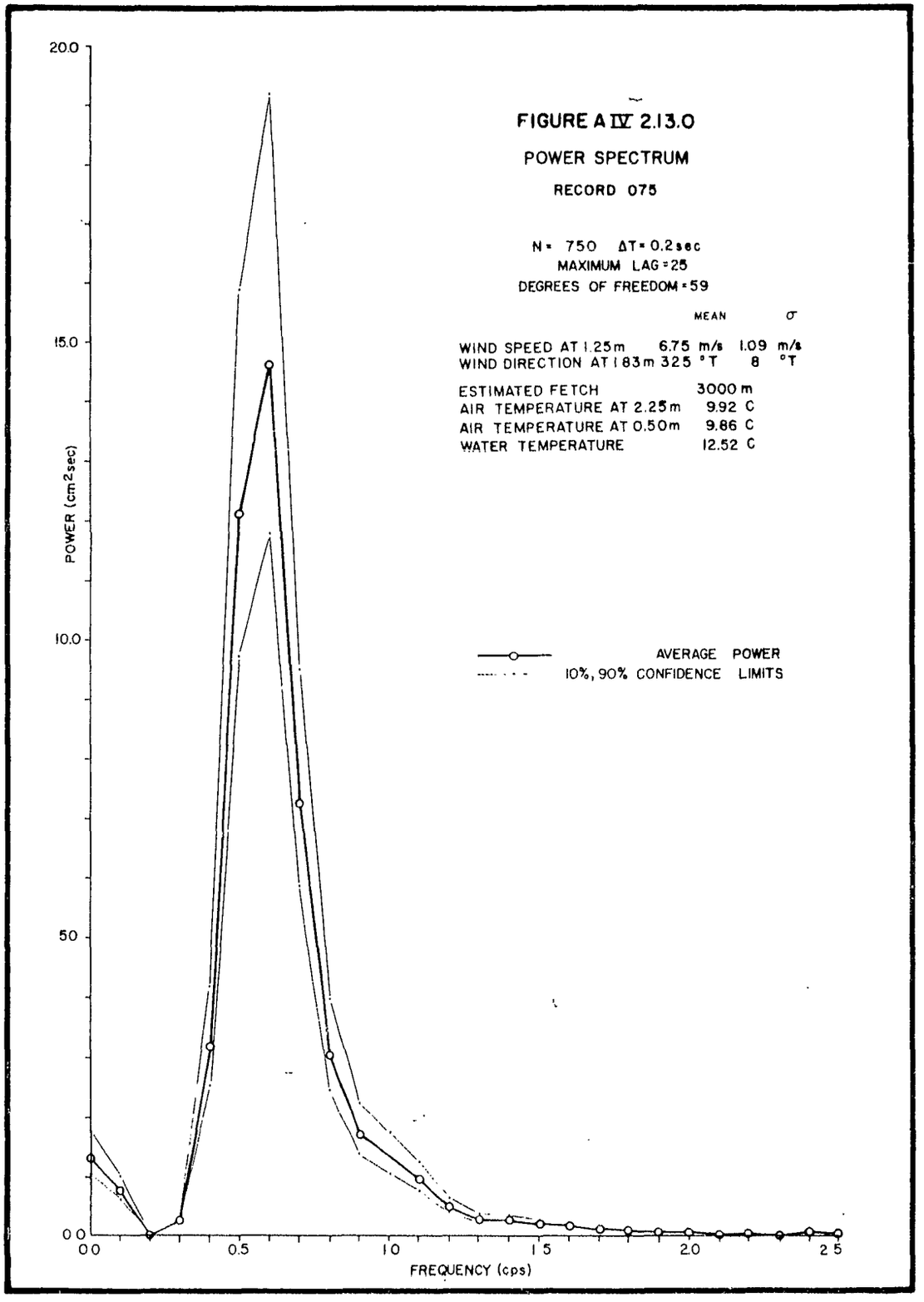

Figure 6.2 An Example of the Rectangular Plots of the Spectra

stage of the analysis, when bimodal spectra would not be appropriate, these two records have been omitted.

Since all the November records were made during a single day, and since all, with the exception of record 087, show about the same power between 0.0 and 0.2 cps, a seiche may have been present. With Round Bay estimated as 12,000 feet long and 20 feet deep, Merian's formula (Proudman, 1953) yields a natural primary period of 15.8 minutes, equivalent to a frequency of 0.001 cps.

In planning this study, as we have already mentioned, it was decided to take records in pairs in order to have some evidence about how stationary time-series models apply. That the process is changing slowly over a 5-minute period can be seen by comparing the spectrum of any odd-numbered record with the spectrum of the succeeding even-numbered record. Although not identical, they generally lie well within each other's confidence limits. This close resemblance does not often extend to records taken half an hour apart. We thus have a loose upper bound on the length of record and consequently on the fineness of resolution realizable with the technique.

There are a number of details which must be explained so that the way the spectra are presented will not mislead the reader. Each power estimate for July records (calculated at a maximum lag of 50) and for November records (at a maximum lag of 25) represents the average power contained in a frequency band 0.2 cps wide, centered at the frequency at which the plotted point or tabular value appears. The end frequencies, f = 0.0 and f = 2.5 cps, are exceptions. For all records the value for f = 0.0 cps, when showed, is the average over the half-sided interval 0.0 to 0.1 cps. For the July records the value for f = 2.5 cps is the average power in the band 2.4 to 2.6 cps, since these records

were computed to f = 5.0 cps. For the November records the power at f = 2.5 cps is the average over the half-sided interval 2.4 to 2.5 cps.

As the average power estimates for July (at maximum lag 50) and November (at maximum lag 25) came from the computer, they were expressed in cm^2 x 0.2 sec so that their sum over all frequencies equaled the variance. As showed in this report, these estimates have been rescaled to unit frequency, cm^2-sec, so that their sum in the November records is five times the variance. This is not true for the July records since the computed values from 2.6 to 5.0 cps have been neglected.

For those November records computed at a maximum lag of 50 the averaging interval is 0.1 cps; the intervals for the end points are half-sided 0.05 cps long, and the units as they came from the computer were cm^2 x 0.1 sec. These too have been rescaled to unit frequency and their sum is ten times the variance.

6.2 The Saturated Side of the Power Spectrum

6.2.1 The "Equilibrium" Range

It has been suggested that the high-frequency end of the spectrum may be an equilibrium range. When the wind, which is always turbulent in nature, blows over the water, the first waves formed are high frequency (large wave number). As time passes energy appears in the wave system at lower and lower frequencies until, for given macroscopic conditions, the process locks into a characteristic spectrum. The notion of an equilibrium range requires that for some range of frequencies the spectra for all macroscopic conditions be identical.

In the linearized version of the problem the amplitudes of the components must be small; each is generated independently, and there can be no interaction between frequencies. If the amplitudes grow to the point where they are not infinitesimally small, then the nonlinear features of the problem become a major consideration, and interaction between different frequencies becomes important. Expressed in a rough way, the wind supplies energy to the waves. The wave heights are built to the point where they are not infinitesimal. Trains of different frequency run through each other. The interference pattern occasionally forms crests so high as to be unstable. These break, draining energy from the waves into turbulence and reducing the height. The wind supplies more energy to rebuild the waves. At high frequencies it is supposed that the gain in energy from the wind is in equilibrium with the energy loss. Any increase in energy from higher winds would accelerate the loss of energy from the system so that, no matter what the wind speed, the balance, once achieved, would be at the same level. The controlling factor is not the energy input from the wind but the physical nature of the wave process at high frequencies.

Phillips (1958) has expressed the idea more elegantly and has suggested a possible mechanism. He says on page 428, "The occurrence of scattered sharp wave crests as a transient limiting configuration corresponds to the occurrence of discontinuities of surface gradient which in spectral terms corresponds to the existence of a certain form of the spectrum of high wave-number. The properties of the instantaneous spatial spectrum at these high wave-numbers will therefore be determined by the physical parameters that determine the extreme configuration of the surface in the limiting condition, the particular property that is relevant being the magnitude of the discontinuity in surface slope developed. It seems likely, therefore, that in a well-developed sea there exists a range of large wave-numbers over which the wave

spectrum is statistically determined by the physical quantities governing the conditions for attachment of the wave crests. Similar remarks can be made concerning the frequency spectrum of the surface displacement at a given point, where rapid changes in the surface displacement are associated with the movement past the point of observation of occasional sharp wave crests near the limiting configuration.

"The basic hypothesis of this paper can therefore be stated briefly as follows. In a well-developed sea, generated by the wind, there is an 'equilibrium range' of large wave-numbers (or high frequencies) in the spectrum, determined by the physical parameters that govern the continuity of the wave surface.

"There are two remarks that should be made at this point. The first is that the concept of an equilibrium range is suggested by consideration of the asymptotic form of the spectrum for large wave-numbers (or frequencies) and that we have little direct evidence upon which to base an a priori estimate of the smallest wave number to which we would expect it to be applicable.* It is clear that a necessary condition for the existence of an equilibrium range over a certain part of the spectrum is the existence of appreciable non-linear interactions among these wave-numbers, but it is not clear whether this condition alone is sufficient. The results of some measurements described in section 3 offer good a posteriori evidence that it may indeed be sufficient but it may be difficult to justify such an assertion in advance. The second remark is that the magnitude of the wave spectrum in the equilibrium range represents an upper limit, dictated by the requirements of crest attachment. In the early stages of wave generation, the equilibrium value may not have been

*This statement was correct at the time it was written. A later paper by Pierson (1959) offers evidence that in sharply peaked spectra the equilibrium range can only begin at frequencies greater than twice the frequency at which the maximum power occurs.

attained at any point in the spectrum, although the wave slopes may be such that non-linear interactions are not negligible, and in a decaying wave system the wave spectrum over the relevant range may have fallen from its equilibrium value through the damping of the components of shorter wavelength."

He then goes on to show that on dimensional grounds the spectrum in the equilibrium range may be expected to have the form

$$\Phi(\omega) \sim \alpha g^2 \omega^{-5}$$

where α = a constant,

g = the gravitational acceleration, and

ω = the angular frequency. We may expect a -5-power dependence of the spectrum on the frequency.

The measurements Phillips refers to in his section 3 (1958) are those of Burling (1955). Burling has computed spectra for 23 wave records from Staines Reservoir, Middlesex, England, made using a capacitance wire recorder developed by Tucker and Charnock (1955). The fetches vary from 400 to 1350 meters. (In our work the fetches vary from 1700 to 3000 meters.) The wind speeds, measured with cup anemometers at a height of 10 meters, ranged from 5 to 8 meters per second. (In our work the wind was measured at only a bit more than 1 meter above mean water level with heated-thermocouple anemometers and ranged from 3.88 to 8.20 meters per second.) Thus our work was done at longer fetches and stronger winds than Burling's. The analysis was performed on an analog machine, a Fourier analyzer, described by Barber, Ursell, Darbyshire, and Tucker (1946). Burling notes that the method of preparing records for the analyzer will probably introduce some noise and also shows that there may have been some malfunctioning of the analyzer itself. No confidence limits are given.

Figure 6.3 shows Burling's spectra. It is striking that for $f \geq 0.85$ the spectral estimates, which are widely dispersed below this value, fall within a quite narrow band. Figure 6.4 shows averaged values of the spectral density weighted by various powers of the frequency and plotted on logarithm-versus-logarithm paper. Burling says, "...they lie almost on a straight line, i.e. the mean power x is inversely proportional to some power of the frequency.... The lines in this figure are (unweighted) mean values of $f^n x$, for n = 4, 5, and 6... There can be little doubt that in this range of frequencies (0.85 to 1.95) w(f) decreases nearly as the inverse fifth power of the frequency, when the spectra arise under the conditions studied in this paper. There is no point in attempting to fit this any more closely."

Hicks (1960) reports a value for the logarithmic slope of the saturated side of the energy spectrum of -4.7 ± 0.5. His value is based on surface records made in small lakes. He also transforms the slope spectra of Cox (1958) to elevation spectra and derives a value of -5.5 from this source.

Our records provided an opportunity to explore the equilibrium range proposal in more detail. Of the 126 records, computation has been completed on 38. Of the 38, there are 24 (table 6.1) with fetches long enough and winds long and strong enough to develop fully an equilibrium range, if there is such a phenomenon.

At the start of the November cruise it was found that the vacuum tube in the blocking oscillator was dead. Various adjustments had to be made in the circuit to make the replacement function properly. All the November records were made with these settings and at the close of the cruise all the adjustment controls were sealed. The calibration tank was completed at a later date and the calibration data taken. The calibration

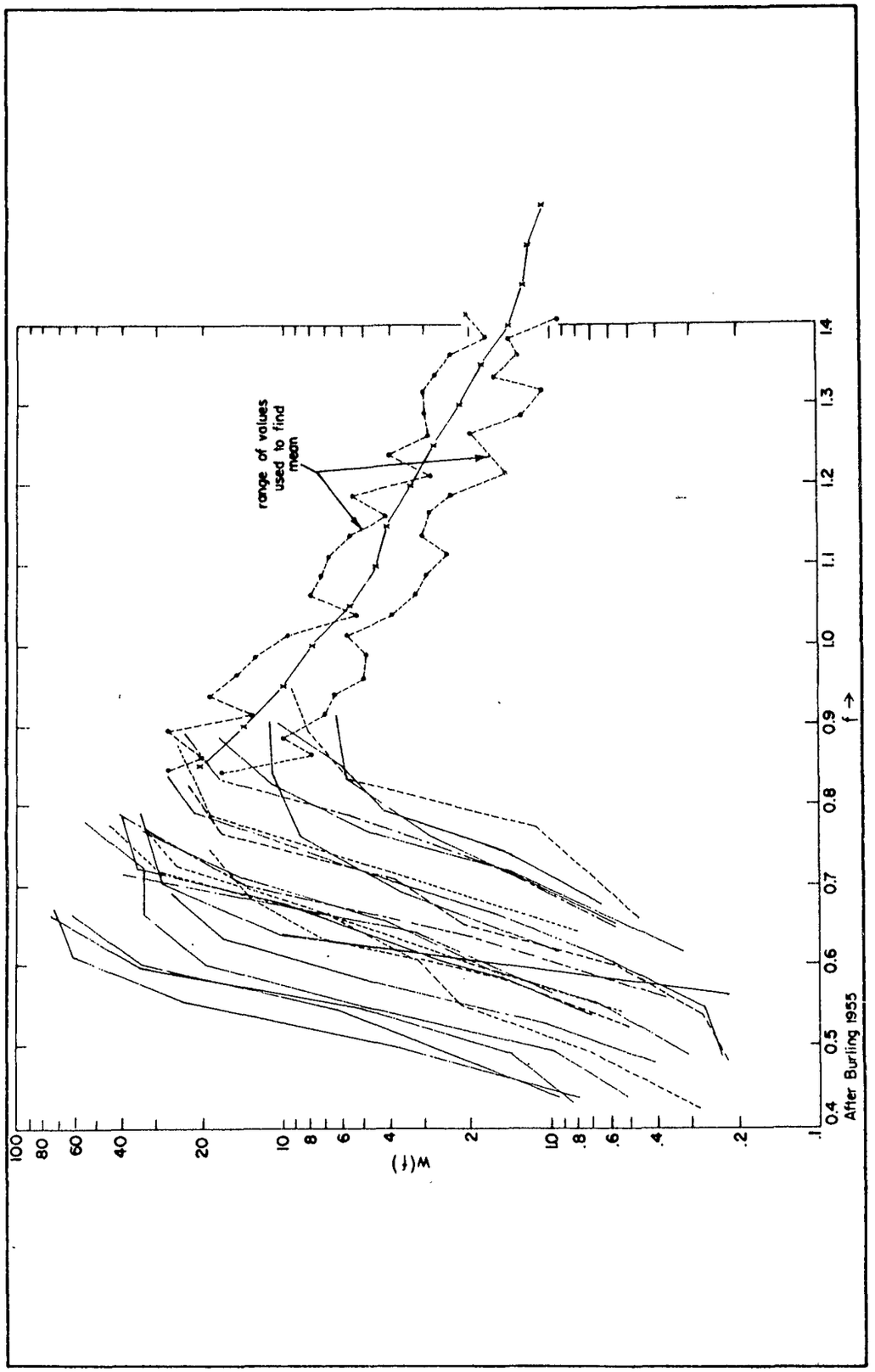

Figure 6.3 Spectra of Wind-Generated Waves as Measured by Burling (1955)

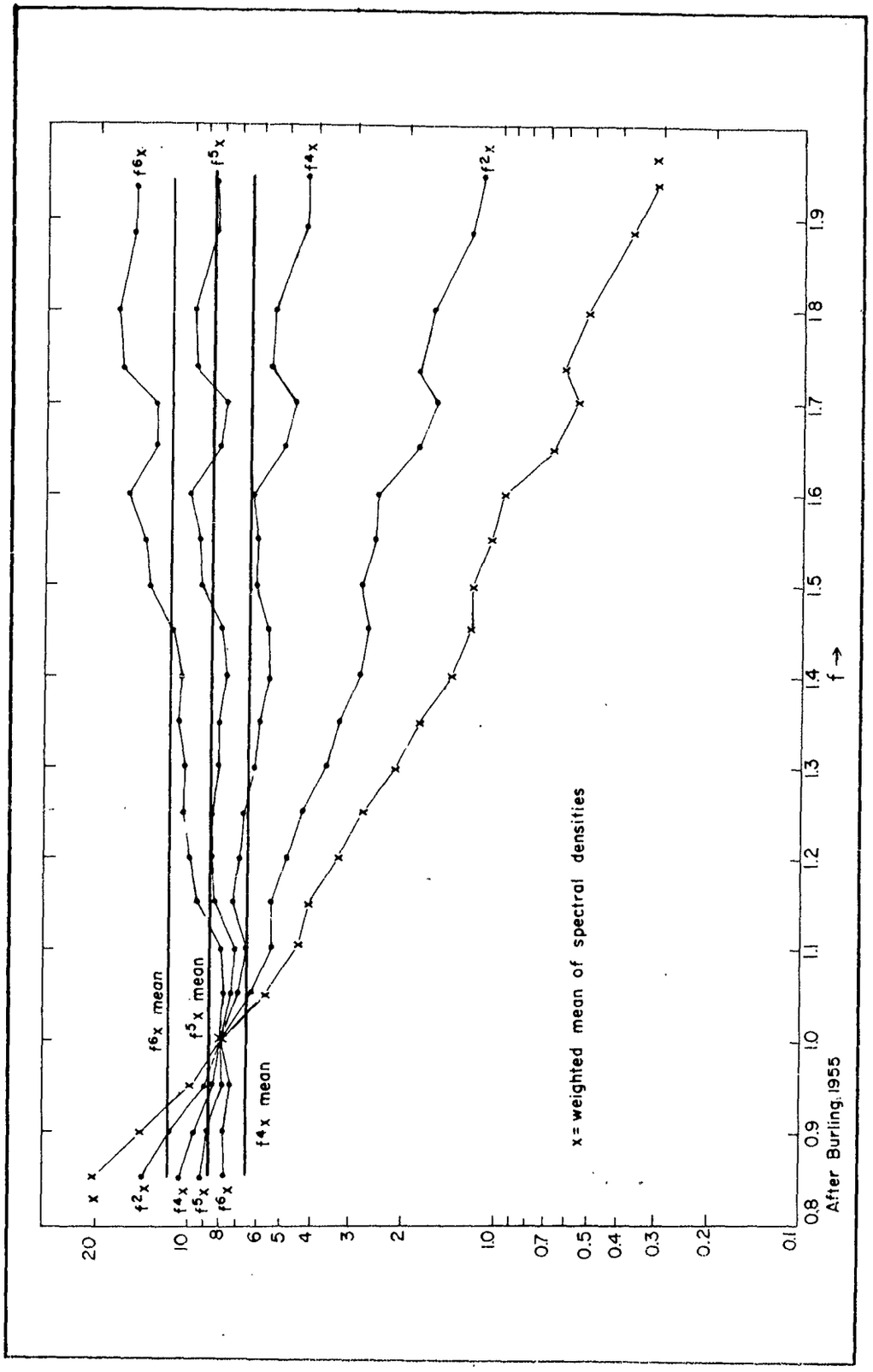

Figure 6.4 The Mean Shape of Spectra at High Frequencies as Computed by Burling (1955)

Table 6.1 Mean Wind Speeds and Estimated Fetches for Records Used in This Study

Record	Mean Wind Speed at About 1.25 m (m/s)	Fetch (m)
009-010	4.92	2100
011-012	5.09	2200
017-018	3.88	1700
027-028	4.64	2300
067-068	6.18	2700
069-070	5.61	3000
075-076	6.75	3000
081-082	6.78	3000
083-084	7.77	2700
085-086	7.87	2800
087-088	7.21	2300
093-094	8.20	2500

data are thus valid for the November records but not for the July records. However, the July records were all made at a single adjustment of the instrument so that they should agree inter se.

In the beginning the July records and the November records were treated as two separate groups. The first step was averaging the spectra frequency-by-frequency. Figures 6.5 and 6.6 show the average power and the standard deviation of the power, frequency-by-frequency, for the July and November records, respectively. The ordinate values for the July records are nominal, having been fixed by applying the November calibration. It is clear that for both records there is a range from 0.8 to 2.1 cps in which the means of the spectral estimates lie substantially on a straight line with relatively small scatter. The November records show an oscillation beyond 2.1 cps that is probably due to noise in the system. From these plots the span 0.8 to 2.1 cps was selected for further study of the equilibrium range. A linear least-squares fit of the form

$$\log P = \log a + b \log f,$$

where $P \equiv$ power and

$f \equiv$ frequency, was made for each set of records. For July $a = 1.220$ and $b = -4.553484$, while for November $a = 0.2545$ and $b = -4.403215$. Thus we have the two equations

$$\hat{P}_J = 1.220\, f^{-4.553} \text{ for July } (\hat{P}_J \text{ in arbitrary units}) \text{ and}$$
$$\hat{P}_N = 0.2545\, f^{-4.405} \text{ for November } (\hat{P}_N \text{ in cm}^2 \times 0.2 \text{ sec}).$$

The powers to which f is raised in these two equations are remarkably close and perhaps the underlying process may obey a -4.5-power law. An attempt to apply Student's t to the hypothesis that the true value of b is -4.5 led to values of t of the order of 10^{-5}, which is associated with a probability extremely close to one. Linear least-squares fits to

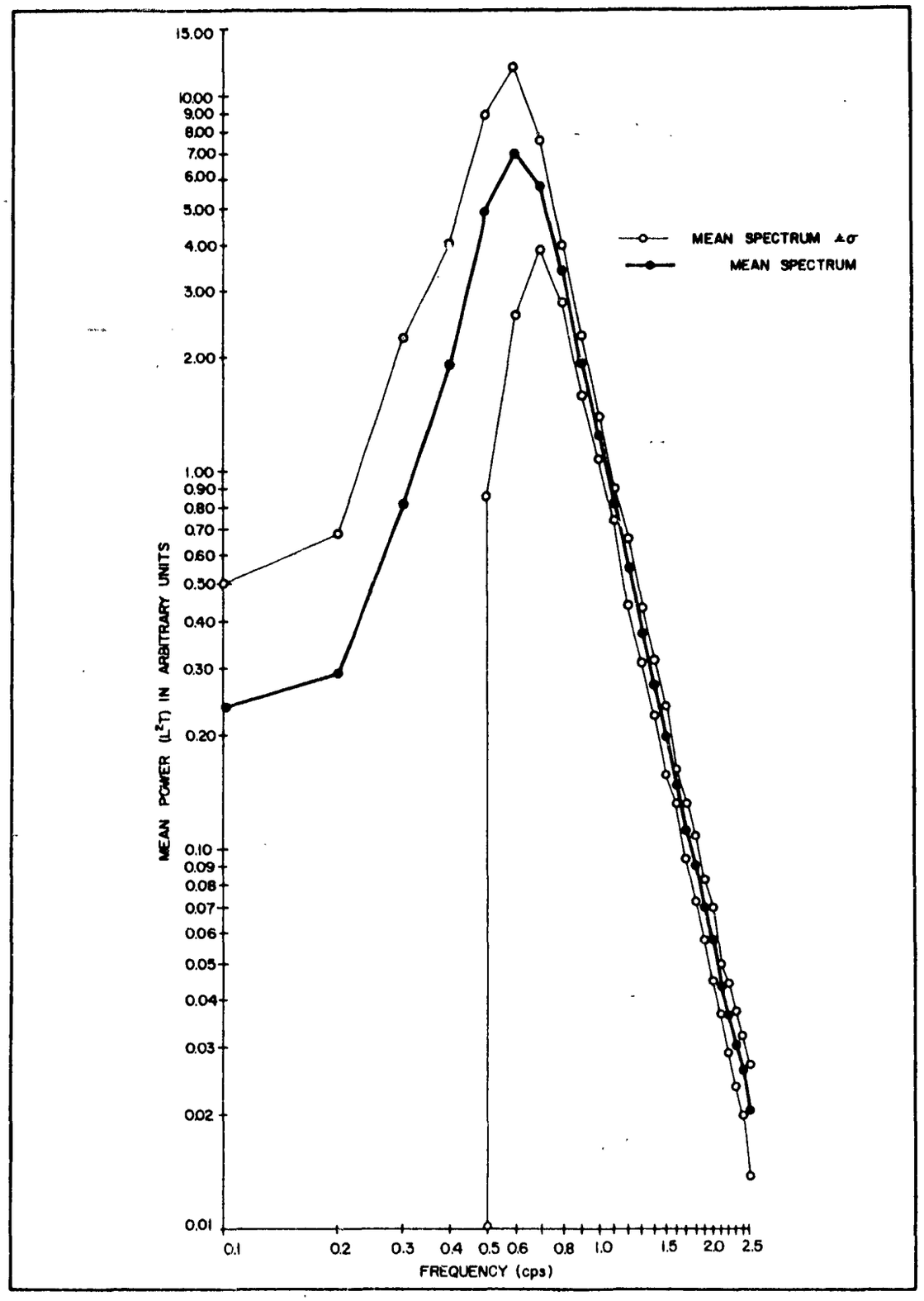

Figure 6.5 The Mean Spectrum of the July Records

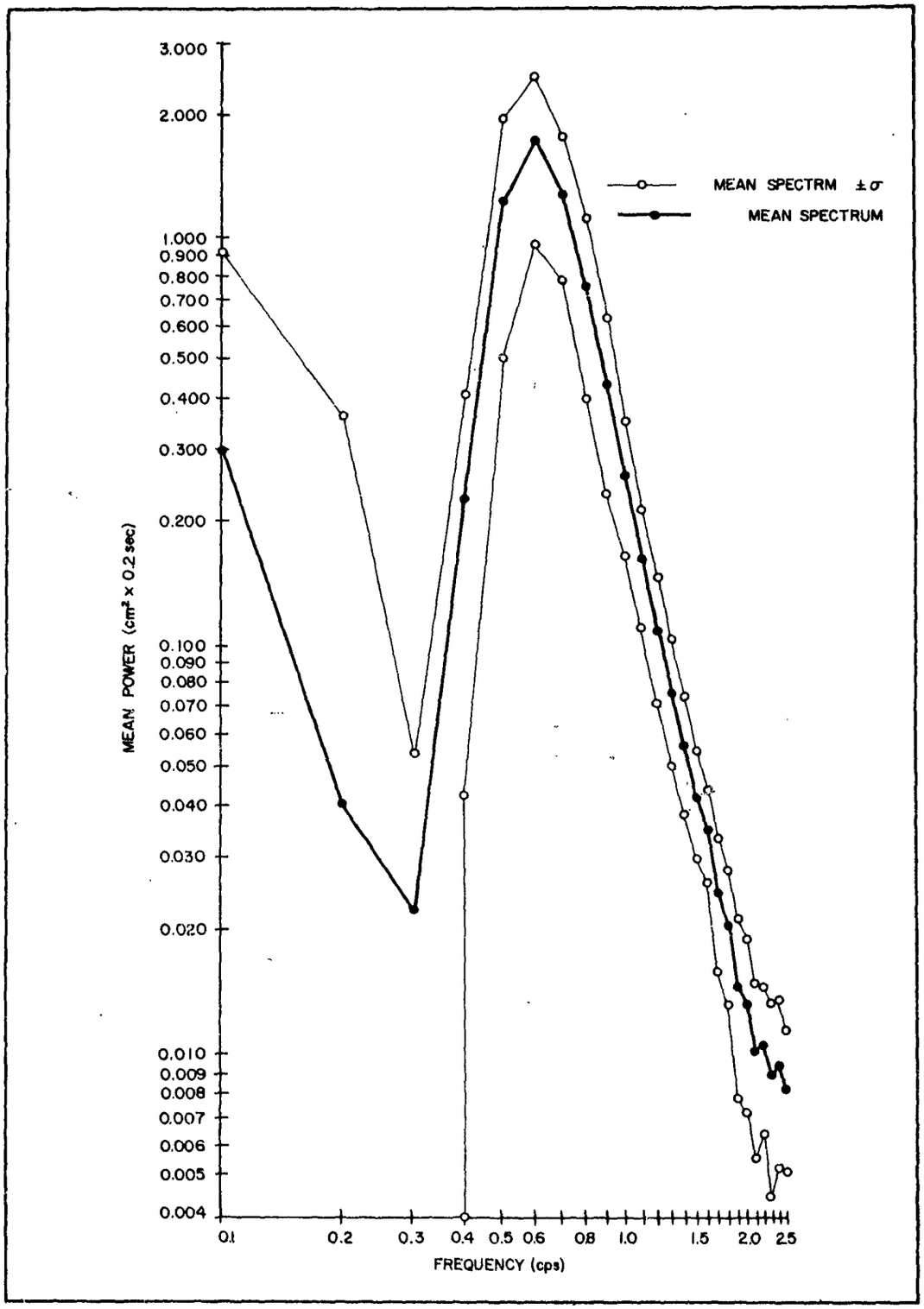

Figure 6.6 The Mean Spectrum of the November Records

the two sets of means with b = -4.5 give

$\hat{\bar{P}}_J = 1.2276\, f^{-4.5}$ for July ($\hat{\bar{P}}_J$ arbitrary units) and

$\hat{\bar{P}}_N = 0.26283\, f^{-4.5}$ for November ($\hat{\bar{P}}_N$ in cm^2 x 0.2 sec).

These equations give us a means of rescaling the July records to bring them in line with the calibrated November records and thus provide July with a calibration of sorts. Let $\hat{\bar{P}}_J \equiv$ the mean power in the July records and $\hat{\bar{P}}_N \equiv$ the mean power in the November records. Then we want

$k\,\hat{\bar{P}}_J = \hat{\bar{P}}_N$; thus

$$k = \frac{\hat{\bar{P}}_N}{\hat{\bar{P}}_J} = \frac{0.26283\, f^{-4.5}}{1.2276\, f^{-4.5}} = 0.21410.$$ In all spectral values for July records except those used in these calculations this correction has been applied.

For further study the entire set of 24 records from 0.8 to 2.1 cps are conceived as 24 random samples of a single process. If the equilibrium hypothesis is true, these 24 records should show a random ordering from frequency to frequency. A systematic ordering would make the hypothesis untenable. Table 6.2 shows the 12 averaged spectra for each run ranked from 1 for the least power to 12 for the greatest. Except for run 093-094, which ranks 12th for all frequencies, the ordering is clearly chaotic. The table also shows the rank correlation coefficient of each column with the previous column:

$$\rho_r = 1 - \frac{6 \sum d^2}{n^3 - n}$$

where $d \equiv$ the difference between rankings, and

$n \equiv$ the number of items ranked. The values of ρ_r are all low, three of them being zero to the nearest one-thousandth and five more being less than one-tenth; also, both positive and negative values occur. A rough sign test using binomial probability paper (Mosteller

Table 6.2 The Rank Correlation

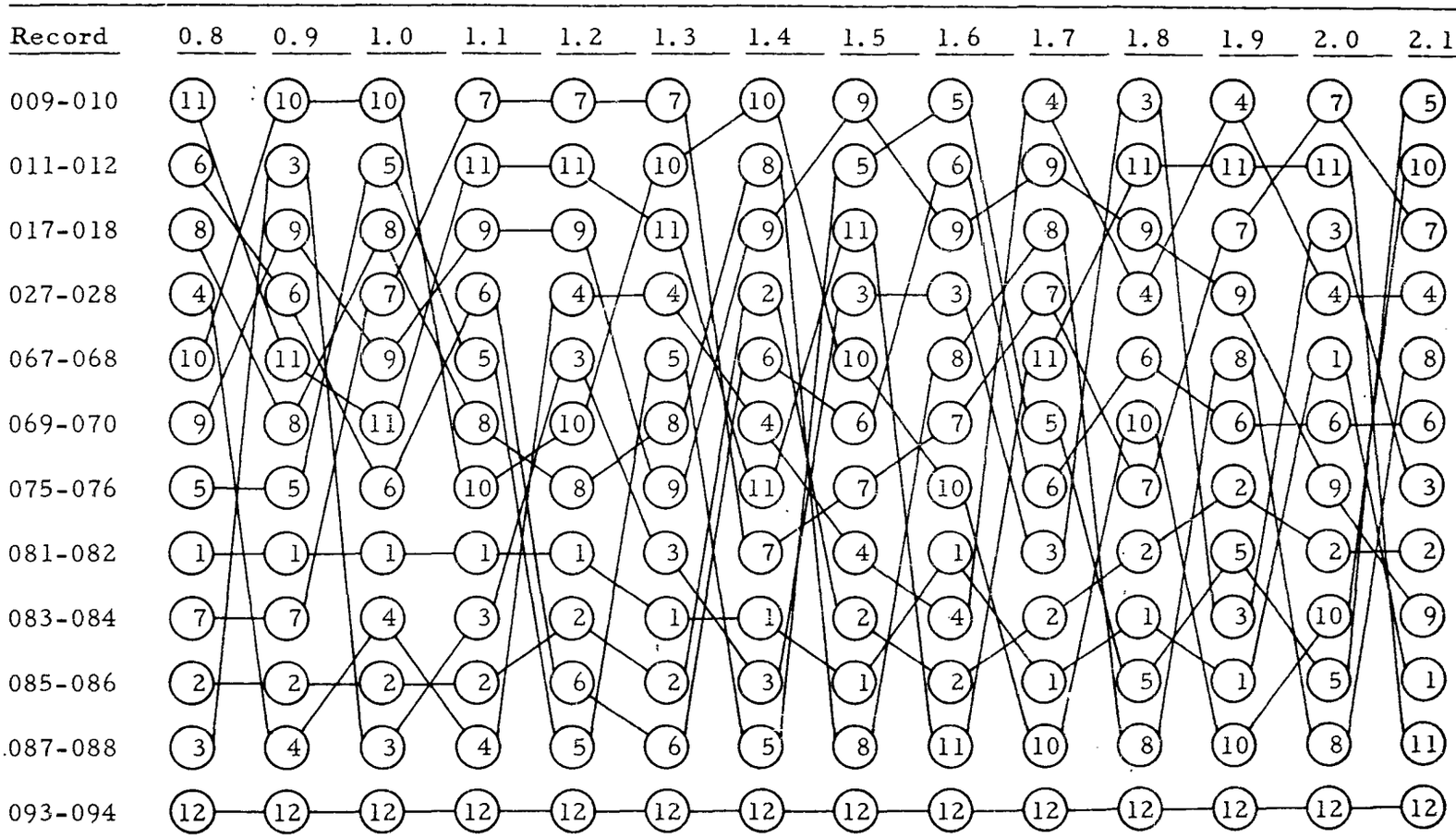

and Tukey, 1949), shows no significant difference from $\rho_r = 0$. The picture could be made even more attractive (although the magnitude of the rank correlation would be increased) if some legitimate reason could be found for discarding record 093-094. A careful search revealed none, so the record has been retained. Even including this record the evidence is apparently strong enough to indicate that there is no systematic variation in power from record to record which demands a physical explanation. Thus we may regard our 24 records as random samples of a single physical process in the range 0.8 to 2.1 cps.

If all the records are rescaled from $cm^2 \times 0.2$ sec to cm^2-sec, i.e., to cm^2 per unit frequency, and averaged, the values showed in table 6.3 and plotted in figure 6.7 occur. The least-squares line for these average points with a slope of -4.5 is $\hat{P} = 1.313\, f^{-4.5}$. Since each record has about 60 degrees of freedom per estimate, the averages have about 1440 degrees of freedom. If we reduce this to a thousand because the spectrum is not flat, we get the confidence limits showed in table 6.3 and figure 6.7. There is an 80% probability that the process measured by the averages has a true value lying within these limits. It is interesting to note that $\hat{P}$ given by the best-fit equation lies within these limits 11 times, coincides with a limit to three decimal places once, and lies outside the limits twice. Counting the coincidence as one-half, the line lies within the 80% interval in 82.1% of the 14 points.

It is clear that the points presented here are incompatible with a line having a -5 slope. However, in exploring the dynamic response we derived an upper bound for a transfer function, figure 2.21. The values have been plotted for sensitivities of 1 and 2 volts/line and an estimate of the upper bound entered in figure 6.8. It must be borne in mind that both of the values entering the ratio which estimates the transfer function

Table 6.3 The Saturated Side of the Mean Spectrum of All the Records

Frequency (cps)	Power (cm^2-sec)	10% Confidence Limit (cm^2-sec)	90% Confidence Limit (cm^2-sec)	50% Confidence Limit (cm^2-sec)
0.8	0.367, 1	0.347, 1	0.389, 1	0.358, 1
0.9	0.209, 1	0.198, 1	0.220, 1	0.211, 1
1.0	0.128, 1	0.121, 1	0.136, 1	0.131, 1
1.1	0.812, 0	0.768, 0	0.861, 0	0.855, 0
1.2	0.549, 0	0.519, 0	0.582, 0	0.578, 0
1.3	0.380, 0	0.359, 0	0.403, 0	0.403, 0
1.4	0.279, 0	0.264, 0	0.296, 0	0.288, 0
1.5	0.208, 0	0.197, 0	0.221, 0	0.212, 0
1.6	0.166, 0	0.157, 0	0.176, 0	0.158, 0
1.7	0.120, 0	0.113, 0	0.127, 0	0.121, 0
1.8	0.990,-1	0.937,-1	0.105, 0	0.932,-1
1.9	0.724,-1	0.685,-1	0.768,-1	0.731,-1
2.0	0.633,-1	0.598,-1	0.671,-1	0.580,-1
2.1	0.487,-1	0.461,-1	0.516,-1	0.466,-1

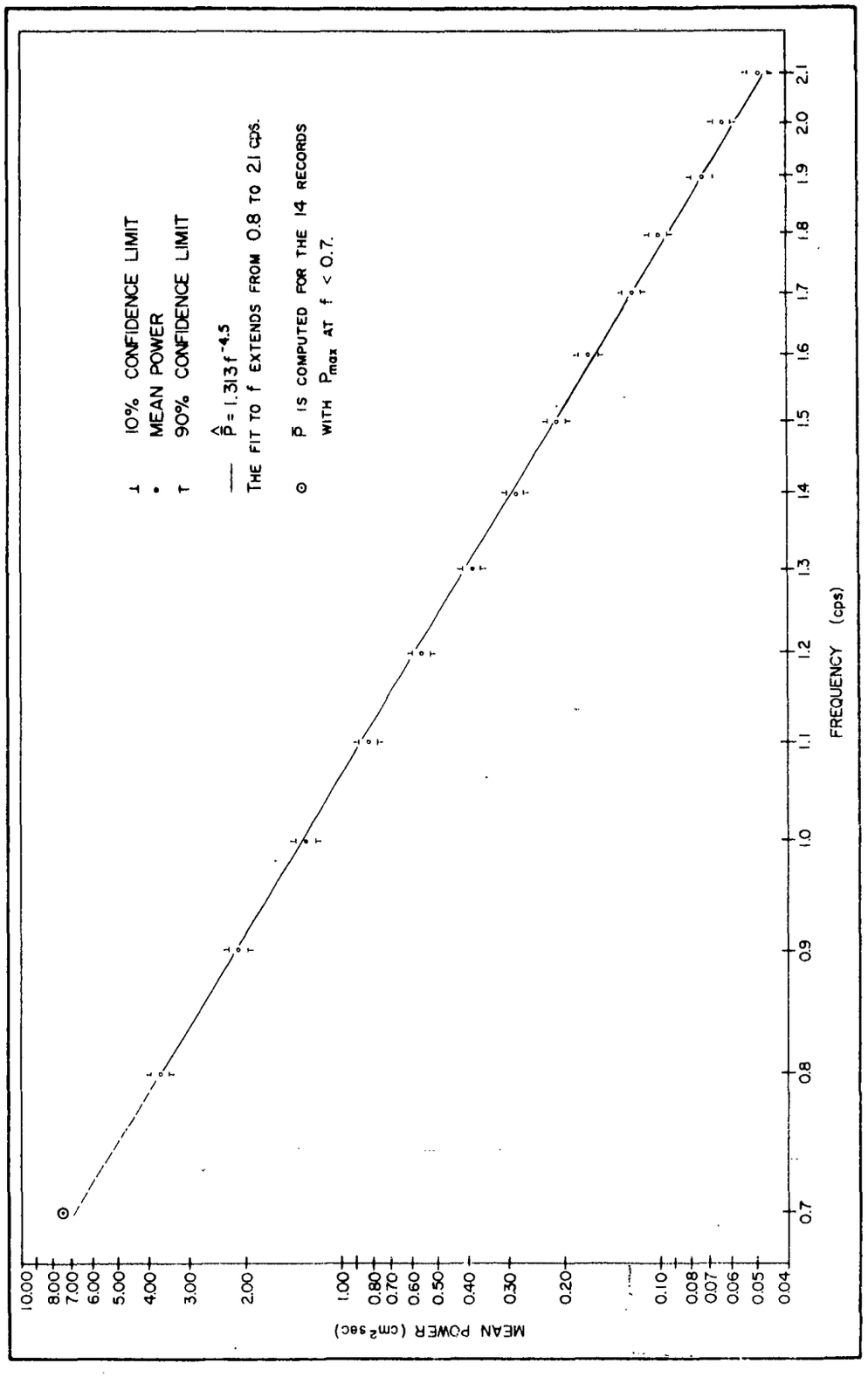

Figure 6.7 The Saturated Side of the Mean Spectrum of All the Records

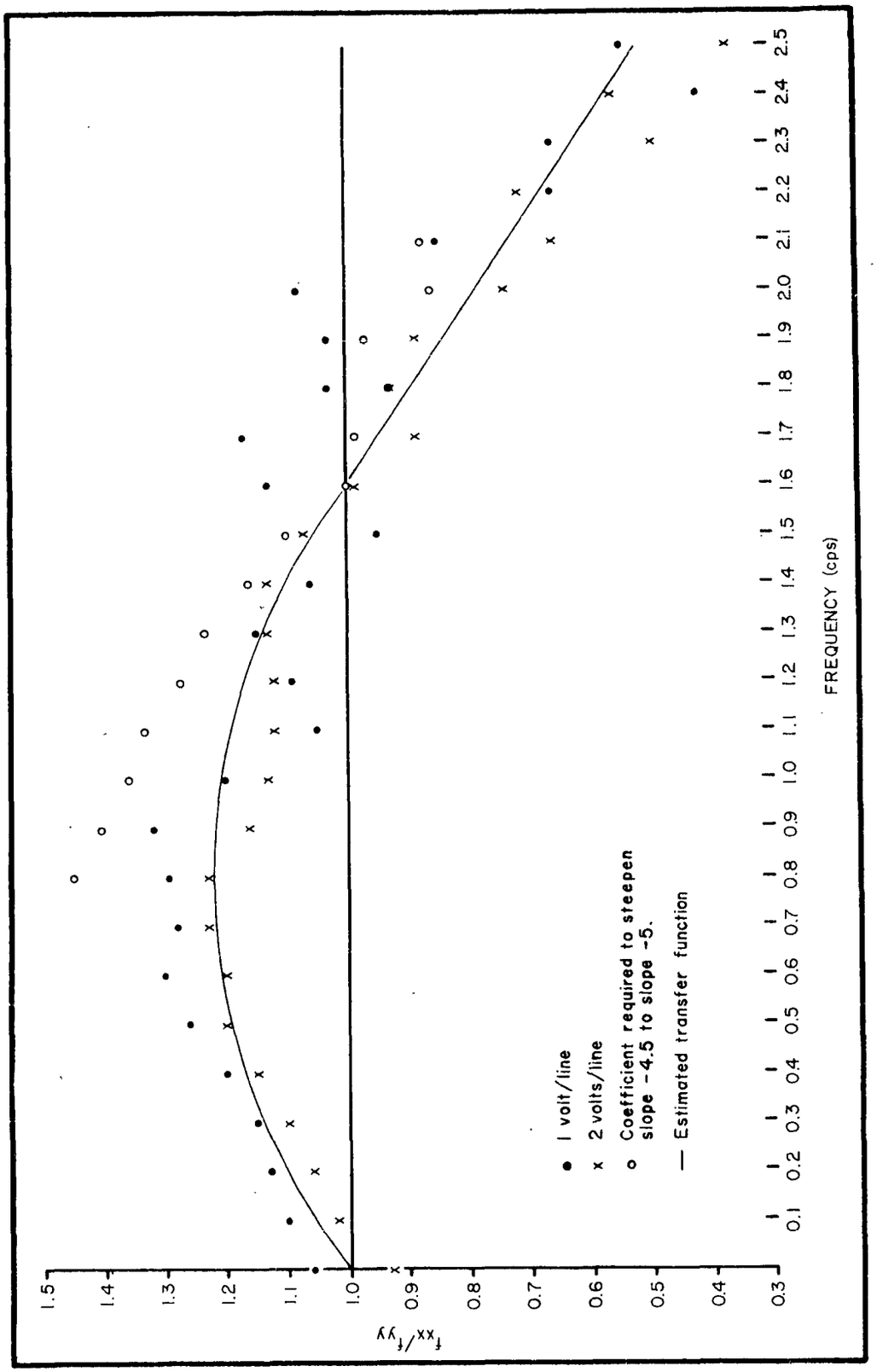

Figure 6.8 The Transfer Function from the Dynamic Response Exploration

are subject to considerable statistical fluctuation; we may therefore anticipate that their ratio will be quite erratic. Showed also in figure 6.8 are the coefficients by which the mean observed power values must be multiplied to bring them into the line

$\overline{P}_{-5} = 1.741 f^{-5}$, which leaves the point f = 1.6 cps, $\overline{P}$ = 0.166 cm^2-sec unchanged. It is clear that even the most extreme correction which might just possibly be applied to the data is insufficient to steepen the curve to a -5-power law in the frequency.

Of the 24 records there are 14 in which the maximum power occurs at 0.6 cps. For these records the power at 0.7 cps was averaged and the value entered in figure 6.7. It is interesting that this point which did not enter the previous analysis agrees so well with the extrapolated -4.5-power line. One may suspect that the equilibrium range, when there has been enough time for it to establish itself, extends down very nearly to the frequency at which the maximum power occurs for records taken at restricted fetches, as these were.

It would almost seem that we were ready to draw some conclusions but we have been getting on far too fast for that. For one thing we have been looking only at mean values which have erased the individual details of the spectra, and for another we have hitherto entirely neglected two papers dealing with the nonlinear aspects of the problem.

6.2.2 Nonlinear Interactions

Tick (1958) uses the Gaussian assumption in a sophisticated way to produce a second-order correction to the linear model for infinite, i.e., long-crested, gravity waves. He retains quadratic terms in the perturbation expansions of the relevant differential equations. He

assumes that the sea surface, η, can be expressed as the sum of two functions,

$\eta = \eta^{(1)} + \eta^{(2)}$, where $\eta^{(1)}$ only is Gaussian and $\eta^{(2)}$ becomes a "correction" that accounts for the departure of the sea surface from a strictly Gaussian distribution. Tick says of his work on page 6, "In a sense we are making a double perturbation: one of the differential equation about some equilibrium condition, and the other, of the probability structure, about the Gaussian 'point.' "

Phillips (1960) has set about exploring the problem of nonlinear effects a bit differently. He begins looking for an efficient transfer of energy from one Fourier component of the sea to another by nonlinear interaction. Phillips describes his results as follows:

"An equation is set up to describe the time history of the Fourier components of the surface displacement in which are retained terms whose magnitude is of order $(\text{slope})^2$ relative to the linear (first order) terms. The second order terms give rise to Fourier components with wave-numbers and frequencies formed by the sums and differences of those of the primary components, and the amplitudes of these secondary components are always bounded in time and small in magnitude. The phase velocity of the secondary components is always different from the phase velocity of a free infinitesimal wave of the same wave-number. However, the third order terms can give rise to tertiary components whose phase velocity is equal to the phase velocity of a free infinitesimal wave of the same wave number, and when this condition is satisfied, the amplitude of the tertiary components grows linearly with time in a resonant manner and there is a continuing flux of potential energy from one wave-number to another. The time scale of the growth of the tertiary component is of order (the geometric mean of the primary wave slopes)$^{-2}$ times the period of the tertiary wave."

In another place he says:

"The principal result of this analysis is the demonstration that, although the tertiary interactions among wave components are given by a perturbation term that is algebraically smaller than that representing the secondary interactions, their cumulative dynamical effect is much more profound because of the existence of resonant wave-numbers whose amplitude grows with time. This implies that, in the development of a dynamical theory to describe a finite amplitude random gravity wave field, the tertiary interactions are essential, and any theory in which they are neglected will ignore the dominant mechanism of energy transfer among the wave components."

The paper cited is part I. It is anticipated that part II will extend these results to a statistical theory.

Tick's theory predicts the existence of a small secondary maximum in the spectrum at a frequency slightly greater than twice the frequency of the primary peak. Phillips' theory, as developed in part I, is not for spectra but for components. He shows that, if we begin with a sine wave of frequency f, the nonlinear interaction of the wave with itself will soon produce waves with frequencies $\sqrt{2}f$, $\sqrt{3}f$, $2f$, $(\sqrt{2})^3 f$, and $3f$. Since our spectra are quite sharply peaked, perhaps it will be worth while to explore them both for surplus energy at this series of frequencies, using f_{max} (the frequency at which the maximum power appears) as the primary frequency, and for surplus energy at slightly more than $2f_{max}$ as suggested by Tick.

Figures AIV 2.01.1 to AIV 2.24.1 show log-log plots of the spectra from 0.7 to 2.1 cps. Figure 6.9 for record 075 is an example. The position of $2f_{max}$ has been entered on the plots. Since P_{max} reported

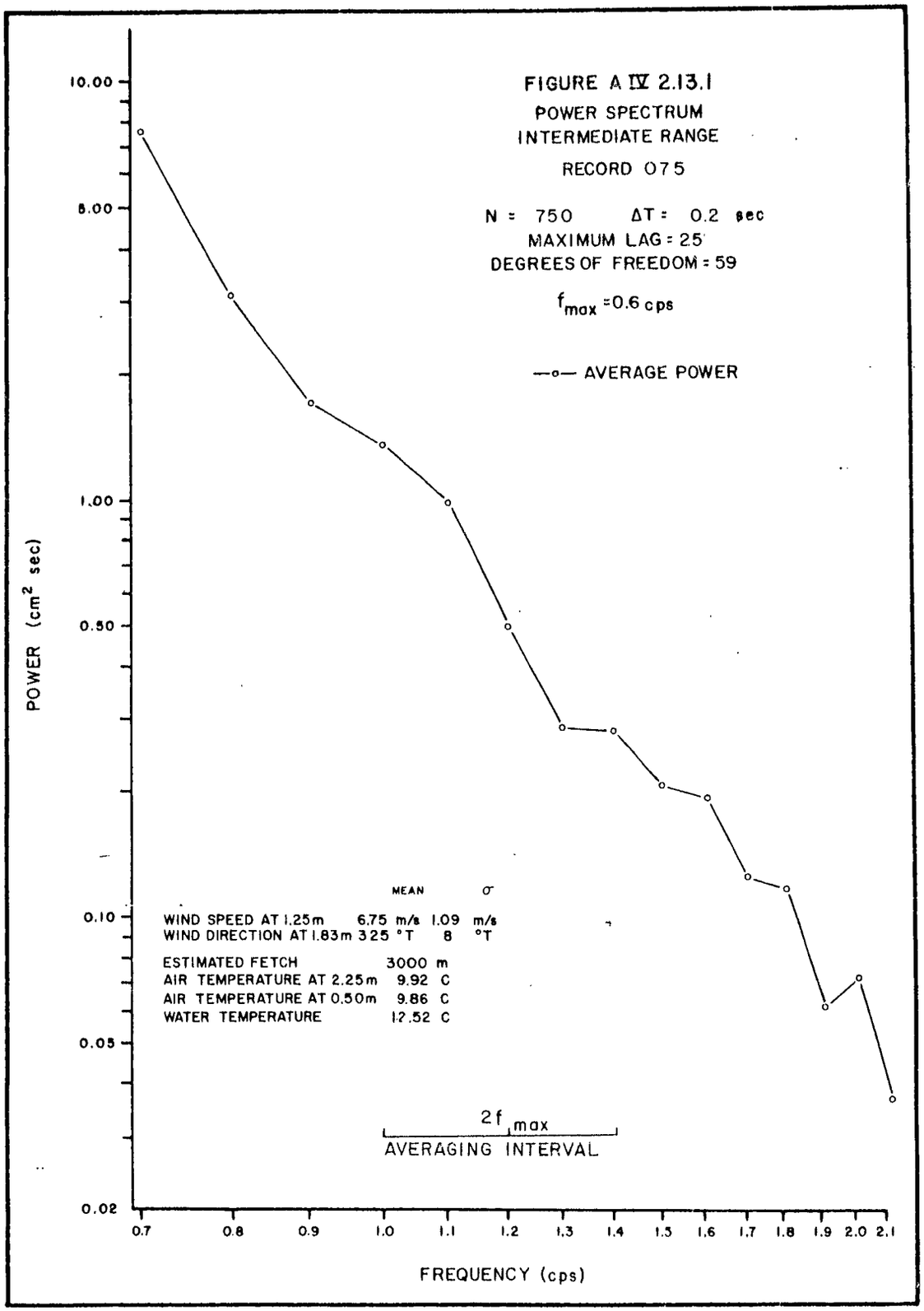

Figure 6.9 An Example of the Log-Log Plots of the Saturated Sides of the Spectra at Low Resolution

at f_{max} is an average over the interval $f_{max} - 0.1$ to $f_{max} + 0.1$, the exact position of $2f_{max}$ is indefinite within the band $2f_{max} - 0.2$ to $2f_{max} + 0.2$. This band is showed around $2f_{max}$ and labeled "averaging interval." Of the 24 spectra, 23 show a palpable excess of energy in the vicinity of $2f_{max}$ although in only 2 instances is a relative maximum achieved. In no single case is the increase in energy statistically significant within a single record, but the persistence of the phenomenon necessitates taking it seriously.

What we really need at this point is a spectral analysis of the records at a higher resolution so that the details can emerge. Fortunately, at the same time the November records were analyzed at a maximum lag of 25, they were also computed at a maximum lag of 50.* These values are showed in table AIV 3.9 to AIV 3.24 and plotted on log-log paper over the range from 0.7 to 2.1 cps in figures AIV 3.09.1 to AIV 3.24.1. Figure 6.10 for record 075 is an example. We have again entered $2f_{max}$ but instead of the "averaging interval" the band showed is derived by determining the frequencies corresponding to $e^{-1}P_{max}$ and doubling them. This is offered purely as a descriptive measure of the peakedness and asymmetry of the power peak which is not showed on the plot. Since the record length has not been increased, the degrees of freedom have been reduced in the course of doubling the number of power estimates between 0.0 and 2.5 cps. Consequently, the detail showed in these figures is no more statistically significant within a given record than it was before. It is persistence that is important.

Inspection of the figures shows that numerous relative maxima, as well as less marked energy excesses, have emerged under higher

*If spectra are computed digitally for the greatest maximum lag that will conceivably be useful, the values for lesser maximum lags, and consequently for lower resolutions and closer confidence limits, may be had for almost no extra machine time.

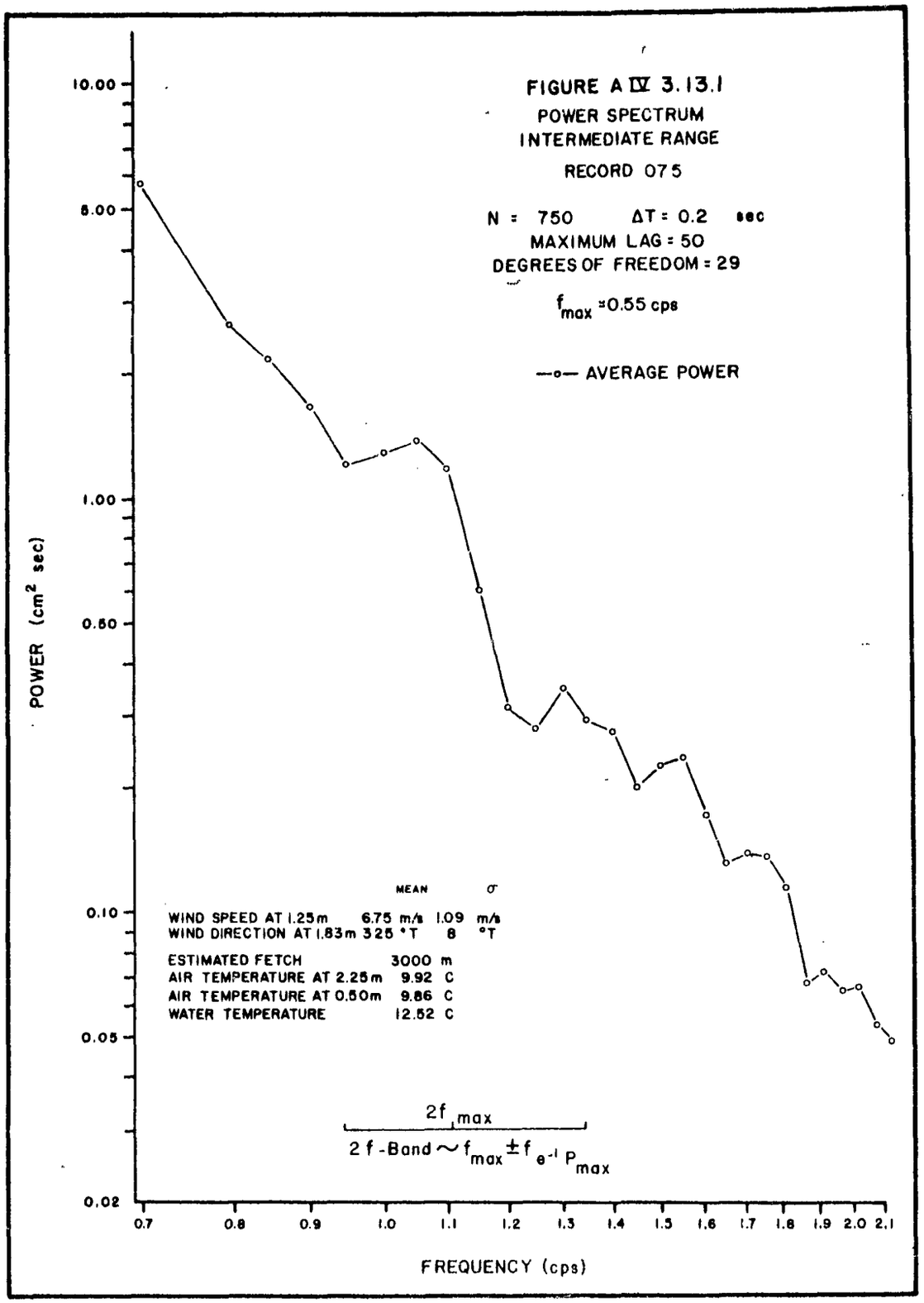

Figure 6.10 An Example of the Log-Log Plots of the Saturated Sides of the Spectra at High Resolution

resolution. Spectral analyses become more and more unstable under higher resolution so that the increased irregularity would have been expected. However, the maximum lag is still comfortably less than 10 per cent of the number of data points so that perhaps we may give some attention to the detail. The frequencies at which the energy excesses occur were read from each figure; to facilitate comparison among the records they were then divided by the frequency at which the maximum power occurs in the record. Table 6.4 shows the results of this rescaling. It was organized by lining up the first relative frequency greater than two and letting the other ratios fall in their natural order except for record 067, in which the first value encountered clearly belongs in the first column rather than the second. In 5 of the 16 records the f_1/f_{max} ratio was absent. There is no overlap between the values in adjacent columns, and the standard deviation seems quite small when one remembers the uncertainty of position introduced by the averaging interval for both terms of the ratio. For example, with nominal values of $f_{max} = 0.55$ and $f_5 = 2.00$, $f_5/f_{max} = 3.64$, but the possible range of values due to position uncertainty within the averaging interval is $1.95/0.60 = 3.27$ to $2.05/0.50 = 4.10$. The means from table 6.4 may be compared with the values predicted by Phillips for frequencies arising from a single sine wave with f = 1.00 (table 6.5). The author finds

Table 6.5 Comparison of the Means of the Relative Frequencies with Those Suggested by Phillips

Phillips' Frequencies (f_P)	Observed Mean Frequencies (f_{ob})	Difference ($f_{ob} - f_P$)	% Difference $\left(\frac{f_{ob}-f_P}{f_P} \times 100\right)$
$\sqrt{2} = 1.41$	1.37	-0.04	- 2.8
$\sqrt{3} = 1.73$	1.79	0.06	3.5
$2 = 2.00$	2.26	0.26	13 0
$(\sqrt{2})^3 = 2.83$	2.69	-0.14	- 4.9
$3 = 3\ 00$	3.17	0.17	5.7

Table 6.4 Positions of Energy Excesses Relative to the Position of the the Maximum Energy for the November Records Analyzed at High Resolution*

Record	f_1/f_{max}	f_2/f_{max}	f_3/f_{max}	f_4/f_{max}	f_5/f_{max}
067	1.48	-	2.08	2.54	3.08
068	-	1.84	2.38	2.69	3.23
069	1.45	1.73	2.18	2.73	3.64
070	-	1.82	2.09	2.82	3.18
075	-	1.91	2.36	2.82	3.45
076	1.45	1.91	2.36	2.73	3.00
081	-	1.67	2.25	2.58	3.50
082	1.23	1.53	2.08	2.77	3.00
083	1.25	1.83	2.33	2.67	3.00
084	-	1.92	2.46	2.69	3.00
085	1.45	1.82	2.36	2.64	3.27
086	1.36	1.73	2.27	2.64	3.00
093	1.42	1.67	2.00	2.58	2.92
094	1.25	1.92	2.42	2.75	3.08
mean	1.37	1.79	2.26	2.69	3.17
σ	0.11	0.15	0.12	0.06	0.18

*Records 087 and 088 have been omitted from this analysis for the reasons given in section 6.1.

this agreement suggestive, although no quantitative analysis can legitimately be undertaken until the results of Phillips' third-order theory for component waves are extended to a statistical theory. The regular appearance of excess energy in the regions where, according to Phillips, the nonlinear processes would place them seems to indicate that a nonlinear theory of gravity surface waves might with profit be extended to at least the third term in the expansion. The mean corresponding to 2 cps is much farther away from the Phillips frequency than the others. This is what one would expect if the Tick secondary maximum which occurs at more than 2 cps were present.

Pierson (1959) computes the size of the secondary maximum predicted by Tick for a spectrum given in Chase et al. (1957) and finds it too small to account for the values showed there. This discrepancy could conceivably be explained by Phillips' result, i.e., second-order components are bounded in time and may well be overwhelmed by resonant tertiaries in the same region. The spectrum showed by Chase et al. in figure 10.1 of their report is an average of three spectra with maxima at very nearly the same frequency. The values entering the average are showed in table 10.1 of the same report. If each of the three spectra is subjected to the same analysis and rescaling as were our records, the results showed in table 6.6 are secured. For comparing these results

Table 6.6 Positions of Energy Excesses Relative to the Position of the Maximum Energy for the SWOP Wave Pole Data

Record	f_1/f_{max}	f_2/f_{max}	f_3/f_{max}	f_4/f_{max}	f_5/f_{max}
No. 1	1.45	-	2.18	2.91	3.27
No. 2	1.42	1.83	2.17	2.67	3.17
No. 3	1.50	1.92	2.33	2.67	3.00
mean	1.46	1.88	2.23	2.75	3.15
σ	0.03	0.05	0.07	0.11	0.11

from the SWOP data with Phillips' frequencies we have table 6.7.

Table 6.7 Comparison of the Means of the Relative SWOP Frequencies with Those Suggested by Phillips

Phillips' Frequencies (f_P)	Mean SWOP Frequencies (f_{SWOP})	Difference ($f_{SWOP} - f_P$)	% Difference $\left(\frac{f_{SWOP}-f_P}{f_P} \times 100\right)$
$\sqrt{2} = 1.41$	1.46	0.05	3.5
$\sqrt{3} = 1.73$	1.88	0.15	8.7
$2 = 2.00$	2.23	0.23	11.5
$(\sqrt{2})^3 = 2.83$	2.75	-0.08	- 2.8
$3 = 3.00$	3.15	0.15	5.0

Again the agreement is suggestive and similar to that from the author's data. It is interesting to note that the records made for this study and those for SWOP are entirely different in scale because the latter was carried out in the open ocean. The author's maximum energies occur around 0.6 cps while for SWOP they occur near 0.125 cps; still the relative spacing of energy excesses for the two is much the same.

The spectra showed in Burling (1955) also show a lumpy structure, and a brief attempt was made to find out whether information of the same sort could be derived from them. The attempt proved useless. From the discussion of the difficulties with the analog device which Burling used for his analysis (Burling, 1955, section 6.2) the author can only conclude that the results are too crude to supply the desired information.* Frequencies near the predicted ones are often present, but so were many others. The entire group of spectra are highly erratic not only between records but for repeated analysis of the same record.

*The author's judgment was confirmed by Phillips (personal communication) who has had an opportunity to observe the analog device under discussion.

The author feels that the evidence presented in this section suggests that attempts to devise a nonlinear theory for a finite-amplitude gravity wave field should include at least the third term in the expansion. It should be clear that the data presented here are insufficient to settle the question of the nonlinear interactions. They do suggest that further work, both field and theoretical, should be undertaken with the aim of laying these ghosts or giving them full-bodied life.

6.2.3 The Equilibrium Range and the Intermediate Range

We must now reconsider our discussion of the averaged spectra from 0.7 to 2.1 cps (section 6.2.1) in the light of the evidence of nonlinear interaction (section 6.2.2). The low-resolution figures AIV 2.01.1 to AIV 2.24.1 each show a longer or shorter interval between f_{max} and $2f_{max}$ which appears substantially straight when plotted on a log-log scale. If least-squares fits of the form

$$\log P = \log a + b \log f$$

are made for the straight section of each record, the resulting slopes range from -7.56 to -4.30. The mean of the 24 slopes is -5.52 and the standard deviation is ±0.83. Thus the mean slope of the straight section just above f_{max} is steeper than Burling's -5, Hicks' -4.7, and the author's -4.5. It matches the -5.5 derived by Hicks from Cox. It falls neatly half way between Phillips' -5 for the equilibrium range and the -6 extrapolated from Neumann's spectrum.

If we consider waves as they occur, we never find all the energy at a single frequency; it is always spread over a band around f_{max}. If we assume that each of these components generates its own secondaries and resonant tertiaries by nonlinear interaction with itself, and if the primaries do not interact with each other, which is an entirely

unrealistic assumption, the bands in which the tertiaries will occur will increase in length with the frequency. With the band $f_{max} - \epsilon/2$ to $f_{max} + \epsilon/2$ for the primaries, figure 6.11 shows the corresponding ranges for the frequencies generated by the interaction process while interactions among the primaries were neglected. It is clear that, were

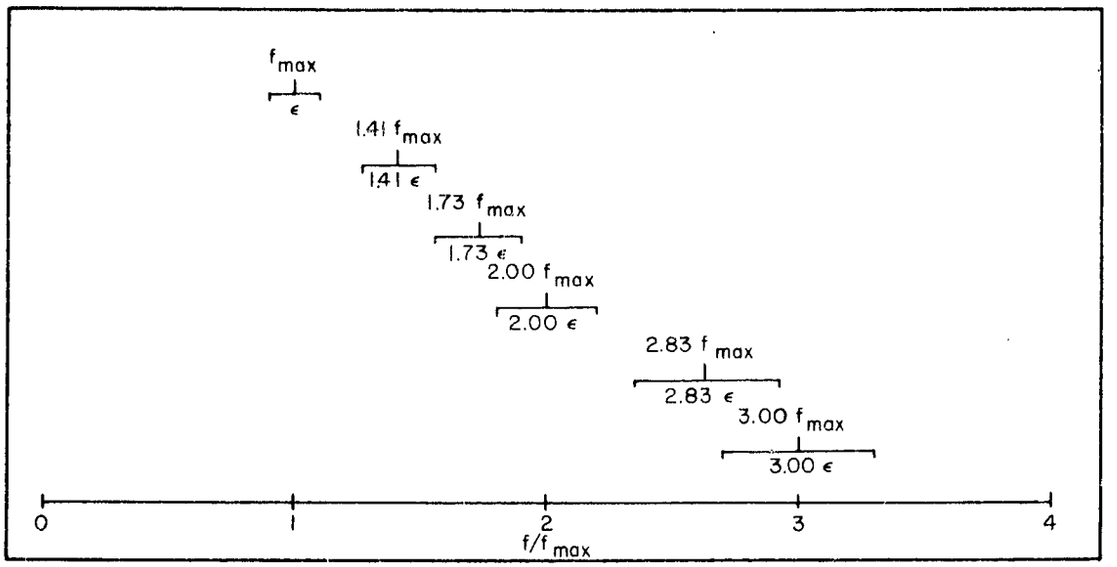

Figure 6.11 Overlapping Multiples of the f_{max} Interval

this figure extended to include higher frequencies, even the modest degree of separation showed would soon be lost and a region encountered where interaction contributions of many kinds would be present in every range of f considered. This region will occur sooner or later as the band width of the primaries is larger or smaller. Such a region of overlap is necessary for the equilibrium range. If the spectrum is very sharply peaked, i.e., if ϵ is comparatively small, the excess energy arising from nonlinear interactions will remain separated up to and beyond $f/f_{max} = 3$. If ϵ is relatively large, the peak in the spectrum is broad, and we may expect the equilibrium range to begin shortly after $f/f_{max} = 2$. This agrees with the suggestion made by Pierson (1959) that the equilibrium range may begin above $f/f_{max} \approx 2$. Of course, the

picture presented in figure 6.11 is wrong. Primaries do interact with each other, and a correct picture must wait for the development of a statistical theory for resonant tertiaries. It will be interesting to see what modifications such a theory will make.

From these considerations it would seem that the range from 0.7 to 2.1 cps discussed in section 6.2.1 may be identified more properly as the intermediate range than as the equilibrium range, since the energy excesses are well separated within each record. It is easy to see that the process of averaging over a number of spectra whose maxima are at different frequencies produces something analogous to a broad ϵ band about the average f_{max}, thus creating an "equilibrium" range in the average spectrum where none exists in the individual records. Since the initial fall from f_{max} is generally steeper than the equilibrium slope, and since the positions and sizes of the energy excesses are an accident of the records selected for the average, the numerical values of the slopes of such averaged spectra in the region from f_{max} to $3f_{max}$ are statistical artifacts. We need not postulate one constant "real" slope applicable to all situations which the various reported slopes are assumed to measure. Consequently, much more may be expected from a study of such averages if the records entering them are carefully scrutinized for their physical properties, and averages are made only for those sets of records which have some reasonable connection with the averaging process. Averages taken indiscriminately over heterogeneous collections of records are likely to produce only profitless arguments about the particular values that result.

7.0 BIBLIOGRAPHY

BARBER, N. F.

1946a Measurements of sea conditions by the motion of a floating buoy. Admiralty Research Laboratory, England, Note A.R.L./103.40/N.2/W.

1946b Ship motion as a guide to sea conditions. Admiralty Research Laboratory, England, Note A.R.L./N.3/103.40 W.

BARBER, N. F., G. COLLINS, and M. J. TUCKER

1946 Proposals for a frequency analyzer to give phase and amplitude. Admiralty Research Laboratory, England, Note A.R.L./103.30/N.2/W.

BARBER, N. F., F. URSELL, and J. DARBYSHIRE

1946 A frequency analyzer used in the study of ocean waves. Nature (London) 158:329.

BENDAT, J. S.

1958 Principles and Applications of Random Noise Theory. John Wiley and Sons, N.Y.

BINDER, R. C.

1955 Fluid Mechanics, third edition. Prentice-Hall, Inc., Englewood Cliffs, N.J.

BIRKHOFF, G., and J. KOTIK

1952 Fourier analysis of wave trains. In Gravity Waves, National Bureau of Standards Circ. 521, pp. 243-253.

BLACKMAN, R. B., and J. W. TUKEY

1958 The Measurement of Power Spectra from the Point of View of Communications Engineering. Dover Publications, Inc. N. Y.

BURLING, R. W.

1955 Wind generation of waves on water. Ph.D. dissertation, Imperial College, University of London.

CHASE, J., L. J. COTE, W. MARKS, E. MEHR, W. J. PIERSON, JR., F. C. RÖNNE, G. STEPHENSON, R. C. VETTER, and R. G. WALDEN

1957 The directional spectrum of a wind generated sea as determined by the stereo wave observation project. Technical Report, Research Division, College of Engineering, New York University.

COULSON, C. A.

1949 Waves, a Mathematical Account of the Common Types of Wave Motion. Interscience Publishers, Inc., N. Y.

COX, C. S.

1958 Measurements of slopes of high frequency wind waves. J. Mar. Res. 16, 199-225.

DE FERIET, J. K.

1954-1955 Introduction to the statistical theory of turbulence, Parts I-IV. J. Soc. Ind. Appl. Maths. 2, 1, 3, 4, 3, 2.

ECKART, C.

1946 The sea surface and its effect on the reflection of sound and light. University of California, Division of War Research, Sonar Data Division File No: 01.75, UCDWR No. M 407.

1953 Theory of noise in continuous media. J. Acoust. Soc. Am, 25, 195-199.

ESTERSON, G. L.

1957 The induction conductivity indicator (ICI), a new method for conductivity measurement at sea. Chesapeake Bay Inst., Technical Report XIV, Ref. 57-3.

GILL, G. C.

1954 A fast response anemometer for micrometeorological investigations. Bull. Am. Meteorol. Soc. 35, 69-75.

HASTINGS, C. E.

1949 A new type instrument for measuring air velocity. Am. Inst. Elec. Eng. miscellaneous paper 49-23.

HASTINGS, C. E., and C. R. WCISLO

1951 A compensated thermal anemometer and flowmeter. Am. Inst. Elec. Eng. miscellaneous paper 51-149.

HASTINGS, C. E., and E. T. DOYLE

1956 Use of the compensated hot thermopile principle in industrial instrumentation. Second IRE Instrumentation Conference (Atlanta, Georgia, December 5-7, 1956).

HICKS, B. L., and C. G. WHITTENBURY

1956 Wind waves on the water. Report R-83, Control Systems Laboratory, University of Illinois, Urbana, Ill.

HICKS, B. L.

1960 The generation of small water waves by the wind, Part I, comparison of data from different sources. Report M-86, Coordinated Science Laboratory, University of Illinois, Urbana, Ill.

LAMB, H.

1932 Hydrodynamics, sixth edition. Dover Publications, Inc., N.Y.

LONGUET-HIGGINS, M. S.

1946 Resolution of the sea into long crested waves. Admiralty Research Laboratory, England, Note A.R.L./103.30/N.1/W.

1950 A theory of microseism generation. Phil. Trans. Roy. Soc. London A 243, 1-35. (Published originally in 1948: Admiralty Research Laboratory Note R2/103.50/W.)

MACKAY, J. H.

1959 On the Gaussian nature of ocean waves. Project A-366, Technical Note No. 8, Engineering Experiment Station, Georgia Institute of Technology, Atlanta, Ga.

MOSTELLER, F., and J. W. TUKEY

1949 The uses and usefulness of binominal probability paper. J. Am. Stat. Assoc. 44, 174-212.

MUNK, W. H., F. E. SNODGRASS, and M. J. TUCKER

1959 Spectra of low-frequency ocean waves. Bulletin of the Scripps Institution of Oceanography, University of California, La Jolla, Calif., 7, 283-362.

PHILLIPS, O. M.

1958 The equilibrium range in the spectrum of wind-generated waves. J. Fluid Mech. 4, 426-434.

1960 On the dynamics of finite amplitude unsteady gravity waves. 1. The elementary interactions. J. Fluid Mech. (in press)

PIERSON, W. J., JR.

1952 A unified mathematical theory for the analysis, propagation and refraction of storm generated ocean surface waves, Parts I and II. Research Division, College of Engineering, New York University, Department of Meteorology and Oceanography. Prepared for the Beach Erosion Board, Department of the Army, and Office of Naval Research, Department of the Navy.

1955 Wind-generated gravity waves. In Advances in Geophysics, 2, Academic Press, N.Y., pp.93-178.

1959 A note on the growth of the spectrum of wind-generated gravity waves as determined by non-linear considerations. J. Geophys. Res. 64, 1007-1011.

PIERSON, W. J., JR., G. NEUMANN, and R. W. JAMES

1955 Practical Methods for Observing and Forecasting Ocean Waves by Means of Wave Spectra and Statistics. U.S. Navy Hydrographic Office Publication No. 603.

PROUDMAN, J.

1953 Dynamical Oceanography. John Wiley and Sons, N.Y.

RICE, S. O.

1954 Mathematical analysis of random noise. In Noise and Stochastic Processes. Dover Publications, Inc., N.Y. pp. 133-294. (Published originally in 1944-1945: Bell System Tech. Jour. 23, 282-332, 24, 46-156.)

RUDNICK, P.

1951 Correlograms for Pacific ocean waves. In Proc. Second Berkeley Symposium on Mathematical Statistics and Probability, University of California Press, Berkeley, Calif., pp. 627-638.

ST. DENIS, M., and W. J. PIERSON, JR.

1953 On the motions of ships in confused seas. Trans. Soc. Naval Arch. and Marine Eng. 61, 280-357.

SMART, W. M.

1958 Combination of Observations. Cambridge University Press, London.

STOKER, J. J.

1957 Water Waves, the Mathematical Theory with Applications. Interscience Publishers, N.Y.

SVERDRUP, H. U., and W. H. MUNK

1947 Wind, sea, and swell: theory of relations for forecasting. U.S. Navy Hydrographic Office Pub. No. 601.

TICK, L. J.

1958 A non-linear random model of gravity waves. Scientific Paper No. 11, Statistics Laboratory, Technical Report No. 11, Research Division, College of Engineering, New York University.

TUCKER, M. J., and H. CHARNOCK

1955 A capacitance wire recorder for small waves. Proc. Fifth Conference on Coastal Engineering (Grenoble, September 1954).

TUKEY, J. W.

1949 The sampling theory of power spectrum estimates. In Symposium on Applications of Autocorrelation Analysis to Physical Problems (Woods Hole, Massachusetts, 13-14 June 1949), Office of Naval Research, Department of the Navy.

UPHAM, S. H.

1955 Electric wave staff (Hydrographic Office model Mark I). Technical Report TR-9, U.S. Navy Hydrographic Office.

U.S. DEPARTMENT OF COMMERCE, COAST AND GEODETIC SURVEY

Annually Tide tables, high and low water predictions, east coast North and South America including Greenland.

U.S. DEPARTMENT OF COMMERCE, WEATHER BUREAU

Monthly Local climatological data, Baltimore, Md.

WHITTENBURY, C. G.

1956 A capacitance probe for recording water waves. Report R-84, Control Systems Laboratory, University of Illinois, Urbana, Ill.

WIENER, N.

1930 Generalized harmonic analysis. Acta Mathematica 55, 117-258.

1949 Extrapolation, Interpolation, and Smoothing of Stationary Time Series. John Wiley and Sons, N.Y. (Published originally in 1942 as a classified report.)

To sum up, then: demonstrative knowledge must be knowledge of a necessary nexus, and therefore must clearly be obtained through a necessary middle term; otherwise its possessor will know neither the cause nor the fact that his conclusion is a necessary connexion. Either he will mistake the non-necessary for the necessary and believe the necessity of the conclusion without knowing it, or else he will not even believe it--in which case he will be equally ignorant, whether he actually infers the mere fact through middle terms or the reasoned fact and from intermediate premisses.

Of accidents that are not essential according to our definition of essential there is no demonstrative knowledge; . . .

Aristotle, Posterior Analytics